

ALMA MATER STUDIORUM · UNIVERSITÀ DI BOLOGNA

DOTTORATO DI RICERCA IN
Scienze e tecnologie agrarie, ambientali e alimentari

Ciclo XXVI

Settore Concorsuale di afferenza: 07/C1

Settore Scientifico disciplinare: AGR/09

**Evaluation of energy level to be absorbed
by tractor ROPS: Actual Tests,
Simulation and Computation**

Presentata da: **Bruno Franceschetti**

Coordinatore Dottorato:
Prof. Giovanni Dinelli

Relatore:
Dott.ssa Valda Rondelli

Correlatore:
Prof. Ing. Adriano Guarnieri
Ing. Roland Lenain

Esame finale 2014

Contents

Contents	iv
List of Figures	v
List of Tables	ix
Preface	1
Introduction	3
1 Tractor rollover	5
1.1 Tractors	5
1.2 Roll-Over Protective Structure (ROPS)	10
1.2.1 Development of the ROPS standards	10
1.2.2 Standard codes for the official testing procedures of tractor ROPS	13
1.2.3 Narrow-track tractor: ROPS testing procedures	16
2 Tractor lateral rollover dynamics	29
2.1 Introduction to the rollover dynamics	29
2.2 Rigid body dynamics	32
2.2.1 Rigid body tractor modeling	32
2.2.2 Equations of motion	37
Annex 1: 3D rigid body model evolution	43
3 Preliminary tests	57

3.1	Introduction	57
3.2	Static tests	60
3.3	Dynamic tests	64
3.4	Comparison between Dynamic and Static tests	71
	Annex 2: Deflection due to bending, strain energy and shock and impact	75
4	Actual test	83
4.1	Tested tractor	83
4.2	Experimental set-up	83
4.3	Experimental results	87
5	Mathematical Model	89
5.1	Lateral rollover model	89
5.2	Different motion phases	91
5.3	Computation of the velocity variations	95
5.3.1	Free falling phases (B, D, F)	95
5.3.2	Impact phases (C, E)	96
5.4	Integration method and kinetic energy computation	103
5.5	Evaluation of energy to be absorbed by the ROPS	106
6	Real data vs. mathematical model	107
6.1	Comparison of the real data and mathematical model	107
7	Conclusions	115
	Bibliography	117

List of Figures

1.1	Wheeled tractor	6
1.2	Track-laying tractor	6
1.3	Narrow-track tractor	7
1.4	ROPS type	8
1.5	ROPS fixing approach	9
1.6	Overturning rig for research on tractor cab design (NIAE, Silsoe; 1973 – 1975)	13
1.7	Clearance Zone	15
1.8	Clearance zone according to OECD Code 6	17
1.9	Lateral stability test	18
1.10	Evaluating of tractor moment of inertia and height of the centre of gravity	19
1.11	Clearance zone for tractors with reversible seat and steering wheel . .	20
1.12	Required levels of energy absorbed by the ROPS for Longitudinal tests (OECD Code 6)	22
1.13	Level of force applied for Crushing test (OECD Code 6)	22
1.14	Required levels of energy absorbed by the ROPS for Side tests (OECD Code 6)	24
1.15	Required levels of energy absorbed by the ROPS for Static tests (OECD Code 6)	24
1.16	Required pendulum height for Dynamic tests (OECD Code 6)	25
1.17	Required levels of energy absorbed by the ROPS for Dynamic tests (OECD Code 6)	25

1.18	Mass intervals considered in the OECD Code 6 , EC Directive 87/402/EEC and ISO 12003-1:2013	26
2.1	Real tractor	33
2.2	Modeling tractor	33
2.3	Rigid body	33
2.4	Representation of the rigid body of a tractor in the impact phase after a rotation	38
2.5	Rigid body in rotation position	39
2.6	Direction cosine	44
2.7	Euler angles	45
2.8	Comparison between Direction cosine and Euler angles	47
2.9	Translation	47
2.10	3D Tractor	49
2.11	Sloping of the ground	51
2.12	Predictable impact points of tractor cab	53
2.13	Tractor rotation axis after the cab impact (rotation of F_1 angle about y-axis)	56
3.1	Data acquisition system	58
3.2	Beam profile	59
3.3	Instrumented beam	59
3.4	Static loading	60
3.5	Elasto-plastic behaviour of the beam	61
3.6	Elastic behaviour of the tested beam	62
3.7	Elasto-plastic behaviour of the tested beam	63
3.8	Dynamic impact phases	65
3.9	Force and deflection vs. time	68
3.10	Dynamic deformation	69
3.11	Velocity of the sphere during the impact on the beam (case $h = 0.2$ m)	70
3.12	Comparison between Dynamic and Static deformation behaviour	73
3.13	Force-deflection linear relationship	77

3.14	Beam bending element	77
3.15	Cantilever beam with a U cross section and a concentrated load F . . .	78
3.16	Impact model	80
4.1	Tested tractor	84
4.2	Tractor positions to determine the moment of inertia by using on oscillating platform	85
4.3	Different phases of the actual experiment	86
4.4	Kinetic energy during the actual lateral rollover, and the energy ab- sorbed by the ROPS	88
5.1	The computing environment: tractor and ground with associated points and angles	91
5.2	Sequence of phases in tractor lateral rollover modelling	94
5.3	Plane motion of a rigid body around a fixed axis	97
5.4	Hard impact phase	98
5.5	Impact of the wheels with the ground slope	101
5.6	Impact of the wheels with the ground slope	104
5.7	Rigid body subject only to gravitational force with initial speed . . .	105
6.1	Kinetic energy and the energy absorbed by the ROPS during impact with respect to the ground slope	108
6.2	Reference system	109
6.3	Model evolution: a) Non-elastic Model,b) Elastic Model,c) Mixed Model	110
6.4	Actual Data vs. Mathematical Model	111
6.5	Energy absorbed by the ROPS vs. slope and tyre elasticity	113

List of Tables

1.1	Pendulum energy during impact against a tractor anchored to the ground with ropes (Dynamic test)	11
1.2	Comparison of OECD Codes, EC Directives and ISO and SAE Standards	15
1.3	Characteristic tractor data for calculation of non-continuous rollover behaviour	19
2.1	Parameters and geometrical factors	35
2.2	Dimensions of the 3D model of tractor	48
3.1	Control, measurement and data acquisition system components of the preliminary tests	58
3.2	Tested beam specification	58
3.3	Data acquisition	61
3.4	Dynamic test notation	64
3.5	Potential energy	66
3.6	Theoretical impact velocity	66
3.7	Strain energy	67
3.8	Differences between theoretical and actual velocity	67
3.9	Differences between theoretical and actual kinetic energy	70
3.10	Differences between kinetic energy and strain energy	71
3.11	Differences between actual and theoretical deflection	71
3.12	Effect of the loading on the strain energy and deflection	72
4.1	Tractor specifications	84

4.2	Control, measurement and data acquisition system components of the test tractor	85
5.1	Points and angles defined for tractor modelling	92
5.2	Parameters and geometrical factors included in the tractor model . .	93
6.1	Tractor geometrical dimension	108
6.2	Energy absorbed by the ROPS in different approaches with respect to the actual value of 1095 J	111

Preface

The thesis is based upon the studies that I performed during my PhD degree and is basically made of two parts, corresponding to the two different approaches adopted in the project. The first one was on the evaluation of energy during a tractor lateral rollover; this approach made it possible to study the lateral rollover dynamic of the tractor on the basis of actual tests. The activity was carried at the Department of Agricultural and Food Sciences (DISTAL) of the University of Bologna, under the guidance of Dr. Valda Rondelli and Prof. Adriano Guarnieri, and with the collaboration of Dr. Enrico Capacci. The second part was based on the activity performed at the National Research Institute of Science and Technology for Environment and Agriculture (IRSTEA) at Clermont-Ferrand (France); the approach was the modellisation of the behaviour of a tractor in phase of lateral rollover, with Dr. Roland Lenain as supervisor. The aim was to predict the amount of energy to be absorbed by Roll-Over Protective Structures (ROPSs) in case of tractor lateral rollover in different boundary conditions.

Introduction

Despite the progress in tractor design with respect to safety, one of the most dangerous situations for the driver in operating conditions is the tractor lateral rollover. Several accidents, involving tractor rollover, have indeed been encountered, requiring the design of a robust Roll-Over Protective Structure (ROPS). The aim of the thesis was to evaluate tractor behaviour in the rollover phase so as to calculate the energy level absorbed by a ROPS to ensure driver safety. A Mathematical Model representing the behaviour of a generic tractor during a lateral rollover, with the possibility of modifying the geometry, the inertia of the tractor and the environmental boundary conditions, is herein proposed. The purpose is to define a method allowing the prediction of the elasto-plastic behaviour of the subsequent impacts occurring in the rollover phase. In particular, it is proposed a tyre impact model capable of analysing the influence of the wheels on the energy to be absorbed by the ROPS. Different tractor design parameters affecting the rollover behaviour, such as mass and dimensions, have been considered. This permitted the evaluation of their influence on the amount of energy to be absorbed by the ROPS. The model was designed and calibrated with respect to the results of actual tests carried out on a narrow-track tractor. The dynamic behaviour of the tractor and the energy absorbed by the ROPS, obtained from the actual lateral upset tests, showed a good match with respect to the results of the model developed. The proposed approach represents a valuable tool in understanding the dynamics (kinetic energy) and kinematics (position, velocity, angular velocity, etc.) of the tractor in the phases of lateral rollover and the factors mainly affecting the event. The prediction of the amount of energy to be absorbed in some cases of accident is possible with good accuracy. It can then help in designing protective structures or active security devices.

The studies performed were divided as follow:

In [chapter 1](#) an introduction to the tractor machine ([section 1.1](#)), the adoption of ROPS structures ([section 1.2](#)) and how the problem of tractor rollover was addressed over the years by developing the ROPS testing procedures are proposed. Chapter [2](#) introduces the study of the dynamics of tractor lateral overturning ([section 2.1](#)) and summarizes the techniques for assessing the level of energy absorbed by the ROPS during a rollover ([section 2.2](#)) through real evidences or simulated studies by modeling.

A real tractor overturning with a narrow-track tractor was analysed and a mathematical model was developed to simulate the actual test. The model was therefore validated and in its present form it allows to simulate an infinite numbers of different boundaries situations quickly and cheaply. The first problem was to rightly instrument the tractor and be able to correctly analyse the data collected in the rollover event.

In [chapter 3](#) laboratory tests carried out on a simple beam before to instrument the tractor are reported. Preliminary tests were made to calibrate the equipment used for data collection during the tractor rollover([section 3.1](#)). The results ([section 3.4](#)) were useful to study the actual behaviour of the impacts and the effect on the deformation and the energy absorbed in case of loading (Static case) ([section 3.2](#)) or impact (Dynamic cases) ([section 3.3](#)). In [chapter 4](#) the evaluation of the dynamics of the overturning of a modern tractor is presented analysing the actual tractor rollover phases. In [chapter 5](#) the actual test simulated by a Mathematical Model is presented. In [chapter 6](#) the comparison between Real Data and Mathematical Model data is proposed ([section 6.1](#)).

Chapter 1

Tractor rollover

1.1 Tractors

Tractors, according to the definition of the Organisation for Economic Co-operation and Development ([OECD Codes, 2013](#)), is a self-propelled wheeled vehicles, having at least two axles, or fitted with tracks, designed to carry out the following operations, primarily for agricultural and forestry purposes:

- to pull trailers;
- to carry, pull or propel agricultural and forestry tools or machinery and, where necessary, supply power to operate them with the tractor in motion or stationary.

Several different types of tractors are commercially available. Manufacturers of tractors over the years were devoted mainly to the production and development of two main types: the standard tractor and the narrow-track tractor ([Figure 1.1](#)).

The first one is used in the context of extensive crops where there are no problems of space around the tractor, while the second one is dedicated to crops, such as orchards and vineyards, causing the need to get into tight spaces. Tractors may be fitted with tyres or crawlers, made of rubber or steel, and depending on this the tractor is defined as wheeled or track-laying tractor ([Figure 1.2](#)).



(a) Wheeled standard tractor



(b) Wheeled narrow-track tractor

Figure 1.1: Wheeled tractor



(a) Rubber track-laying tractor



(b) Steel track-laying tractor

Figure 1.2: Track-laying tractor

In the case of wheeled narrow-track tractors there is a further diversification because there are tractors with isodiametric wheels, that is, all the wheels of the same size on the two axles. (Figure 1.3).

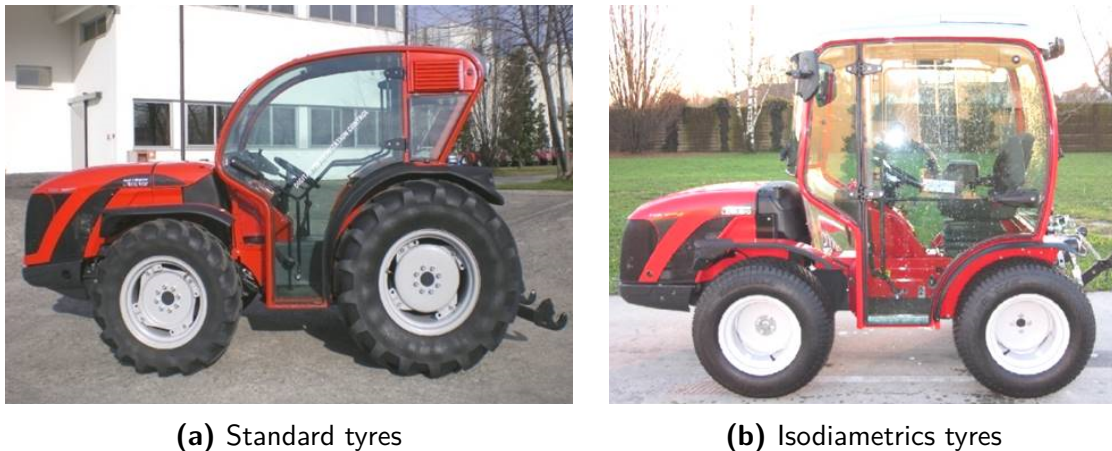


Figure 1.3: Narrow-track tractor

The tractor is the machine mostly used in agriculture and, due to its wide diffusion, it is the first cause of injury for the operator (Harris et al., 2010). The overturning, and specifically the lateral rollover, is the most serious and frequent accident that may occur in field. A solution to this problem, which has been adopted worldwide, has been to provide a passive protection during the rollover by fitting Roll-Over Protective Structures (ROPS) (Figure 1.4). Tractors are normally used in field operation in the farms and the variable conditions (such as slopes, slippery surfaces, drainage ditches, etc.) introduce the risk of instability, potentially leading to tractor rollover. Roll-Over Protective Structure (safety cab or frame), hereinafter called "protective structure or ROPS", means the structure on a tractor the essential purpose of which is to avoid or limit risks to the driver resulting from rollover of the tractor during normal use. The Roll-Over Protective Structure is characterized by the provision of space for a "clearance zone" large enough to protect the driver when seated either inside the envelope of the structure or within a space bounded by a series of straight lines from the outer edges of the structure to any part of the tractor that might come into contact with flat ground and that is capable of supporting the tractor in that position if the tractor overturns (OECD Codes, 2013). Historically, before the widespread introduction of ROPS, tractor rollover caused



(a) Front dual pillars ROPS



(b) Rear dual pillars ROPS



(c) 4 pillars ROPS



(d) ROPS cab

Figure 1.4: ROPS type

the deaths of many tractor drivers each year: the risk of severe injury or fatality was very high (Chisholm, 1972; Moberg, 1964). Fortunately ROPS have long been recognised as an effective means to greatly reducing the likelihood of operator injury during overturning accidents involving agricultural tractors (Springfeldt, 1996). However, the fixing of the ROPS on the tractor has changed considerably over the years (Rondelli et al., 2012). Indeed these structures were initially rigidly mounted on the tractor axles, then elastic elements were introduced to limit vibration and noise till to design solutions with cabin completely suspended above the chassis of the tractor (Figure 1.5).

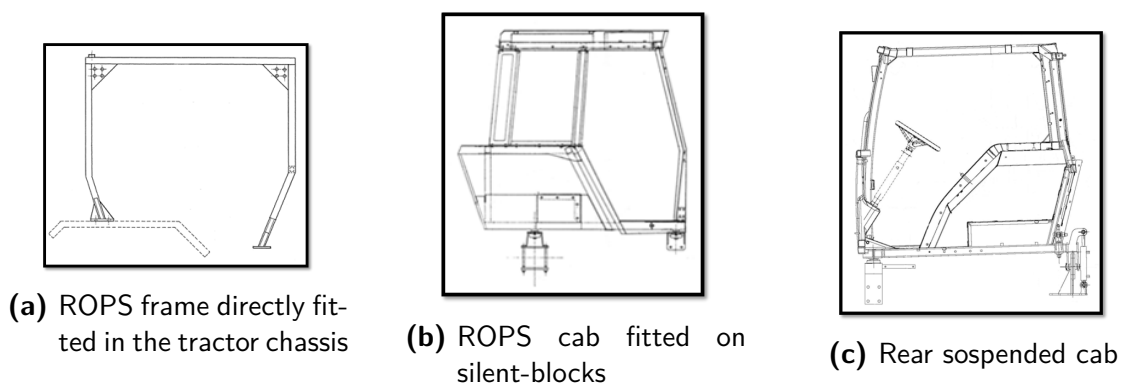


Figure 1.5: ROPS fixing approach

Special interest by the scientific community is currently facing the stability of agricultural tractors. Specifically, the goal is to focus attention on tractor dynamic to improve the safety aspects for the driver. Deep studies need to be carried out because the variability of the tractor geometry and the external environmental conditions affects the dynamics of the rollover. Nonetheless, intensive work has been already done on the effect of the slope and the angles of rollover measured in static conditions (Liu and Ayers, 1998; Spencer and Gilfillan, 1976). Another important issue concerns the design of the ROPS structures. Improving the ROPS performance can be reached both experimentally, through laboratory tests (Etherton et al., 2002; Silleli et al., 2007, 2008), and/or adopting dedicated softwares, such as those based on finite element (Alfaro et al., 2010; Fabbri and Ward, 2002). The present study is focusing on the dynamics of tractor lateral rollover and the energy shared between the tractor body and the ground during the different impacts, analysing the influ-

ence of parameters such as geometry, inertia, mass and environmental conditions. The goal is to evaluate the actual energy that the ROPS absorbs at the impact point during a lateral rollover, varying the boundaries conditions. To know this data will permit to improve the design of safety ROPS.

1.2 Roll-Over Protective Structure (ROPS)

1.2.1 Development of the ROPS standards

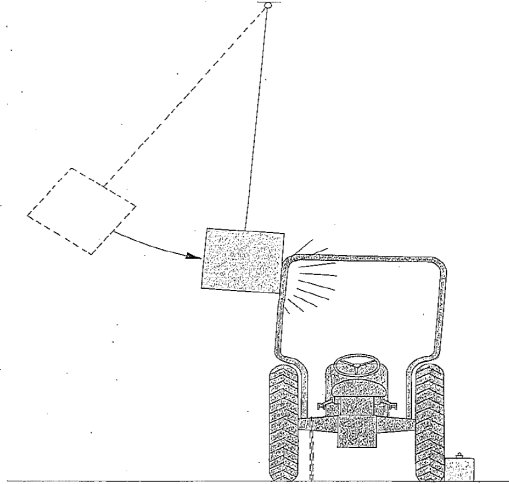
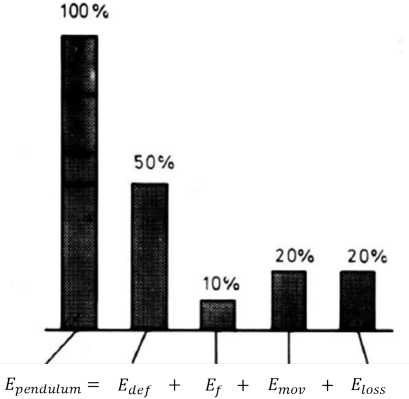
The use of wheeled vehicles in certain off-road conditions inevitably introduces a risk of instability and rollover. In the absence of adequate operator rollover protection, the risk of severe injury or fatality in such instances is very high. Having introduced as a mandatory requirement on agricultural tractors in Sweden in the late-1950s the ROPS fitting (Moberg, 1973) a similar ROPS approach followed in many countries during the subsequent decade. Development and publication of relevant laboratory test criteria proceeded in parallel to ensure the adequacy of ROPS designs for their intended purpose. The OECD test codes have been at the forefront of ROPS performance test criteria development for agricultural tractors, initially with the Code 3 (Dynamic test, OECD Code 3) from the 1960s and subsequently the Code 4 (Static test, OECD Code 4), as introduced in the late-1970s and still widespread used today. Codes 6 and 7 were developed for the narrow-track tractors in the early-1990s. Later on Code 8 for track-laying tractors was introduced (OECD Code 8). Other organisations have developed in parallel ROPS testing procedure (EC/EU in Europe, ISO, SAE, OSHA in the United States of America, etc.).

All ROPS test criteria are based on a series of empirical test relationships mainly referred to the tractor reference mass to calculate the minimum level of strain energy a ROPS must absorb under loading without the structure fails or infringes the driver's "clearance zone". The dynamic procedure was developed by combining of research results, testing activity and examination of real rollover accidents. Details of the pendulum impact tests for the dynamic ROPS testing procedure is depicted in Table 1.1. As tractor power and mass increased during the late-1960s and

early-1970s, it became evident that the dynamic test procedure (Code 3-type) embodied certain limitations, particularly concerning the testing difficulties for ROPS on heavier vehicles (Moberg, 1973). The limitation of this method was recognised by researchers in Germany, France, the UK, and the European Commission (EC) (Schwanghart, 1978; Söhne and Schwanghart, 1978). The EC subsequently commissioned to a multinational group of experts to research and find a solution to the problem, (Boyer et al., 1976). In the mid-1970 the findings leading to develop the static ROPS test criteria adopted by the EU and the OECD nowadays.

For drafting the new static code the results obtained from Schwanghart (1978) were taken into account, he stated that on average during the dynamic tests, only 50% of the total energy supplied by the pendulum was absorbed from the ROPS in the form of deformation energy (Table 1.1).

Table 1.1: Pendulum energy during impact against a tractor anchored to the ground with ropes (Dynamic test)

Diagram of the arrangement for pendulum impact tests	Possible breakdown of pendulum energy during impact										
	 <p style="text-align: center;">$E_{pendulum} = E_{def} + E_f + E_{mov} + E_{loss}$</p> <table border="1" data-bbox="850 1552 1394 1706"> <tbody> <tr> <td>$E_{pendulum}$</td> <td>Total potential energy</td> </tr> <tr> <td>E_{def}</td> <td>Deformation energy</td> </tr> <tr> <td>E_f</td> <td>Energy lost on pendulum oscillation</td> </tr> <tr> <td>E_{mov}</td> <td>Energy absorbed by the tractor movements</td> </tr> <tr> <td>E_{loss}</td> <td>Loss of energy</td> </tr> </tbody> </table>	$E_{pendulum}$	Total potential energy	E_{def}	Deformation energy	E_f	Energy lost on pendulum oscillation	E_{mov}	Energy absorbed by the tractor movements	E_{loss}	Loss of energy
$E_{pendulum}$	Total potential energy										
E_{def}	Deformation energy										
E_f	Energy lost on pendulum oscillation										
E_{mov}	Energy absorbed by the tractor movements										
E_{loss}	Loss of energy										

Over the last 40 years ROPSs have made a major contribution to agricultural vehicle safety, even if it is worldwide accepted that it is impossible to protect the operator in all the rollover instances: certain accident scenarios will undoubtedly lead to a so high levels of energy which a ROPS could not be expected to withstand. Consequently the ROPS test criteria have to ensure that the tested ROPS will

provide "the highest reasonable probability of driver protection" in the event of rollover in "a normal operation" for the vehicle.

However, tractor design evolved during the years: increasing in the agricultural mechanisation and decreasing manpower labour required fewer operators to use larger and more powerful tractors. The need of increased power tractors has encouraged the development and widespread adoption of four-wheel-drive (4wd) systems with higher travel speeds, greater braking capability and increased hydraulic lift capacity, to handle wider and heavier mounted implements. Developments in agricultural tyre design allowed improved tractive performance and greater load capacity. These factors potentially may affect the adequacy of the ROPS test criteria currently in use, being these mainly unchanged in the energy and force equations.

The (static) ROPS test criteria currently used in the EC directives and in the OECD Codes was developed and validated by a broad multinational research effort. Tractor accident investigation to determine typical dynamic rollover behaviour (Chisholm, 1979b,d) was carried out, computer simulation modelling of tractor rollover behaviour was developed (Chisholm, 1979a) and practical, instrumented vehicle rollover testing to validate the simulation was then performed (Chisholm, 1979b; Schwanghart, 1982) (Figure 1.6). Chisholm stated that simulation modelling was needed to cover the wide range of rollover conditions involved and to study the detailed effect of parameter changes (Chisholm, 1979c). Rollover experiments alone were considered to be too costly, time-consuming, and insufficiently reliable to meet these requirements. However, the research in question was based mainly on the tractor designs of 40 years ago, which were primarily two-wheel-drive and of limited payload capacity.



Figure 1.6: Overturning rig for research on tractor cab design (NIAE, Silsoe; 1973 – 1975)

1.2.2 Standard codes for the official testing procedures of tractor ROPS

Over the years the ROPSs have changed significantly (Job, 2008). In Europe most of the development for ROPS design was done under the auspices of OECD, which developed **OECD Code 3** and **OECD Code 4** for the standard agricultural tractors, **OECD Code 6** for the narrow-track tractor fitted with front rollbar and **OECD Code 7** for the narrow-track tractors fitted with rear rollbar or cab ROPS. **OECD Code 3** is the dynamic ROPS testing procedure and **OECD Code 4** is the static one. Inside the **OECD Code 6** and **OECD Code 7** there are both ROPS testing procedures: dynamic and static. In Europe the European Union developed over the years tractor Directives and required as compulsory ROPS structures fitted on the tractors. Currently all the tractors in the European Union need to have tested and certified ROPS. ROPS are tested according to the armonized OECD testing procedure or the specific EC directives. Tractor ROPS are approved as in compliance with the EC Directives/OECD codes and this allows a registration of the structure design. As already mentioned during the late-1950s OECD introduced the zone of clearance (Moberg, 1973). The zone of clearance is defined by planes

as follows, the tractor being on a horizontal surface: "Horizontal 950 mm above the compressed seat; Vertical, at right angles to the median plane of the tractor and 100 mm behind the back of the seat; Vertical, parallel to the median plane of the tractor and 250 mm to the left of the center of the seat; Vertical, parallel to the median plane of the tractor and 250 mm to the right of the center of the seat; An inclined plane in which lies a horizontal line which is at right angles to the median plane of the tractor, 950 mm above the compressed seat and 450 mm plus the normal fore and aft movement of the seat in front of the back of the seat. This inclined plane passes in front of the steering wheel and at its nearest point is 40 mm from the rim of the steering wheel. The back of the seat shall be determined ignoring any padding thereon. The seat shall be in its rearmost adjustment for normal seated operation of the tractor and in its highest position if this is independently variable. Where the springing of the seat is adjustable it shall be at its mean setting and the load on it shall be 75 kg".

During the strength tests, the ROPS frame shall be examined to determine whether any part of the "zone of clearance" is outside the protection of the frame. For this purpose "it shall be considered to be outside the protection of the frame if any part of it would have come in contact with flat ground if the tractor had overturned towards the direction from which the blow was struck or the load was applied. For this purpose the tires and track setting shall be assumed to be the smallest standard fitting".

As more organizations and standards developing organizations became involved in the process, the operator clearance zone was defined as the volume which the ROPS could not enter during the strength tests. Nevertheless there are some different definitions in the ROPS standards. For example, [OECD Code 3](#) and [OECD Code 4](#) use the clearance zone depicted in [Figure 1.7](#). The clearance zone is designed on the basis of the Seat Index Point (SIP), as defined in the ISO Standard (ISO 5353:1995).

In the early standards, the static tests were very simple; indeed the ROPS was loaded from the side, was then checked for failure and loaded from the rear. Through the development process crush tests were added to assure the ROPS were adequate.

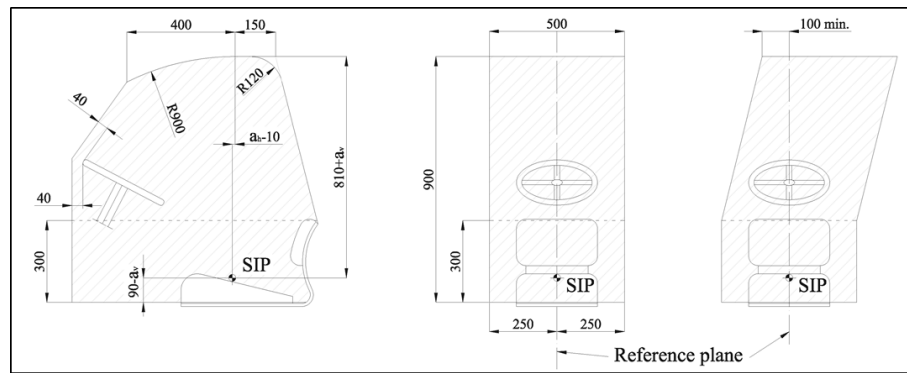


Figure 1.7: Clearance Zone

Today in **OECD Codes** there are three longitudinal loads, the front, side and rear, and two crush loads applied. The energy inputs and crushing forces to be used in the tests are based on the mass selected by the manufacturer for calculation (reference mass). That mass must not be less than the unballasted mass and must be sufficient to ensure the Mass Ratio does not exceed 1.75. This ratio is the result of the tractor maximum permissible mass with respect to the reference mass.

In the early standards of other Organisations, the tractor mass used was the the nominal mass of the tractor. Some standards used the maximum allowable mass of the tractor ("gross vehicle weight") as tested mass. The subsequent development essentially made the ROPS testing more sophisticated to increase the protection. [Table 1.2](#) gives an indication of different Codes, Standards and Directives adopted for the ROPS fitted on agricultural tractors.

Table 1.2: Comparison of OECD Codes, EC Directives and ISO and SAE Standards

Tractor and ROPS type	OECD Code	EC/EU Directive	ISO Standard	SAE/ASAE Standard
	Code 3	2009/57/EC	ISO 3463	SAE J2194
	Code 4	2009/75/EC	ISO 5700	
	Code 6	87/402/EC	ISO 12003-1	
	Code 7	86/298/EC	ISO 12003-2	SAE J1194

As shown in [Table 1.2](#) for each type of tractor different procedures to test the ROPS are offered. The choice falls on where the tractor need to be commercialized. The homologation for road circulation of the tractor in Europe is addressed by the Directive [2003/37/EC](#) with the addition of Directive [2010/52/EU](#). Directive [2005/67/EC](#) introduced the possibility for tractor ROPS in Europe to be tested according to the OECD standardized codes because these were defined equivalent to the specific EC/EU directives. The test report according to the OECD codes may be used in place of the test reports drawn up in compliance with the corresponding directives. ROPS SAE Standards are national standards in the USA. ROPS ISO standards have some correspondences with the SAE standards and are partly harmonised with the OECD Codes. As written in [SAE J 2194](#), "Any ROPS meeting the performance requirement of [ISO 5700:2013](#) (Static ROPS Test Standard) or [ISO 3463:2006](#) (Dynamic ROPS Test Standard) meets the performance requirements of the SAE Standard if the ROPS temperature/material and seat belt requirements are also met". Moreover the [SAE J 2194](#) and the [OECD Code 3](#) and [OECD Code 4](#) have the same strength equations.

1.2.3 Narrow-track tractor: ROPS testing procedures

With reference to the narrow-track tractor considered in the actual tests described in the following chapters the ROPS procedures considered is the one referred to **front mounted ROPS on narrow-track wheeled agricultural tractor** ([OECD Code 6, 2013](#)). During the ROPS tests no parts may intrude into the driver's clearance zone, because this ideally is the area occupied by the driver during the rollover event. For this ROPS type a reduced clearance zone is provided ([Figure 1.8](#)).

In Europe, as mentioned above, the EC/EU Directives, or alternatively, the OECD Standardised Codes are followed, according to the provisions of the Directive [2003/37/EC](#) as amended by the Directive [2005/67/EC](#).

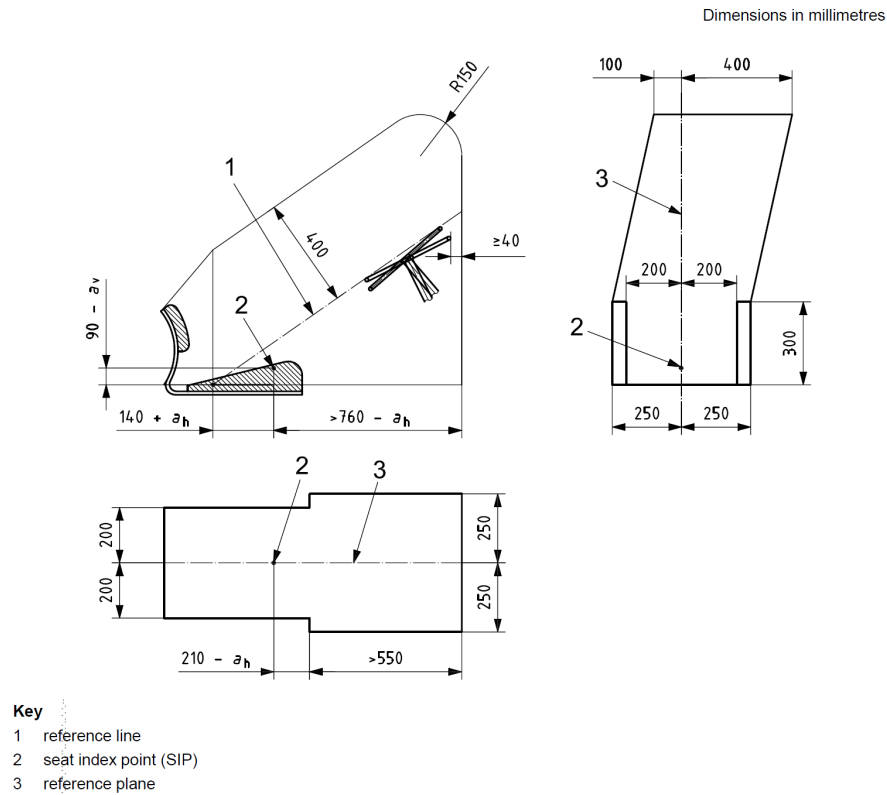


Figure 1.8: Clearance zone according to **OECD Code 6**

Narrow-track tractor: preliminary tests

In case of narrow track tractors fitted with front Roll-bar ROPS the testing procedures, **OECD Code 6** or the equivalent Directive **87/402/EEC** are completed by two preliminary tests. The protective structure may only be subjected to the strength tests if both the Lateral Stability Test and the Non-Continuous Rolling Test have been satisfactorily completed (**OECD Code 6, 2013**). For Lateral Stability Test, the angle of inclination of the tractor must be at least 38° at the moment when it is resting in a state of stable equilibrium with its 2 wheels touching the ground (**Figure 1.9**). The Non-Continuous Rolling Test is intended to check whether a structure can satisfactorily prevent continuous rollover of the tractor in the event of its overturning laterally on a slope with a gradient of 1 in 1.5. Evidence of non-continuous rolling can be provided in accordance with one of the two methods:

- > Demonstration of non-continuous rolling behaviour by means of the overturning test;

> Demonstration of non-continuous rolling behaviour by calculation.

Demonstration of non-continuous rolling behaviour by calculation require data (Figure 1.10) to be included in a specific computer programme for determining the continuous or interrupted rollover behaviour of a laterally overturning narrow-track tractor (Table 1.3). This method permits to simulate the angular velocity during the overturning; the velocity decreases after the protective structure hits the ground and the angular velocity decreases till zero if the tractor stop the rolling. If the tractor after the impact shows an angular velocity, the tractor has a continuous rolling behaviour.

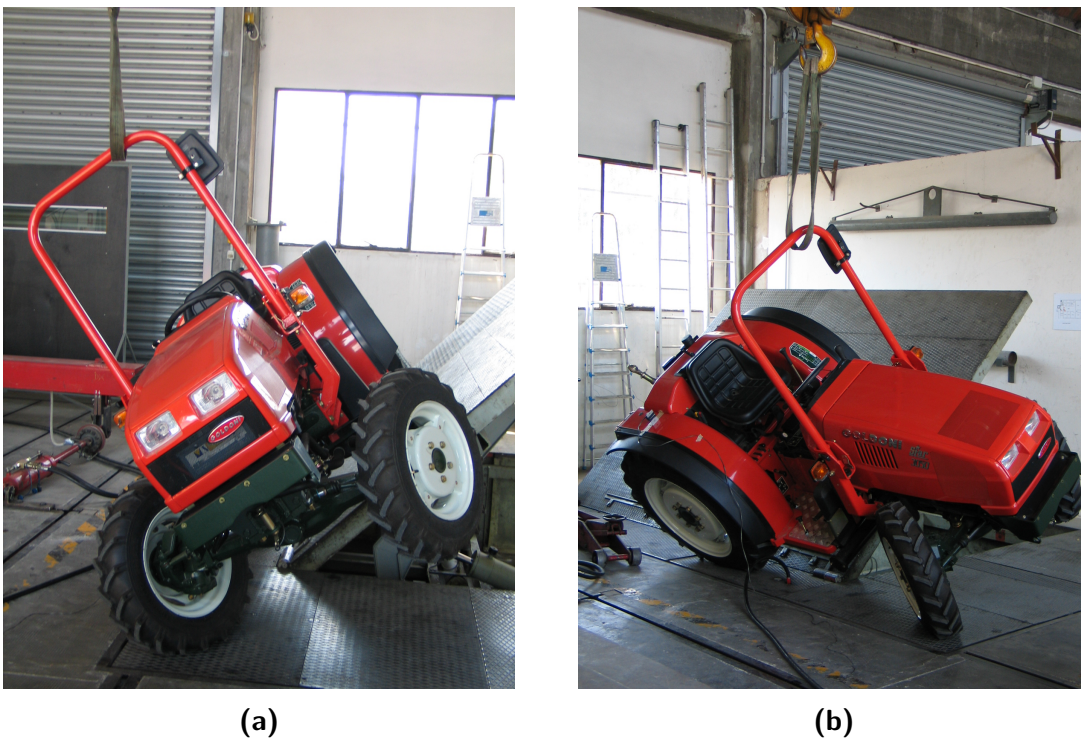


Figure 1.9: Lateral stability test



Figure 1.10: Evaluating of tractor moment of inertia and height of the centre of gravity

Table 1.3: Characteristic tractor data for calculation of non-continuous rollover behaviour

Tractor parameter		Unit
	Rear tyre width	B_0 m
	Width of protective structure between the right and left points of impact	B_6 m
	Width of engine bonnet	B_7 m
	Front-axle swing angle from zero position to end of travel	D_0 rad
	Height of front tyres under full axle load	D_2 m
	Height of rear tyres under full axle load	D_3 m
	Height of the front-axle pivot point	H_0 m
	Height at the point of impact	H_6 m
	Height of engine bonnet	H_7 m
	Rear track width	s m
	Horizontal distance between the centre of gravity and front axle	L_2 m
	Horizontal distance between the centre of gravity and rear axle	L_3 m
	Horizontal distance between the centre of gravity and the leading point of intersection of the protective structure	L_6 m
	Horizontal distance between the centre of gravity and the front corner of the engine bonnet	L_7 m
	Tractor mass used for calculation	M_c kg
	Moment of inertia about the longitudinal axis through the centre of gravity	Q kg m ²
	Height of centre of gravity	H_1 m

Narrow-track tractor: strength tests

A protective structure is regarded as having satisfied the strength requirements if during the tests no part of the protective structure enters the clearance zone as defined in [Figure 1.8](#). For tractors with reversible seat and steering wheel, the clearance zone is shown in [Figure 1.11](#) as the sum of two clearance zones.

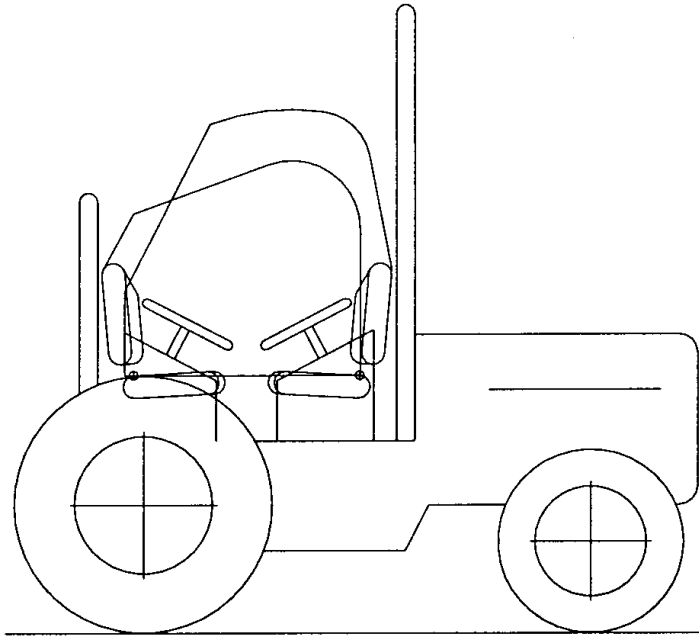


Figure 1.11: Clearance zone for tractors with reversible seat and steering wheel

The sequence of strength tests for **OECD Code 6** is as follows:

1. Impact (Dynamic test) or loading (Static test) at the rear of the structure;
2. Rear crushing test (Dynamic or Static test);
3. Impact (Dynamic test) or loading (Static test) at the front of the structure;
4. Impact (Dynamic test) or loading (Static test) at the side of the structure;
5. Crushing at the front of the structure (Dynamic or Static test).

Longitudinal tests (Figure 1.12). In the Static test the longitudinal loading tests are stopped when the energy absorbed by the protective structure is equal to, or greater than, the required energy input established. The required energy input is given by:

$$E_{LS} = 500 + 0.5 M \quad \text{Longitudinal Static loading} \quad (1.1)$$

where E_{LS} is the required absorbed energy (J), and M is the tractor reference mass (kg). In the Dynamic test the longitudinal impact tests are satisfied when the pendulum mass (m_p), equal to 2000 kg, is pulled back so that the height of its center of gravity (H_{LD}) above the point of impact is as follows:

$$\left. \begin{aligned} H_{LD} &= 25 + 0.07 \cdot M && \text{(if } M < 2000 \text{ kg)} \\ H_{LD} &= 125 + 0.02 \cdot M && \text{(if } M > 2000 \text{ kg)} \end{aligned} \right\} \quad \text{Longitudinal Dynamic impact} \quad (1.2)$$

Crushing tests (Figure 1.6). The first crushing test must be applied at the same end of the protective structure as the rear longitudinal loading test. The crushing force is given by:

$$F = 20M \quad (1.3)$$

where F is the applied force (N), and M is the tractor reference mass (kg). This force is maintained for 5 second after cessation of any visually detectable movement of the protective structure. The test is the same in both Static and Dynamic procedures.

Side tests. The energy required in the side static loading test is:

$$E_{SS} = 1.75 M \cdot \left(\frac{B_6 + B}{2 \cdot B} \right) \quad \text{Side Static loading} \quad (1.4)$$

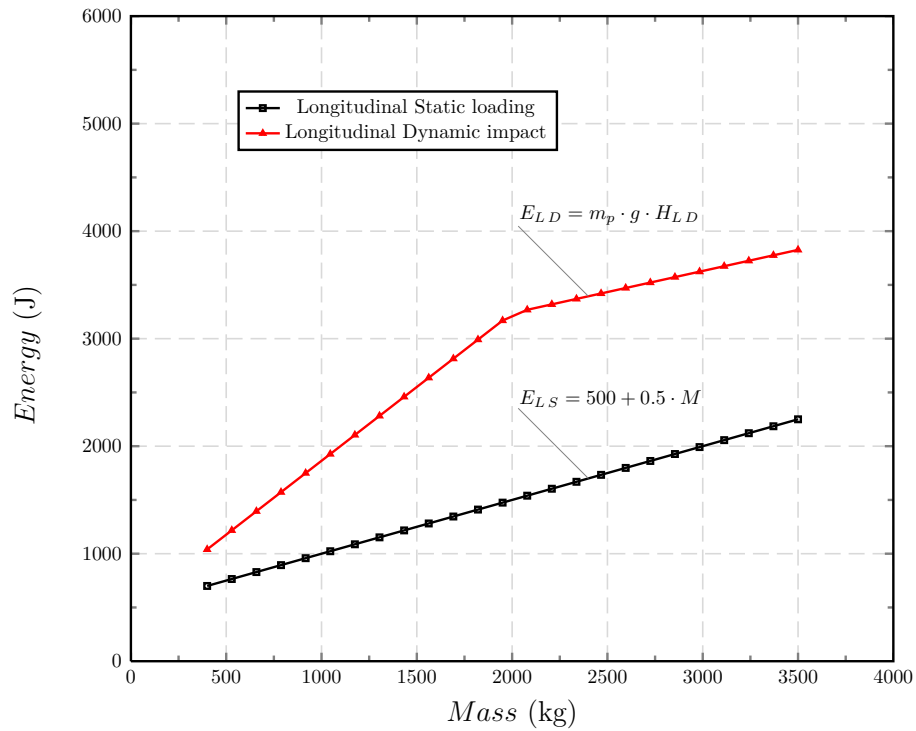


Figure 1.12: Required levels of energy absorbed by the ROPS for Longitudinal tests (OECD Code 6)

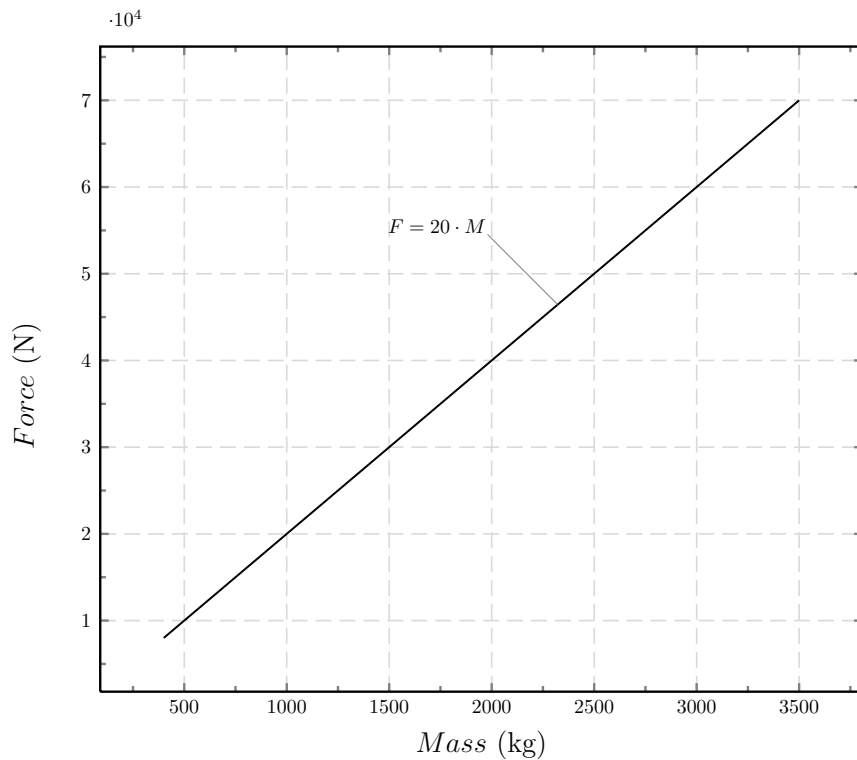


Figure 1.13: Level of force applied for Crushing test (OECD Code 6)

where E_{SS} is the required absorbed energy (J), and M is the tractor reference mass (kg). B (m) is the minimum overall width of the tractor; B_6 (m) is the width of protective structure between the right and left points of impact. The side impact test is satisfied when the pendulum mass (2000 kg) is pulled back so that the height of its center of gravity (H_{SD}) above the point of impact is as follows:

$$\left. \begin{aligned} H_{SD} &= 25 + 0.2 M \cdot \left(\frac{B_6 + B}{2 \cdot B} \right) && \text{(if } M < 2000 \text{ kg)} \\ H_{SD} &= 125 + 0.15 M \cdot \left(\frac{B_6 + B}{2 \cdot B} \right) && \text{(if } M < 2000 \text{ kg)} \end{aligned} \right\} \text{Side Dynamic impact} \quad (1.5)$$

where B (m) is the minimum overall width of the tractor; B_6 (m) is the width of protective structure between the right and left points of impact.

Side tests for tractor with reversible driver's position (Figure 1.14). $\left(\frac{B_6+B}{2 \cdot B} \right)$ is not adopted if the tractor has a reversible driver's position (reversible seat and steering wheel). In this case the formulas are as follow:

$$E_{SS} = 1.75 M \quad \text{Side Static loading} \quad (1.6)$$

$$\left. \begin{aligned} H_{SD} &= 25 + 0.2 M && \text{(if } M < 2000 \text{ kg)} \\ H_{SD} &= 125 + 0.15 M && \text{(if } M < 2000 \text{ kg)} \end{aligned} \right\} \text{Side Dynamic impact} \quad (1.7)$$

The second crushing test must be applied at the end of the protective structure as the front longitudinal loading test. In the case of two-post designs, the second crush may be at the same point as the first crush. The second crushing force applied is equal to the first (1.3). The required levels of energy absorbed by the ROPS for Static strength procedures are shown in Figure 1.15. The required pendulum height for Dynamic strength procedure are shown in Figure 1.16. The corresponding levels of energy for Dynamic strength procedure are shown in Figure 1.17.

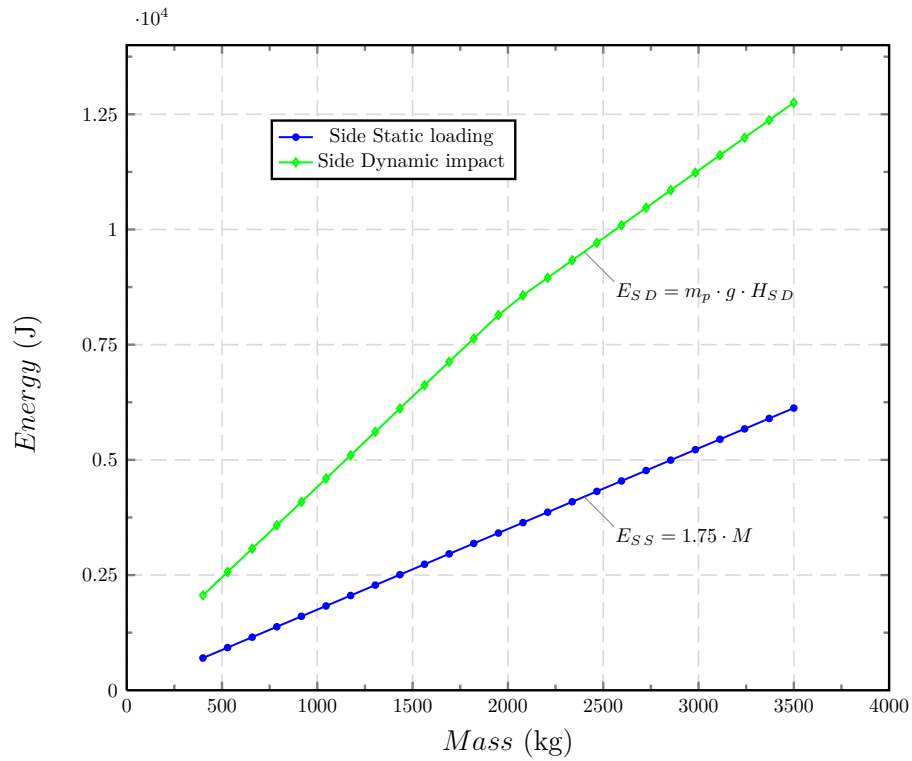


Figure 1.14: Required levels of energy absorbed by the ROPS for Side tests (OECD Code 6)

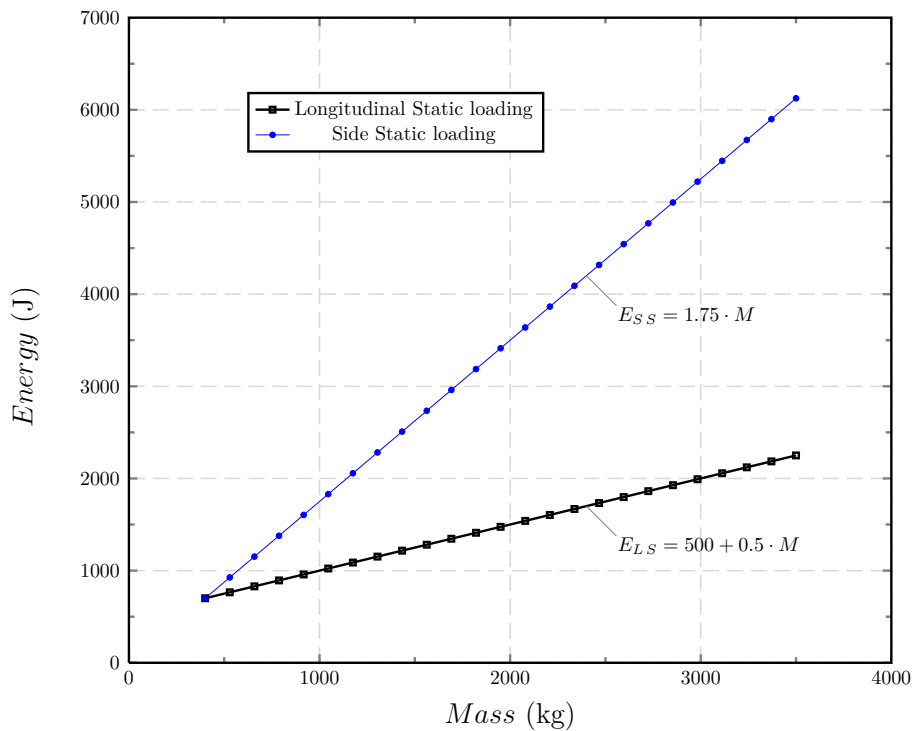


Figure 1.15: Required levels of energy absorbed by the ROPS for Static tests (OECD Code 6)

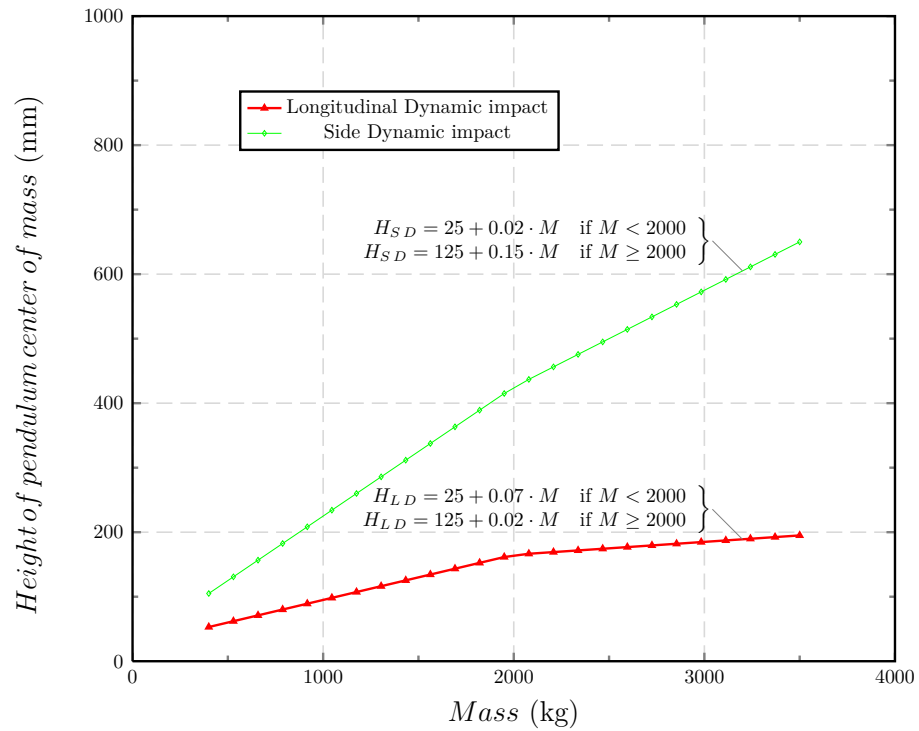


Figure 1.16: Required pendulum height for Dynamic tests (OECD Code 6)

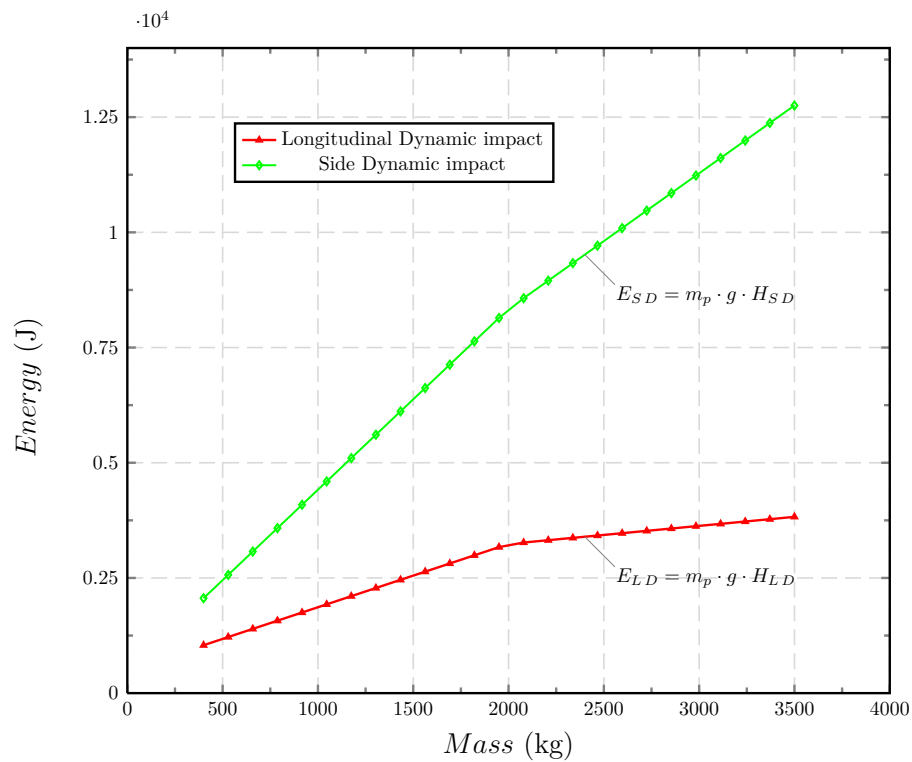


Figure 1.17: Required levels of energy absorbed by the ROPS for Dynamic tests (OECD Code 6)

Narrow-track tractor: Field of application and Mass definition in the different ROPS testing procedures

Simplifying, it is defined "Narrow-track tractor" a tractor with a minimum track width lower than 1150 mm. However it is interesting to compare different definitions of narrow-track tractor, as considered in the OECD Code 6, EC Directive and ISO Standard. The mass intervals considered are depicted in [Figure 1.18](#).

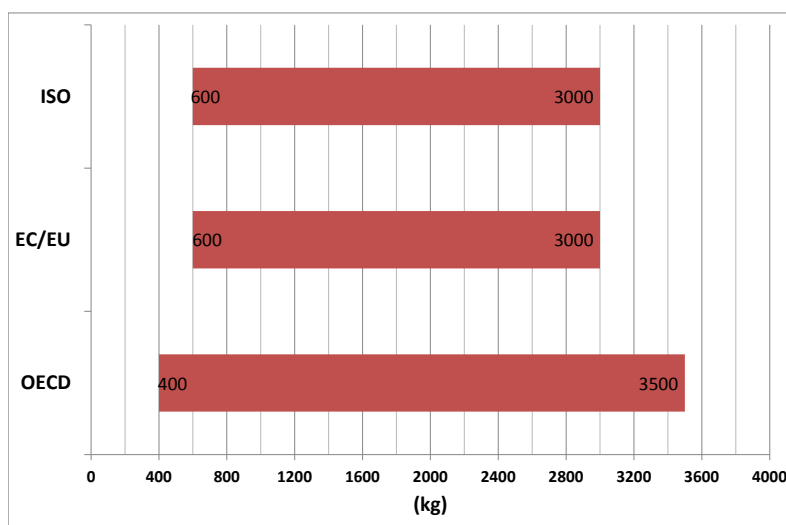


Figure 1.18: Mass intervals considered in the [OECD Code 6](#), [EC Directive 87/402/EEC](#) and [ISO 12003-1:2013](#)

OECD Standard Code 6: A fixed or adjustable minimum **track width** of one of the two axles of less than 1150 mm when fitted with the widest specified tyres. A mass greater than 400 kg but less than 3500 kg, unladen, including the ROPS and tyres of the largest size recommended by the manufacturer. **Unballasted / Unladen Mass** is the mass of the tractor excluding optional accessories but including coolant, oils, fuel, tools plus the protective structure. Not included are optional front or rear weights, tyre ballast, mounted implements, mounted equipment or any specialised components. The **Maximum Permissible Mass** is the maximum mass of the tractor stated by the manufacturer to be technically permissible and declared on the vehicle's identification plate and/or in the Operator's Handbook. The **Refer-**

ence Mass is the mass, selected by the manufacturer, used in formulae to calculate the height of fall of the pendulum block, the energy inputs and crushing forces to be used in the tests. It must not be less than the unballasted mass and must be sufficient to ensure the Mass Ratio does not exceed 1.75, i.e. $\frac{\text{Maximum Permissible Mass}}{\text{Reference Mass}} < 1.75$.

In the equivalent **Directive 87/402/EC** the definition is: A minimum **track width** of less than 1150 mm, with an unladen **mass**, in running order, of more than 600 kg and below 3000 kg.

Standard ISO 12003-1: A fixed or adjustable minimum **track width** of one of the two axles of less than 1150 mm when fitted with the widest specified tyres. A mass greater than 600 kg but less than 3000 kg, unladen, including the ROPS and tyres of the largest size recommended by the manufacturer. **Tractor mass** is the mass of the unladen tractor in working order with tanks and radiator full, front-mounted ROPS and any equipment required for normal use (The operator, optional ballast weights, additional wheel equipment, and special equipment and tools are not included). **Reference Mass** is the mass, not less than the tractor mass, selected by the manufacturer for calculation of loading energies and forces to be applied in the tests.

Chapter 2

Tractor lateral rollover dynamics

2.1 Introduction to the rollover dynamics

The problem of tractors and agricultural machinery overturning has been studied in depth by the scientific community. Indeed, the different operating conditions lead to a high risk of instability and, hence, consequent rollover situations. The majority of the rollover accidents in agriculture resulted in fatal injuries ([Harris et al., 2010](#)). As a result, rollover accidents have been investigated over the years, since the 1930s, with a peak of interest in the 1970s ([Chisholm, 1972](#)). Renewed attention in recent years has been observed ([Harris et al., 2010](#)), considering the recent evolution of tractor design (shape and overload masses). The difficulty in avoiding fatal tractor accidents has led to the introduction of Rollover Protective Structures (ROPSs), not to prevent the event but to reduce injury to the operator involved in the accident. The first mandatory requirement for ROPS tested on agricultural tractors was introduced in Sweden in the 1950s ([Moberg, 1964](#)); subsequently, many countries followed, encouraged by the first standardised testing procedure of the Organisation for Economic Co-operation and Development ([OECD Code 3, 2013](#)). In-depth research activities on the subject of tractor rollover then continued and led to the definition of additional OECD normalised testing procedures ([OECD Codes, 2013](#)). Official ROPS tests are normally mainly based on the energy to be absorbed by the ROPS, defined according to the reference mass of the tractor ([Rondelli and Guzzomi, 2010](#)). However, the rollover protective structures are verified in terms of strength

through test criteria based mostly upon studies carried out more than forty years ago (Boyer et al., 1976; Chisholm, 1977; Chisholm and Seward, 1976; Moberg, 1973; Schwanghart, 1982). Over the years, many research approaches have involved the development of mathematical models dedicated to understanding rollover dynamics via computer simulation. Since 1920, the static and dynamic behaviour of tractors has been investigated (McKibben, 1927). Research increased in the 1960s as a result of the introduction of computers, with the first examples of numerical modelling applied to the tractor, mainly based on the Newtonian approach or the Lagrange method (Kim and Rehkugler, 1987). Tractor lateral rollover (Chisholm, 1979a,b,c,d; Davis and Rehkugler, 1974a,b; Schwanghart, 1971, 1973) and longitudinal overturning (Goering and Buchele, 1967a,b; Koch et al., 1970; Smith and Liljedahl, 1972) were simulated. Research on the subject continued to the present day in order to investigate the real behaviour and the energy dynamics during tractor rollover (Ahmadi, 2011; Guzzomi et al., 2009; Lenain et al., 2010). These approaches were referred to a totally rigid body, mainly based on a simulation software approach requiring important computing skills, and were then useless in the framework of testing procedures. The ROPS approach was also considered with respect to small agricultural vehicles, such as lawn mowers, brush cutters, load carriers and multi-utility vehicles with an operating mass of 300 to 600 kg (Scarlett et al., 2006; Wang, 2005).

Studies were carried out using Finite Element in order to predict deflection, without carrying out actual tests (Arana et al., 2011; Harris et al., 2000; Wang et al., 2009). In general, the deflection of the mechanical parts of the tractor (depending on shape and material) and the amount of energy to be absorbed by the ROPS during a shock must be known for design purposes when a generic tractor is considered. An analytical model could be extremely important in agriculture in order to assess the risks for the operators. Many parameters are linked. Nowadays taking into consideration the high number of accidents having a great impact on the health of the operator and the evolution of modern tractors, it is advisable to evaluate the current ROPS standardised procedures with respect to the level of safety for the operator (Guzzomi and Rondelli, 2013; Rondelli et al., 2012). To investigate a

model dedicated to computing the amount of energy to be absorbed by the actual protective structures fitted on modern tractors varying the environmental conditions has been the goal to reach in the current study. A generic and adaptable dynamic model, based on the equations of the dynamics of the rigid body adapted to a real environment, was developed to define the kinetic energy of the tractor and to estimate the amount of energy absorbed by the ROPS in case of a lateral tractor rollover onto a surface with a constant slope. The model developed was based on the Schwanghart's approach (Schwanghart, 1982) for checking non-continuous rolling behaviour in narrow-track tractors. This model is basically the one currently adopted in the preliminary tests of OECD Code 6 (OECD Code 6, 2013). Starting from this approach, the model development was focused on the phases characterizing the tractor-ground impact. Actual preliminary tests were carried out in order to compare the real behaviour of the tractor during a lateral upset with the one simulated in the mathematical model. Analysis of the actual test results made it possible to understand the behaviour of the wheels and the ROPS at the time of impact with the ground. The study of the dynamics of the rigid body combined with the evaluation of the actual tests allowed the development of an advanced model capable of depicting the real behaviour in all phases of the lateral tractor rollover, including the absorption of the non-rigid element, such as the tyres. The model could represent a useful tool in the design of the machines, as it was capable of anticipating the kinetic energy and the energy exchanged in the machine-ground impact. It allows to modify the geometry of the machine and the elasto-plastic properties of its components, such as the wheels and the ROPS, without using a complex analysis. Moreover, the model could also be useful for establishing safety rules. Indeed, analysis of the energy exchanged between the ROPS and the ground allows the evaluation and, if necessary, the updating of the strain energy required in normalised testing procedures. In the approach adopted experimental tests allowing the analysis of a rollover situation are first proposed. The variation of energy during a normalized rollover sequence could then be known and analysed. It represented a reference to be reached by the mathematical model then proposed. After having described the different assumptions and rollover phases, the dynamic equations were

detailed since hard and soft shocks had to be considered (depending on the part touching the ground). To be representative, a mixed impact model was proposed in order to preserve accuracy and simplicity, in particular with respect to tyre deflection. The performance of the proposed model was then investigated by means of comparison to the experimental data.

2.2 Rigid body dynamics

A rigid body is an idealization of a solid body in which deformation is neglected. In other words, the distance between any two given points of a rigid body remains constant in time regardless of external forces exerted on it. In classical mechanics a rigid body is usually considered as a continuous mass distribution, while in quantum mechanics a rigid body is usually thought of as a collection of point masses.

Rigid-body dynamics studies the movement of systems of interconnected bodies under the action of external forces. The assumption that the bodies are rigid, which means that they do not deform under the action of applied forces, simplifies the analysis by reducing the parameters that describe the configuration of the system to the translation and rotation of reference frames attached to each body. The dynamics of a rigid body system is defined by its equations of motion, which are derived using either Newton's laws of motion or Lagrangian mechanics. The solution of these equations of motion defines how the configuration of the system of rigid bodies changes as a function of time. The formulation and solution of rigid body dynamics is an important tool in the computer simulation of mechanical systems.

2.2.1 Rigid body tractor modeling

The tractor, even if it is a complex machine and consists of many components of different geometry and material (Figure 2.1), can be studied using the theory of rigid body (Figure 2.2). In fact, the tractor can be studied and approximated to a single component with the tractor size to which always apply the assumptions made for the rigid body. The mass of the tractor can be calculated $m = \int_m dm = \int_V \rho dV$ if the density is known $\rho = \frac{dm}{dV}$.



Figure 2.1: Real tractor

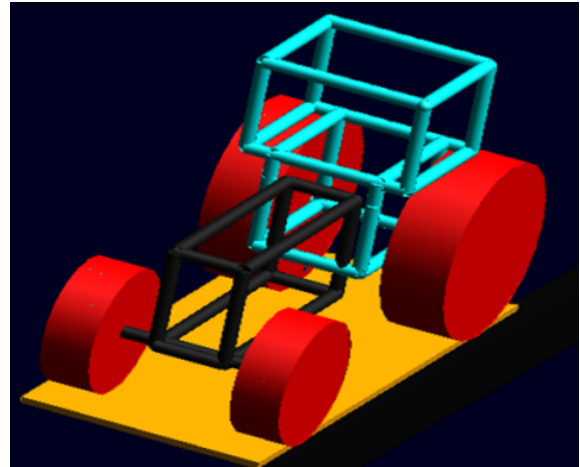


Figure 2.2: Modeling tractor

A rigid body can be considered as a continuous system m or a system of particles m_i in which the relative positions of the particles do not change (Figure 2.3).

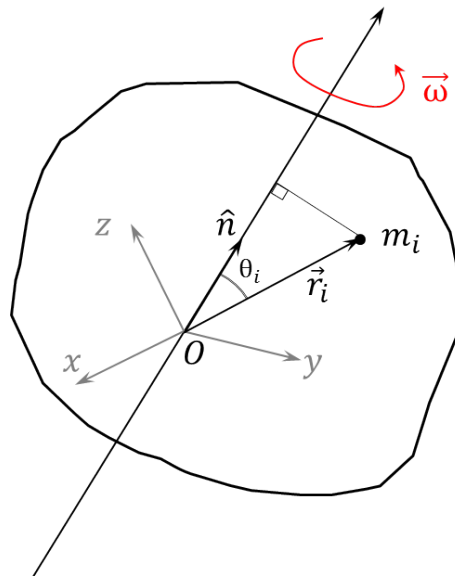


Figure 2.3: Rigid body

The centre of mass \vec{R}_{cm} is defined (2.1) (in relation to its reference system) and the moment of inertia with respect to the axis of rotation can be expressed as shown in (2.2).

Centre of mass:

$$\left\{ \begin{array}{l} \vec{R}_{cm} = \frac{\int \vec{r} dm}{\int dm} \quad \text{Continuous} \\ \vec{R}_{cm} = \frac{\sum_{i=1}^N m_i \vec{r}_i}{\sum_{i=1}^N m_i} \quad \text{Discrete} \end{array} \right. \quad (2.1)$$

Moment of inertia:

$$\left\{ \begin{array}{l} I = \int_m R^2 dm \quad \text{Continuous} \\ I = \sum_{i=1}^N (m_i \cdot R_i^2) \quad \text{Discrete} \end{array} \right. \quad (2.2)$$

Angular momentum:

Angular momentum is a vector quantity that represents the product of a body's rotational inertia and rotational velocity about a particular reference system. The angular momentum can be written in matrix form and represented by equation (2.3) or (2.4). The terms of the equations are defined in Table 2.1.

$$\begin{pmatrix} L_{cm_{x'}} \\ L_{cm_{y'}} \\ L_{cm_{z'}} \end{pmatrix} = \begin{pmatrix} I_{x'x'} & -I_{x'y'} & -I_{x'z'} \\ -I_{y'x'} & I_{y'y'} & -I_{y'z'} \\ -I_{z'x'} & -I_{z'y'} & I_{z'z'} \end{pmatrix} \begin{pmatrix} \omega_{x'} \\ \omega_{y'} \\ \omega_{z'} \end{pmatrix} \quad (2.3)$$

$$\vec{L} = \vec{I} \cdot \vec{\omega} \quad (2.4)$$

\vec{I} is the tensor of inertia (written in matrix form) about the center of mass "cm" and

with respect to the $x'y'z'$ axes. The tensor of inertia gives an idea on how the mass is distributed in a rigid body.

Table 2.1: Parameters and geometrical factors

Notation	
\vec{F}	Vectors of body external force
\vec{T}	Vectors of body external moments
\vec{p}	Vectors of linear momentum
\vec{L}	Vectors of angular momentum
I_i	Moment of inertia on point i (i=0,1)
I_{cm}	Moment of inertia on centre of mass
m	Body mass
\vec{g}	Gravitational acceleration
\vec{v}_{cm}	Velocity of the centre of mass
$\vec{\omega}_{z_i}$	The body angular velocity ($i = 0, 1$)
cm	Centre of mass
b	Horizontal distance between the axis of rotation and the cm
\vec{r}_i	Distance between the impact point and the centre of mass ($i = 0, 1$)
ψ	Angle between the gravitational acceleration vector (\vec{g}) and \vec{r}_i

Principal Axes of Inertia:

For a general three-dimensional body, it is **always** possible to find 3 mutually orthogonal axis (an x, y, z coordinate system) for which the products of inertia are zero, and the inertia matrix takes a diagonal form. In many subjects, this is the preferred way to formulate the problem. For a rotation about only one of these axis, the angular momentum vector is parallel to the angular velocity vector.

$$\begin{pmatrix} L_{cm_x} \\ L_{cm_y} \\ L_{cm_z} \end{pmatrix} = \begin{pmatrix} I_{xx} & 0 & 0 \\ 0 & I_{yy} & 0 \\ 0 & 0 & I_{zz} \end{pmatrix} \begin{pmatrix} \omega_x \\ \omega_y \\ \omega_z \end{pmatrix} \quad (2.5)$$

$$\vec{L} = I_{xx} \vec{\omega}_x + I_{yy} \vec{\omega}_y + I_{zz} \vec{\omega}_z \quad (2.6)$$

For a rigid body rotating around an axis of symmetry (e.g. the blades of a ceiling fan), the angular momentum, \vec{L} (2.7), can be expressed as the product of the body's moment of inertia, \vec{I} , (a measure of an object's resistance to changes in its rotation velocity) and its angular velocity $\vec{\omega}$.

If z-axis is axis of symmetry and axis of rotation ($\vec{\omega} = \vec{\omega}_z$):

$$\vec{L} = I_{zz} \vec{\omega}_z \quad (2.7)$$

Change of axis of rotation (outside to the center of mass) is described, according to [Figure 2.4](#).

$$\begin{cases} \vec{L} = I_{cm} \vec{\omega}_{z_1} + \vec{r}_1 \wedge m \vec{v}_{cm} \\ \vec{v}_{cm} = \vec{\omega}_{z_0} \wedge \vec{r}_0 \end{cases} \quad (2.8)$$

It can be written:

$$\vec{L} = I_{cm} \vec{\omega}_{z_1} + \vec{r}_1 \wedge m (\vec{\omega}_{z_0} \wedge \vec{r}_0) \quad (2.9)$$

According to the Lagrange's formula $\vec{a} \wedge (\vec{b} \wedge \vec{c}) = \vec{b}(\vec{a} \cdot \vec{c}) - \vec{c}(\vec{a} \cdot \vec{b})$

If $\vec{r} \perp \vec{\omega}$, the angular momentum for rigid body after the impact phase ([Figure 2.4](#)) is:

$$\boxed{\vec{L} = I_{cm} \vec{\omega}_{z_1} + m \vec{\omega}_{z_0} r_0 r_1 \cos(\psi)} \quad (2.10)$$

If $r = r_0 = r_1$ and $\psi = 0$ (i.e. $\Rightarrow \vec{r}_0 = \vec{r}_1$), the angular momentum for rigid body in rotation position ([Figure 2.5](#)) is:

$$\boxed{\vec{L} = (I_{cm} + m \cdot r^2) \vec{\omega}_z} \quad (2.11)$$

2.2.2 Equations of motion

$$\begin{cases} \vec{F} = \frac{d\vec{p}}{dt} \\ \vec{T} = \frac{d\vec{L}}{dt} \end{cases} \quad (2.12)$$

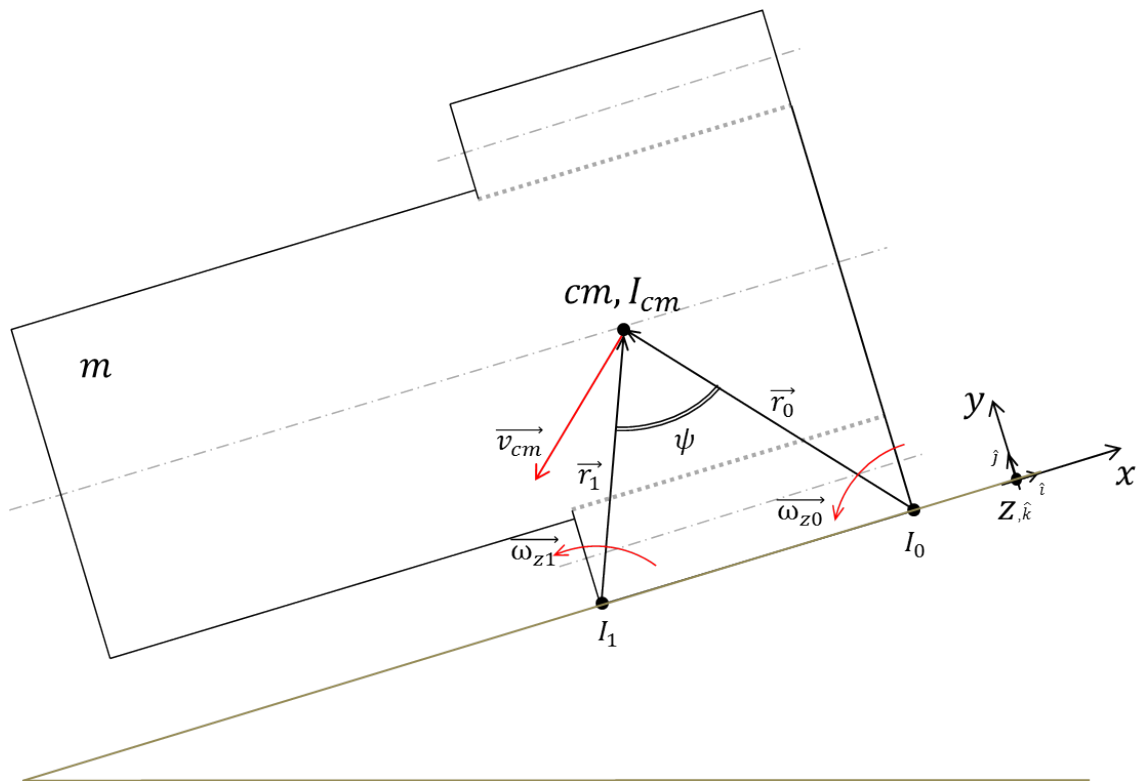


Figure 2.4: Representation of the rigid body of a tractor in the impact phase after a rotation

Rotation around a fixed axis:

$$\begin{cases} \vec{F} = m \cdot \frac{d(\vec{v}_{cm})}{dt} \\ \vec{T} = \frac{d(I \cdot \vec{\omega})}{dt} \end{cases} \quad (2.13)$$

Rotation around a fixed axis and without external forces:

$$\begin{cases} \vec{F} = m \cdot \vec{g} \\ \vec{T} = I \cdot \frac{d(\vec{\omega})}{dt} \end{cases} \quad (2.14)$$

Where I is the moment of inertia of the body, ω is the angular velocity of the body in the same direction of moment of inertia.

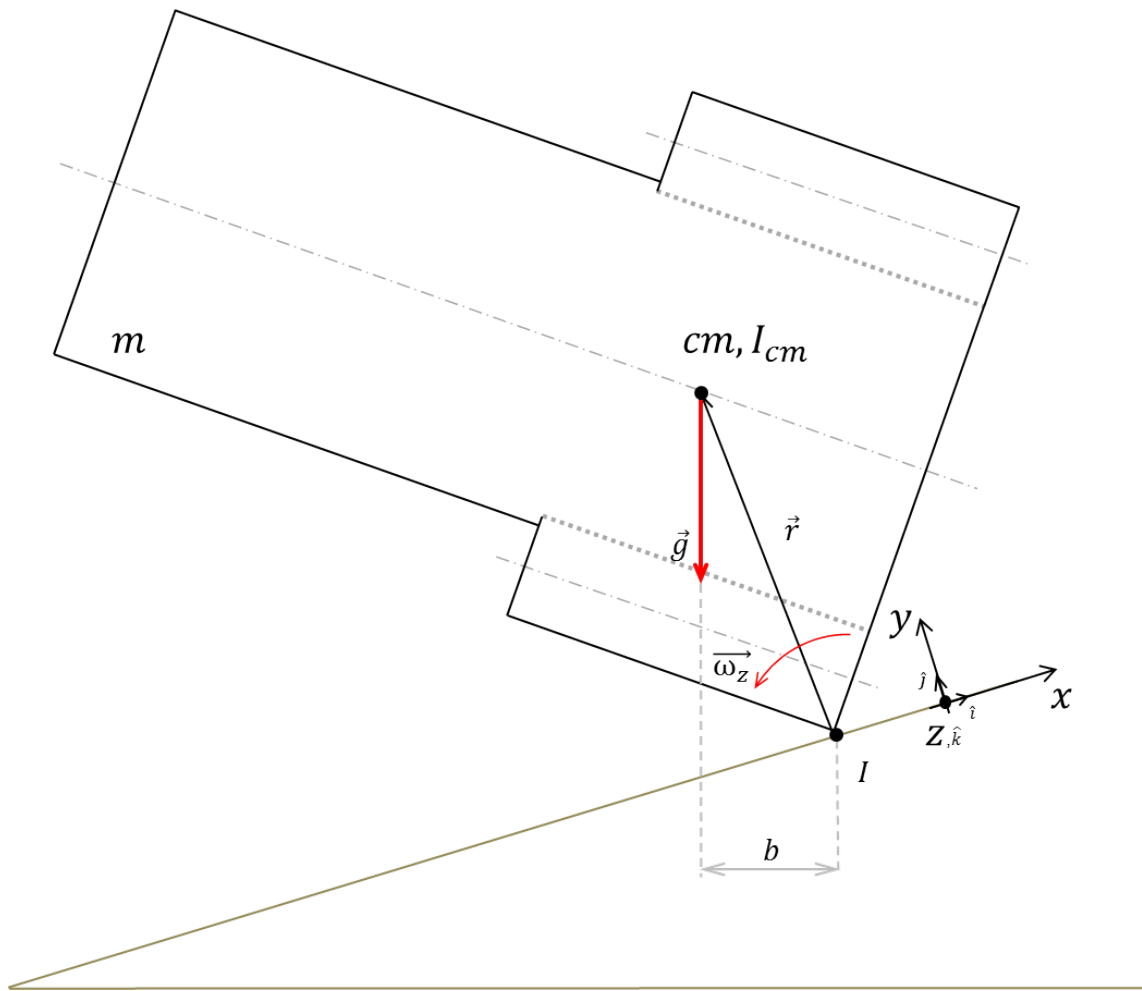


Figure 2.5: Rigid body in rotation position

Euler's equations (rigid body dynamics):

$$I \cdot \frac{d(\vec{\omega})}{dt} = m \cdot \vec{g} \cdot b \quad (\text{Figure 2.5}) \tag{2.15}$$

$$\dot{\vec{\omega}} = \frac{m \cdot \vec{g} \cdot b}{I} \tag{2.16}$$

if there is no net external force on the system as a whole, the force and momentum are conserved

$$\begin{cases} \sum \vec{F} = 0 \\ \sum \vec{T} = 0 \end{cases} \tag{2.17}$$

Conservation of Angular Momentum:

$$\vec{L}_{tot} = I \cdot \vec{\omega} = const. \quad (2.18)$$

Conservation of Energy:

$$E_{tot} = KE + PE \quad (2.19)$$

$$E_{tot} = \frac{1}{2} \cdot I_{cm} \cdot \omega^2 + \frac{1}{2} \cdot m \cdot v_{cm}^2 + PE \quad (2.20)$$

E_{tot} , KE and PE are respectively the total energy, the kinetic energy and the potential energy of the body. An elastic collision is a collision between two bodies in which the total kinetic energy of the two bodies after the impact is equal to their total kinetic energy before the impact. Elastic collisions occur only if there is no net conversion of kinetic energy into other forms. During the collision of small objects, kinetic energy is first converted to potential energy associated with a repulsive force between the particles, then this potential energy is converted back to kinetic energy (when the particles move with this force, i.e. the angle between the force and the relative velocity is acute). When considering energies, possible rotational energy before and/or after a collision may also play a role. A consequence of the conservation of energy is that it is not necessarily the conservation of kinetic energy. The kinetic energy can be destroyed but somehow if energy is destroyed, it must come out in some other forms. In case of completely inelastic collision the lost kinetic energy is converted into heat or friction and in its most general form, the kinetic energy before the collision plus "some number Q " equals the kinetic energy after the collision. If Q is bigger than zero, there is a gain of kinetic energy. $Q > 0$ corresponds to a superelastic collision, $Q = 0$ is called elastic collision and $Q < 0$ inelastic collision.

In general the **Equation of Energy** is as follow:

$$KE + Q = KE' \quad (2.21)$$

$$\begin{cases} Q > 0 & \text{super elastic collision} \\ Q = 0 & \text{elastic collision} \\ Q < 0 & \text{inelastic collision} \end{cases} \quad (2.22)$$

Where KE is the kinetic energy before impact and KE' is the kinetic energy after impact. As example $Q = \frac{1}{2} \cdot k \cdot \Delta x^2$ is the (elastic) potential energy of a springs of stiffness k stretched to x .

Annex 1: 3D rigid body model evolution

In the current annex considerations are provided for the tractor modeling from a 2D to a 3D. This approach could help in modeling tractor cases referred to ROPS cab and/or standard tyres fitting.

Principal axes of inertia: $X = (\hat{x}, \hat{y}, \hat{z})$ for the rigid body. Tensor of inertia (with principal axes of Inertia) is defined in **cartesian coordinate system** ($0xyz$) as:

$$I_0 = \begin{pmatrix} I_{xx} & 0 & 0 \\ 0 & I_{yy} & 0 \\ 0 & 0 & I_{zz} \end{pmatrix} \quad (2.23)$$

If exists an axis of rotation passing through zero

$$\hat{n} = \begin{pmatrix} \hat{n}_x \\ \hat{n}_y \\ \hat{n}_z \end{pmatrix} \quad (2.24)$$

It is possible define a tern called direction cosine ([Figure 2.6](#)), which identifies the direction of the axis of rotation with respect to the cartesian coordinate system.

$$\hat{n} = \begin{pmatrix} \cos(\alpha) \\ \cos(\beta) \\ \cos(\gamma) \end{pmatrix} \quad (2.25)$$

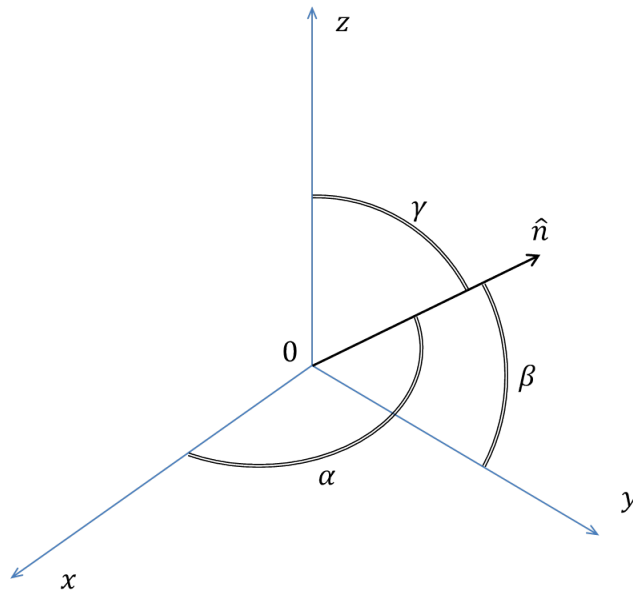


Figure 2.6: Direction cosine

Moment of inertia

If the rotation is not in one of the principal axes of inertia, using the rotation behaviour, it is possible:

1. The matrix referred to the new axis of rotation;
2. Rotation of the matrix according to the axis of rotation.

The matrix referred to the new axis of rotation

$$I = \hat{n}^T \cdot I_0 \cdot \hat{n} = \begin{pmatrix} \cos(\alpha) & \cos(\beta) & \cos(\gamma) \end{pmatrix} \cdot \begin{pmatrix} I_{xx} & 0 & 0 \\ 0 & I_{yy} & 0 \\ 0 & 0 & I_{zz} \end{pmatrix} \cdot \begin{pmatrix} \cos(\alpha) \\ \cos(\beta) \\ \cos(\gamma) \end{pmatrix} \quad (2.26)$$

Angles linearly dependent:

$$\cos^2(\alpha) + \cos^2(\beta) + \cos^2(\gamma) = 1 \quad (2.27)$$

Rotation of the matrix according to the axis of rotation

The Euler angles are three angles to describe the orientation of a rigid body. To describe the orientation in 3-dimensional Euclidean space, three parameters are required (Figure 2.7).

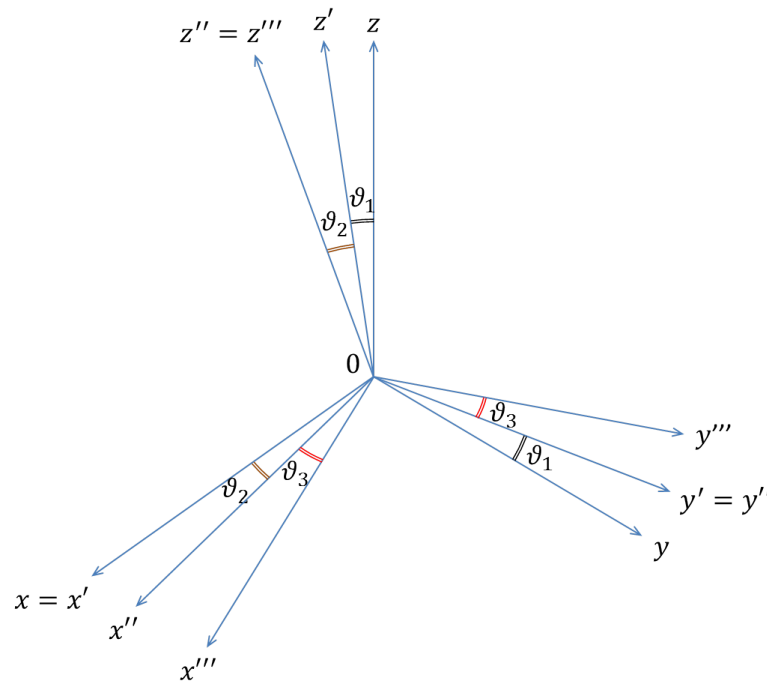


Figure 2.7: Euler angles

The angles θ_1 , θ_2 , and θ_3 are the **Euler angles**. A rotation matrix can be represented as the matrix product,

$$R = R_z R_y R_x \quad (2.28)$$

This matrix can be simplified into a sequence of three rotations, one about each principle axis. Since matrix multiplication does not commute, the order of the axes of rotation will affect the result. For this analysis, first rotation is about the x-axis, then the y-axis, and finally the z-axis.

A rotation of θ_1 radians about the x-axis is defined as

$$R_x = \begin{pmatrix} 1 & 0 & 0 \\ 0 & \cos(\theta_1) & -\sin(\theta_1) \\ 0 & \sin(\theta_1) & \cos(\theta_1) \end{pmatrix} \quad (2.29)$$

Similarly, a rotation of θ_2 radians about the y-axis is defined as

$$R_y = \begin{pmatrix} \cos(\theta_2) & 0 & \sin(\theta_2) \\ 0 & 1 & 0 \\ -\sin(\theta_2) & 0 & \cos(\theta_2) \end{pmatrix} \quad (2.30)$$

Finally, a rotation of θ_3 radians about the z-axis is defined as

$$R_z = \begin{pmatrix} \cos(\theta_3) & -\sin(\theta_3) & 0 \\ \sin(\theta_3) & \cos(\theta_3) & 0 \\ 0 & 0 & 1 \end{pmatrix} \quad (2.31)$$

The modified moment of inertia from the old coordinates to the new ones becomes

$$I'_0 = R^T \cdot I_0 \cdot R = R^T \cdot \begin{pmatrix} I_{xx} & 0 & 0 \\ 0 & I_{yy} & 0 \\ 0 & 0 & I_{zz} \end{pmatrix} \cdot R \quad (2.32)$$

In our case the rotation axis is one of the axes of the coordinates system:

$$\hat{n} = \begin{pmatrix} 1 \\ 0 \\ 0 \end{pmatrix}; \hat{n} = \begin{pmatrix} 0 \\ 1 \\ 0 \end{pmatrix}; \hat{n} = \begin{pmatrix} 0 \\ 0 \\ 1 \end{pmatrix} \quad (2.33)$$

$$I = \hat{n}^T \cdot I'_0 \cdot \hat{n} \quad (2.34)$$

A comparison between Direction cosine and Euler angles in order to define the same spatial rotation is depicted in [Figure 2.8](#)

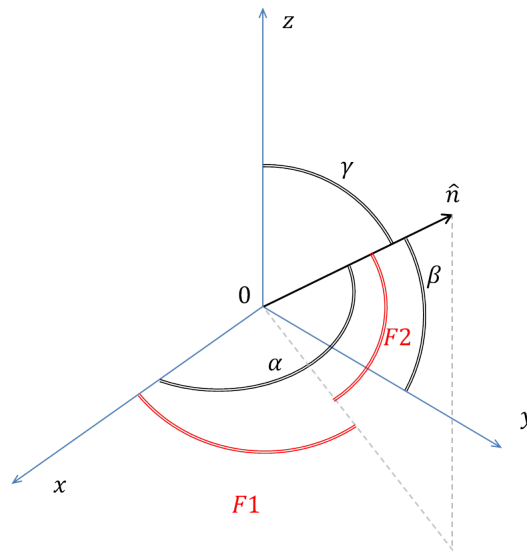


Figure 2.8: Comparison between Direction cosine and Euler angles

If there is translation component:

$$I = \hat{n}^T \cdot I_0 \cdot \hat{n} - m \cdot \tilde{\Omega} \cdot \tilde{\Omega} \tag{2.35}$$

$$\tilde{\Omega} = \begin{pmatrix} 0 & -\Omega_z & \Omega_y \\ \Omega_z & 0 & -\Omega_x \\ -\Omega_y & \Omega_x & 0 \end{pmatrix} \tag{2.36}$$

$\tilde{\Omega}$ =component of the vector that provides the starting point and the end point are the centre of mass (Figure 2.9).

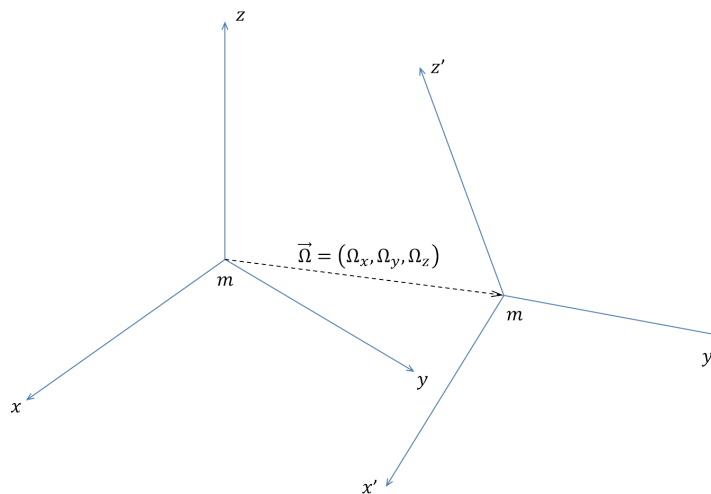


Figure 2.9: Translation

Lateral rollover (2D-3D)

The geometry of the tractor is provided considering the dimensions of the tractor 3D model (Figure 2.10 and Table 2.2).

$$W_F = \frac{V_F + RR_F}{2} \quad (2.37)$$

$$W_R = \frac{V_R + RR_R}{2} \quad (2.38)$$

$$F_1 = \arctan\left(\frac{W_R - W_F}{L}\right) \quad (2.39)$$

$$F_2 = \arctan\left(\frac{\left(\frac{RR - R_F}{L}\right)}{1 - \left(\frac{RR - R_F}{2L}\right)^2}\right) \quad (2.40)$$

$$K = R_R(1 + \cos(F_2)) + (L_F + R_F \cdot \sin(F_2)) \cdot \tan(F_2) \quad (2.41)$$

$$W = W_F + (W_R - W_F) \cdot \frac{L_F}{L} \quad (2.42)$$

Table 2.2: Dimensions of the 3D model of tractor

Notation	
H_{cm}	Height of cm
L	Wheelbase
L_F	Horizontal distance cm-front axle
L_R	Horizontal distance cm-rear axle
RR_F	Width front tire
RR_R	Width rear tire
R_F	Front radius tire
R_R	Rear radius tire
V_F	Front wheeltrack
V_R	Rear wheeltrack

According to the equations described in section "Moment of inertia" it was possible to define the new moments of inertia in two different modalities for each rotation.

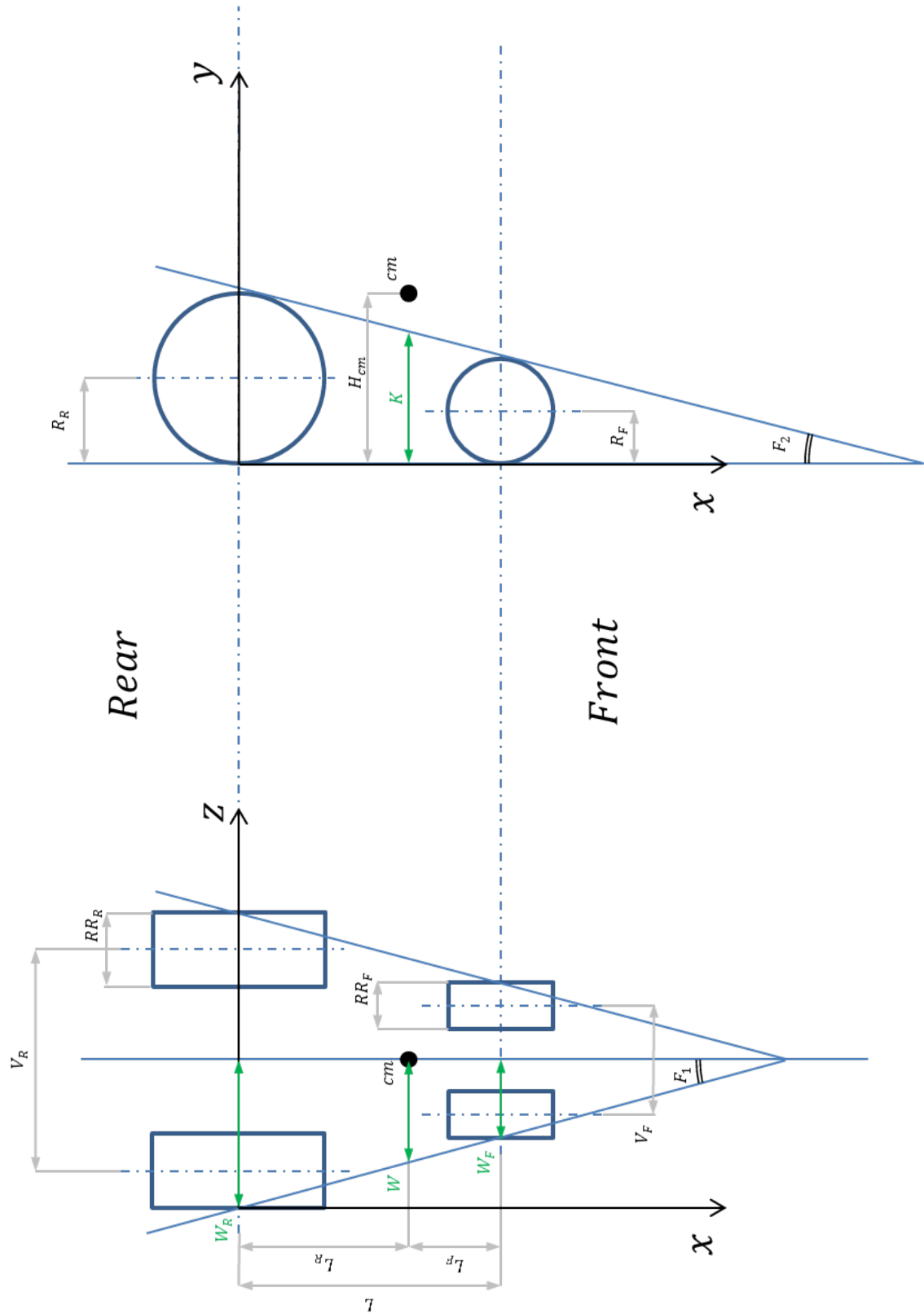


Figure 2.10: 3D Tractor

1. The matrix referred to the new axis of rotation

$$\hat{n} = \begin{pmatrix} A \\ B \\ C \end{pmatrix} = \begin{pmatrix} \cos(\alpha) \\ \cos(\beta) \\ \cos(\gamma) \end{pmatrix} = \begin{pmatrix} \sin(F_1) \cos(F_2) \\ \sin(F_2) \\ \cos(F_1) \cos(F_2) \end{pmatrix} \quad (2.43)$$

$$I = \hat{n}^T \cdot I_0 \cdot \hat{n} \quad (2.44)$$

2. Rotation of the matrix according to the axis of rotation

$$R = R_y(F_1) \cdot R_z(F_2) \quad (2.45)$$

$$I'_0 = R^T \cdot I_0 \cdot R \quad (2.46)$$

$$\hat{n}' = \begin{pmatrix} 0 \\ 0 \\ 1 \end{pmatrix} \quad (2.47)$$

$$I = \hat{n}'^T \cdot I'_0 \cdot \hat{n}' \quad (2.48)$$

Moment of inertia along the axis tangent to the *bottom* of the *rear tyre* and to the *bottom* of the *front tyre*:

$$\begin{cases} I_{cm_{F_1}} = I_{xx} \cdot \sin^2(F_1) + I_{zz} \cdot \cos^2(F_1) \\ d_{F_1} = \sqrt{W^2 + H_{cm}^2} \end{cases} \\ \Rightarrow I = I_{cm_{F_1}} + m \cdot d_{F_1}^2 \quad (2.49)$$

Moment of inertia along the axis tangent to the *top* of the *rear tyre* and to the *top* of the *front tyre*:

$$\begin{cases} I_{cm_{F_1 F_2}} = I_{xx} \cdot \sin^2(F_1) \cos^2(F_2) + I_{yy} \cdot \sin^2(F_2) + I_{zz} \cdot \cos^2(F_1) \cos^2(F_2) \\ d_{F_1 F_2} = \sqrt{W^2 + (H_{cm} - K)^2} \end{cases} \\ \Rightarrow I = I_{cm_{(F_1 \rightarrow F_2)}} + m \cdot d_{F_1 F_2}^2 \quad (2.50)$$

If $F_1 = 0$ (minimum overall width of the rear axles of the tractor equal to the one of the front axles)

$$\Rightarrow I_{cm_{F_2}} = I_{yy} \cdot \sin^2(F_2) + I_{zz} \cdot \cos^2(F_2) \quad (2.51)$$

When there is a change of axis and ω is not null:

$$\omega_{new} = \omega_{old} \cdot \cos(\gamma) \quad (2.52)$$

Where γ is the angle between the two axes

The angle of slope ground changes depending on the axis of rotation (Figure 2.11):

$$\alpha' = \arctan \left(\frac{\tan(\alpha)}{\sqrt{1 + \left(\frac{\tan(F_1)}{\cos(\alpha)}\right)^2}} \right) \quad (2.53)$$

$$\alpha'' = \arctan \left(\frac{\tan(\alpha')}{\sqrt{1 + \left(\frac{\tan(F_2)}{\cos(\alpha')}\right)^2}} \right) \quad (2.54)$$

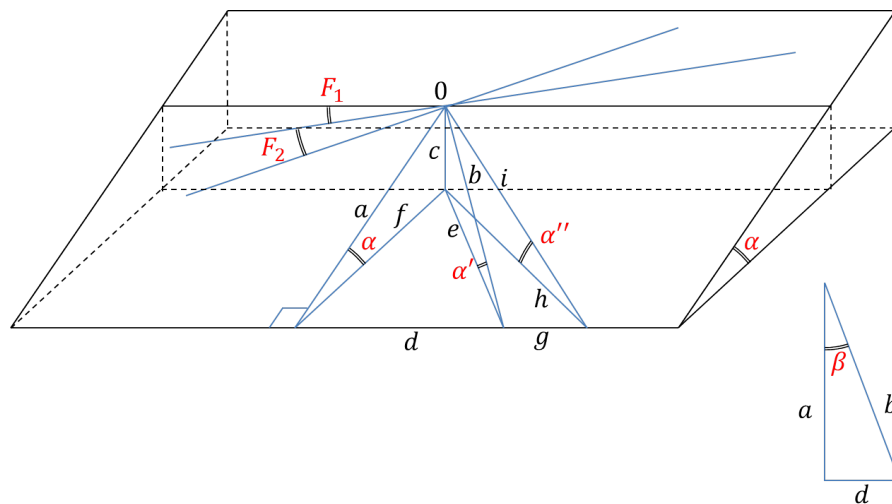


Figure 2.11: Sloping of the ground

Impact points for cab (2D-3D)

When the ROPS is a cab shape two impact points are predictable. The distances of the two points of impact are shown in [Figure 2.12](#). The coordinates of the centre of mass are: $cm = (x_{cm}, y_{cm}, z_{cm})$.

$$a = \tan(F_1) \cdot x_2 \quad (2.55)$$

$$b = \tan(F_1) \cdot (x_1 - x_2) \quad (2.56)$$

$$c = \cos(F_2) \cdot (z_2 - a) \quad (2.57)$$

$$d = \cos(F_2) \cdot (z_1 - a - b) \quad (2.58)$$

$$ff = (\tan(F_2) \cdot (L - x_2) + 2 \cdot R_F) \quad (2.59)$$

$$gg = (\tan(F_2) \cdot (L - x_1) + 2 \cdot R_F) \quad (2.60)$$

$$f = \cos(F_2) \cdot (y_2 - ff) \quad (2.61)$$

$$g = \cos(F_2) \cdot (y_1 - gg) \quad (2.62)$$

Where x_1, y_1, z_1 are the front impact point coordinates and x_2, y_2, z_2 are the rear impact point coordinates.

On the basis of these dimensions it is possible to know the first point of impact by analysing the angle formed by the plane created by the wheels and the points of impact relative to the axis of rotation. The point of impact which gives the smaller θ value will be the actual point of impact. After the impact it is interesting to know whether the tractor continues rolling along the axis formed by the point of impact and the rear tyre or front tyre. This is evaluable analysing the position of the centre of mass. Using the same notation for both the front or rear points it is as follow.

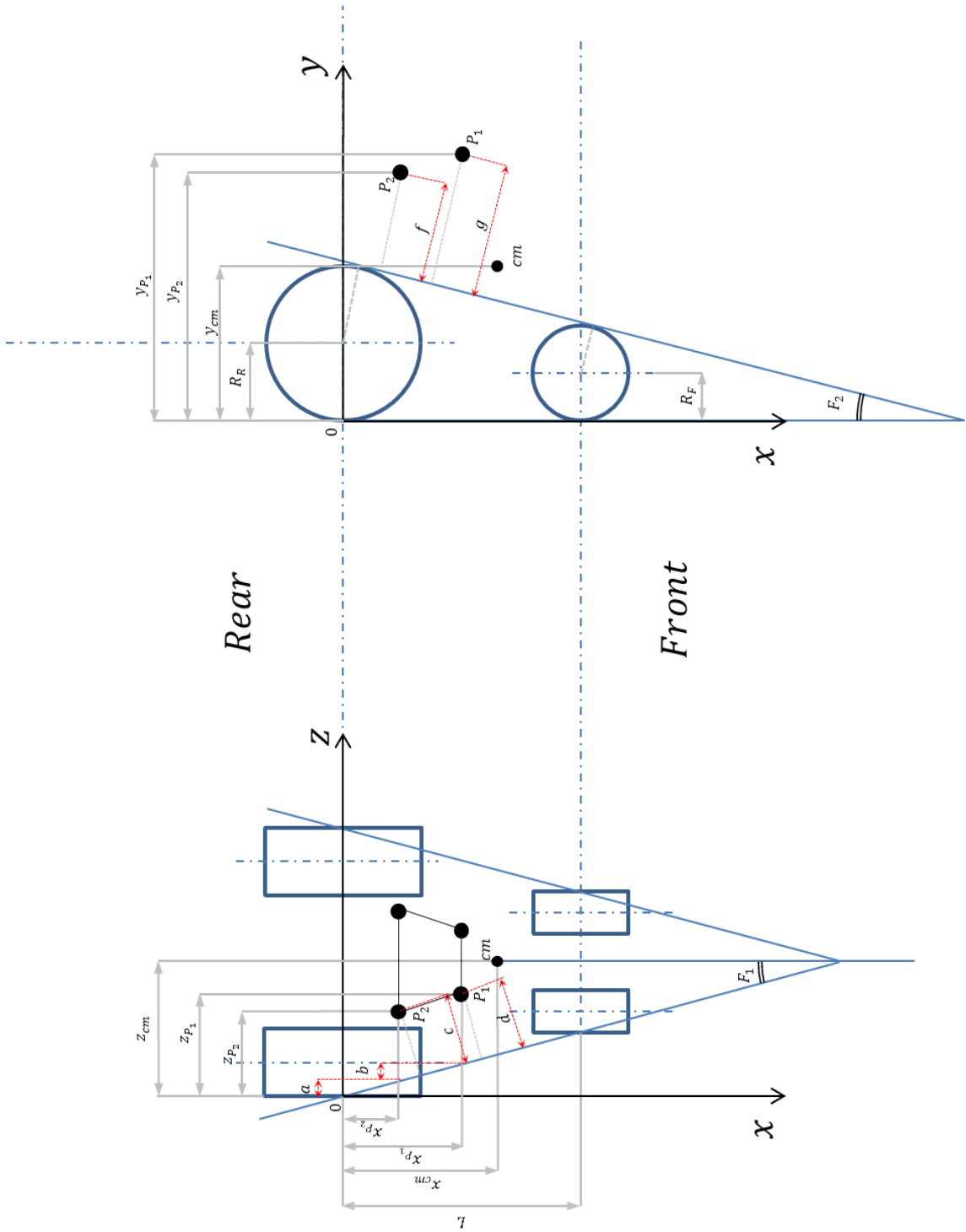


Figure 2.12: Predictable impact points of tractor cab

Front impact point:

if $\arctan\left(\frac{d}{g}\right) < \arctan\left(\frac{c}{f}\right)$;

$$\theta_3 = \arctan\left(\frac{d}{g}\right) \quad (2.63)$$

$$x_{imp} = x_1 \quad (2.64)$$

$$y_{imp} = y_1 \quad (2.65)$$

$$z_{imp} = z_1 \quad (2.66)$$

Rear impact point:

if $\arctan\left(\frac{d}{g}\right) > \arctan\left(\frac{c}{f}\right)$;

$$\theta_3 = \arctan\left(\frac{c}{f}\right) \quad (2.67)$$

$$x_{imp} = x_2 \quad (2.68)$$

$$y_{imp} = y_2 \quad (2.69)$$

$$z_{imp} = z_2 \quad (2.70)$$

The point of impact is identified as \mathbf{P} . After the impact, the tractor rotates about an axis passing through the point \mathbf{P} and tangent to a tyre. The following relations defines if the rotation occurs around the front tyre or the rear tyre ([Figure 2.13](#)).

$$\begin{cases} \gamma = z_{imp} \cdot \tan(F_1) \\ A = (x_{imp} + \gamma) \cdot \cos(F_1) \end{cases} \quad (2.71)$$

$$\begin{cases} \varphi = z_{cm} \cdot \tan(F_1) \\ CM_A = (x_{cm} + \psi) \cdot \cos(F_1) \end{cases} \quad (2.72)$$

$$\begin{cases} \rho = (y_{imp} - R_R) \cdot \tan(F_2) \\ B = (A - \rho) \cdot \cos(F_2) \end{cases} \quad (2.73)$$

$$\begin{cases} \psi = (y_{cm} - R_R) \cdot \tan(F_2) \\ CM_B = (CM_A - \psi) \cdot \cos(F_2) \end{cases} \quad (2.74)$$

If $CM_B > B$ the axis of rotation is about the *front tyre*, else the axis of rotation is about the *rear tyre*.

Chapter 3

Preliminary tests

3.1 Introduction

The aim of preliminary tests was to define the tractor instrumentation and to calibrate the instruments used in the actual upset test. Preliminarily a simple beam was tested, suitably instrumented and subjected to the procedure of static load and dynamic impact. Instruments used for control, measurement and data acquisition are shown in [Figure 3.1](#) and the specifications are in [Table 3.1](#). Sensors represented by dynamic load cell and linear displacement transducers were used to acquire signals of force and deflection. The output signals from the sensors (Volt) were sent to Voltage input module included in the Data acquisition system (DAQ - National Instruments) for signal conditioning and to Analog-to-Digital converter. A Computer connected allowed to process data with dedicated software (LabView). The force signal was amplified before the DAQ by means of a charge amplifier (Kistler). In addition to this instrumentation, high speed camera recorded the event to better understand the dynamic phases.

Three instrumented beams, with the same dimensions and technical specifications, were submitted to strength tests ([Table 3.2](#)). In [Figure 3.2](#) the image of profile beam used. The first beam was subjected to a static test with a hydraulic cylinder loading almost "statically" the beam, the other two beams were subjected to dynamic tests using a sphere of 45 kg mass which impacted the beam at two different velocities. The tests allowed to understand the influence of strain rate with

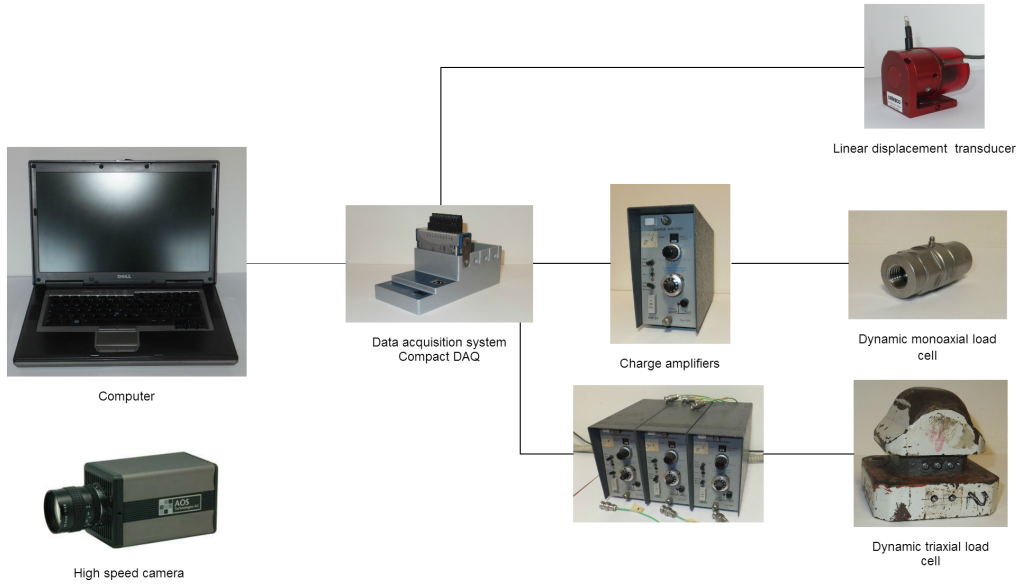


Figure 3.1: Data acquisition system

Table 3.1: Control, measurement and data acquisition system components of the preliminary tests

Quantity	Instrument	Purpose	Specifications
1	Monoaxial dynamic load cell (Kistler)	1 component of force	Range $F \pm 40$ kN
1	Triaxial dynamic load cell (Kistler)	3 perpendicular components of force	Range $F_x \pm 40$ kN; $F_y, F_z \pm 20$ kN
1	Linear displacement transducer (Celesco)	Linear displacement	Range 360 mm, Max cable acc. 136 g
1	NI cDAQ-9184 (National Instruments)	Data acquisition system	DC Input alimentation 12 V
1	NI 9215 (National Instruments)	Voltage input module	Range ± 10 V
1	Charge amplifier Type 5007 (Kistler)	Voltage input	AC Input alimentation 220 V
1	High speed camera (AOS)	Event video recording	Range 1000 frames/s

Table 3.2: Tested beam specification

UPN 80 beam (ISO 5680-73)	
Nominal dimensions	
Height	$h = 80$ mm
Thickness _h	$a = 6$ mm
Base	$b = 45$ mm
Thickness _b	$e = 8$ mm
Radius	$r = 8$ mm
Moment of Inertia	$I_{yy} = 194\,000$ mm ⁴
Elastic modulus _{Fe360}	$E = 190\,000$ N/mm ²
Length	$l = 1500$ mm

respect to the deflection of the beam structure.



Figure 3.2: Beam profile

It was decided to carry out strength tests on a simply cantilever beam in order to better explain and evaluate the behavior. By applying the elastic theory was possible to formulate theoretical considerations on the deflection, the stiffness of the beam and the strain energy. These theoretical results were compared to the experimental data recorded during the tests. In [Figure 3.3](#) the instrumented beam in the static test is shown. This approach allowed to analyze the behavior in case of plasticization of the structure, not considered by the elastic theory.



Figure 3.3: Instrumented beam

Experimental results compared to the theoretical data are proposed. Main relations considered are reported in Annex 2.

3.2 Static tests

The beam was subjected to very slow increasing load applied by means of a hydraulic cylinder (Figure 3.4). The rate of load application (0.004 m/s) was so low that it can be considered static. In Figure 3.5 is shown the behaviour of the beam: a first elastic deflection till 84 mm then the slope of the curve changes due to the change of behavior from elastic to plastic. At 104 mm load was released and there was an springback. Be noted that the residual deflection is 20 mm approximately equal to the deflection in the plastic range.

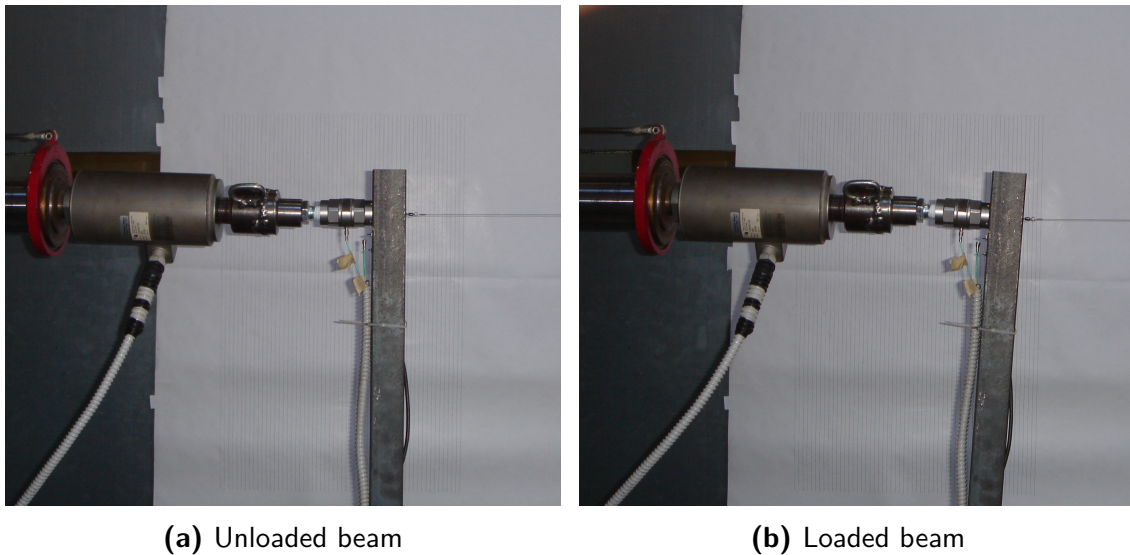


Figure 3.4: Static loading

Linearly interpolating in the elastic range (the blue line in Figure 3.6) is possible to derive the relationship between the force and deflection. The coefficient of proportionality between the force and the deformation is the bending stiffness in the elastic range. Similarly way it is possible to derive the bending stiffness interpolating the strain energy obtained considering the integration of the force applied on the deformation. The coefficient of proportionality between the energy and the square term of the deflection is half of the bending stiffness. The equations which allowed to obtain the strain energy (U) are as follow. The terms of the equations are defined in Table 3.3.

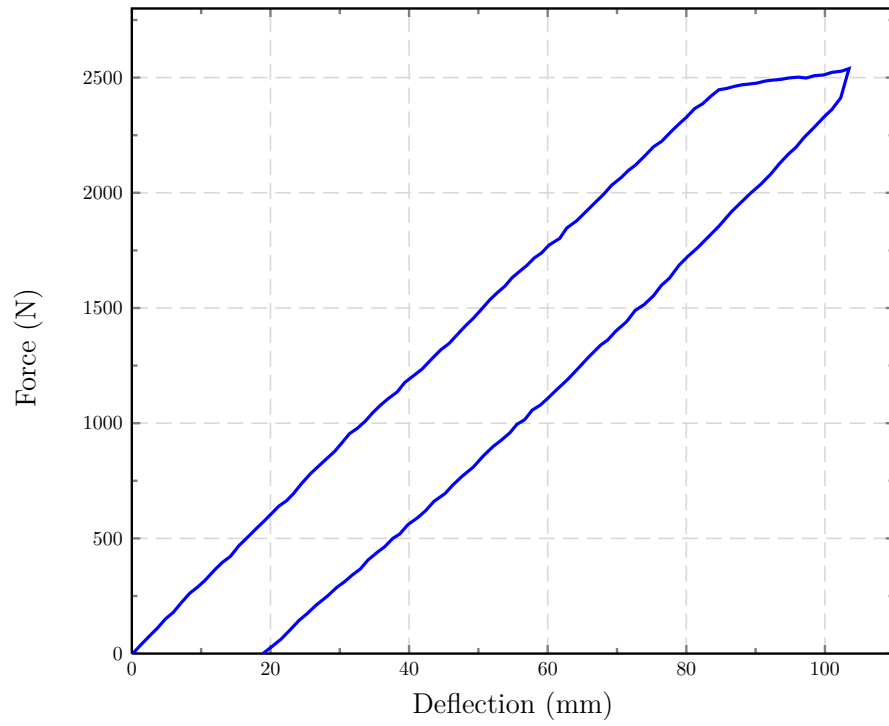


Figure 3.5: Elasto-plastic behaviour of the beam

$$dU = F(\delta) d\delta \quad (3.1)$$

$$U = \int_{\delta_1}^{\delta_2} F(\delta) d\delta = \lim_{n \rightarrow \infty} \sum_{i=1}^n [F_i (\delta_i - \delta_{i-1})] \quad (3.2)$$

$$\underbrace{\sum_{i=1}^n}_{f_s \uparrow \uparrow} [F_i (\delta_i - \delta_{i-1})]$$

Table 3.3: Data acquisition

Data acquisition	
n	Sampled data (number sampled data signal)
Δt	Sampled period (the time step between two adjacent sampled data)
$f_s = \frac{1}{\Delta t}$	Sampling rate
$T = (n - 1) \Delta t = [t_1, t_n]$	Acquisition time (data record length)
$F = f(t)$	Force in time
$\delta = g(t)$	Deflection in time
$F_1 = F(t_1); \delta_1 = \delta(t_1)$	First sampled acquisition data
$F_n = F(t_n); \delta_n = \delta(t_n)$	Last sampled acquisition data

The values of the the bending stiffness of the beam obtained by interpolating the acquired data (Figure 3.6) and the theoretical analysis of the bending stiffness for a cantilever beam was computed.

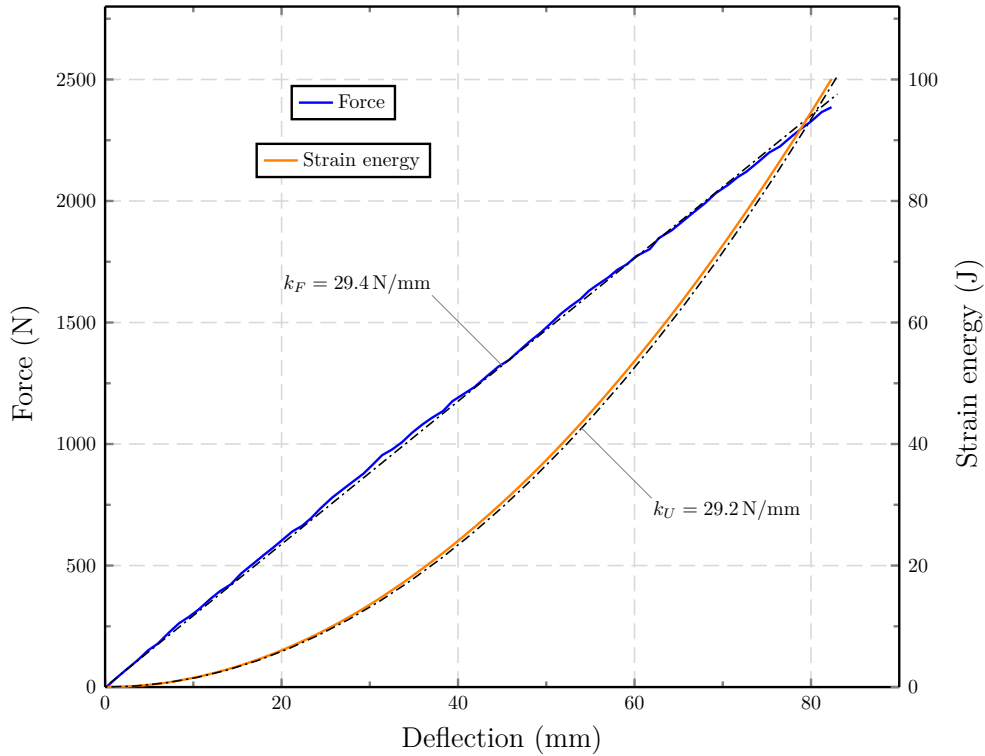


Figure 3.6: Elastic behaviour of the tested beam

$$\text{Theoretical: } k_{\text{theoretical}} = \frac{3 \cdot E \cdot I}{l^3} = 32.7 \text{ N/mm} \quad (3.3)$$

$$\text{Actual: } \begin{cases} F = k_F \delta \Rightarrow k_F = 29.4 \text{ N/mm} \\ U = \frac{1}{2} k_U \delta^2 \Rightarrow k_U = 29.2 \text{ N/mm} \end{cases} \quad (3.4)$$

The difference between the measured and theoretical bending stiffness can be justified by the fact that there are errors on the measurement systems and on the fixing of the beam. In the elastic range, the bending stiffness of a structure can be obtained by knowing the applied load or the strain energy absorbed and the relative deflection. The approach was a similar consideration in the plastic range. The elastic theory is not applicable, no small swings, the structure tends to be softer and there is no a linear relationship between strength and deflection. It is not possible to derive

a kind of stiffness of the structure by linearly interpolating force and deflection. An interpolation which approximates the curve has to use a polynomial of order, higher than the order fourth. In the case of the deformation energy is good curve fitting is a polynomial of order two, as in the elastic case. The coefficient between energy and the square of the deflection is called "bending stiffness equivalent" and, in addition to give an indication of the stiffness, it can be useful in the comparison of different structures or frames subjected to strength tests, as the cases of ROPS strength tests. The bending stiffness equivalent calculated on the basis of the strain energy absorbed by the beam (Figure 3.7), equation (3.5), is less than the elastic stiffness of about 5%.

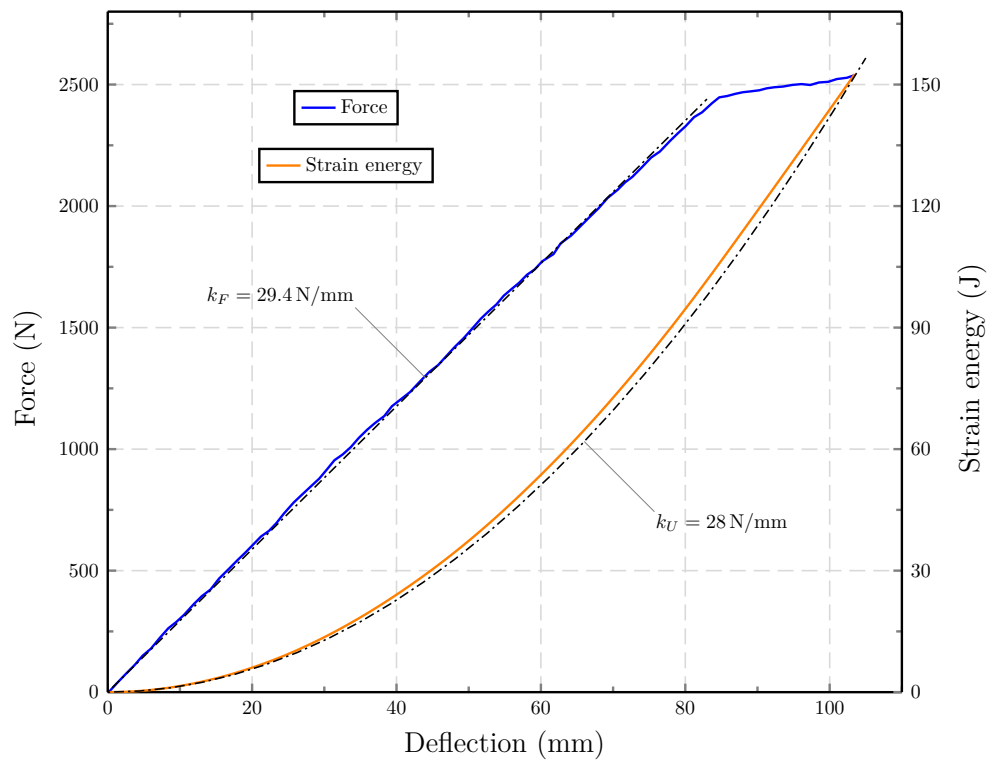


Figure 3.7: Elasto-plastic behaviour of the tested beam

$$k_{eq} = 28 \text{ N/mm} \quad (U = 152.5 \text{ J}) \quad (3.5)$$

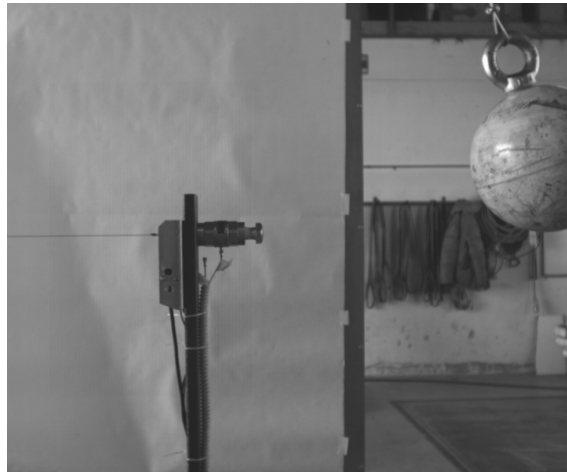
3.3 Dynamic tests

The dynamic tests were performed on the beam instrumented as in the static test. Two tests with different energy levels were carried out, in order to analyze the influence of the impact velocity on the deflection. Then the results were compared with those of the static test. The approach was an impact loading: a sphere (Table 3.4) impacted against the beam from two drop heights (h). The height of the sphere with respect to the point of impact allows to evaluate the initial potential energy (mgh), and produces a variation on the impact velocity (v) leading to a transformation into kinetic energy ($\frac{1}{2}mv^2$). The sphere after the impact decreased progressively the velocity due to the contact with the beam, transferring energy and causing the deflection of the beam (Table 3.4).

Table 3.4: Dynamic test notation

Sphere used against cantilever beam	
	<i>Nominal dimensions</i>
	<i>Mass</i> $m = 45 \text{ kg}$
	<i>Diameter</i> $\phi = 0.22 \text{ m}$
	<i>Height</i> $h = 0.20 \text{ m}$
	<i>Height</i> $h = 0.30 \text{ m}$
<i>Gravitational acceleration</i> $g = 9.80665 \text{ m/s}^2$	

In analysing the data the approach was to divide the impact event in three phases (Figure 3.8). On the basis of the conservation of energy, the amount of initial potential energy (PE) is transformed into kinetic energy (KE) of the sphere. At the impact time the sphere deforms the beam and decelerates till stop. The kinetic energy is transferred to the beam as strain energy (U). The strain energy of the beam can be considered as a potential energy which increases the energy level of the beam. The energy absorbed produces a deflection of the structure. If the structure is able to release this energy, this will be "elastic energy", but if the structure will not be able to release all the energy absorbed part of the energy will change the physical properties of the structure.



(a) Phase 1: Before impact



(b) Phase 2: Impact



(c) Phase 3: Impact end

Figure 3.8: Dynamic impact phases

In the impact event three phases have been considered.

1. Sphere before the free fall ($v = 0$)
2. Sphere impacts the beam ($v \neq 0$)
3. Impact end, corresponding to the maximum deflection of the beam ($v = 0$)

$$E_{tot} = PE + KE + U = const. \quad (3.6)$$

Phase 1 : $E_{tot} = PE$

The two impact tests were carried out at two different fall heights of the sphere: $h = 0.20$ m and $h = 0.30$ m corresponding to two different potential energy values (Table 3.5).

Table 3.5: Potential energy

	$PE = m \cdot g \cdot h$
$h = 0.20$ m	88.3 J
$h = 0.30$ m	132.5 J

Phase 2 : $KE = PE$

The two theoretical impact velocity of the sphere were analysed using the theory of the conservation of energy (Table 3.6).

$$\frac{1}{2} m v_t^2 = m g h \Rightarrow v_t = \sqrt{2 g h} \quad (3.7)$$

Table 3.6: Teoretical impact velocity

	$v_t = \sqrt{2 g h}$
$h = 0.20$ m	1.981 m/s
$h = 0.30$ m	2.426 m/s

Phase 3 : $E_{tot} = U$

The integration of the impact force measured by the load cell (blue data in Figure 3.9) and the deflection measured by the displacement transducer (green data in Figure 3.9) (3.2) is depicted in Figure 3.10. The strain energy is shown in Table 3.7 for the two heights.

Table 3.7: Strain energy

	$U = \sum_i F_i \Delta\delta_i$
$h = 0.20 \text{ m}$	91.1 J
$h = 0.30 \text{ m}$	130.1 J

The strain energies (Phase 3) are different if compared to the energy values considered in the previous two phases. Friction and air resistance are factors that greatly affect the energy transferred. It is possible to evaluate the energy lost in Phase 3 by measuring the actual impact velocity of the sphere on the beam. Using the high speed camera it was possible to measure the velocity and compare it with the theoretical one. Considering a loss on the impact velocity (it is estimated that a loss of 3% is due to the friction losses of the pendulum, including air resistance) and by introducing a coefficient that takes into account losses during the fall (Ψ) it is possible to redefine the actual velocity v_a (3.8). Table 3.8 shows the results obtained. The energy at the impact time is shown in Table 3.9.

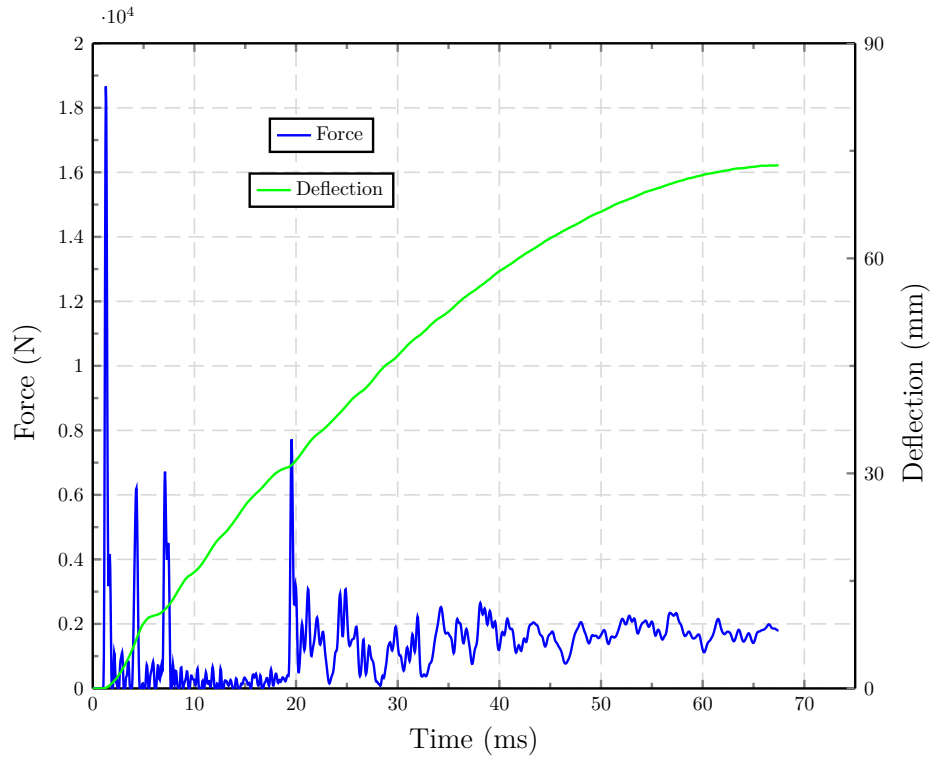
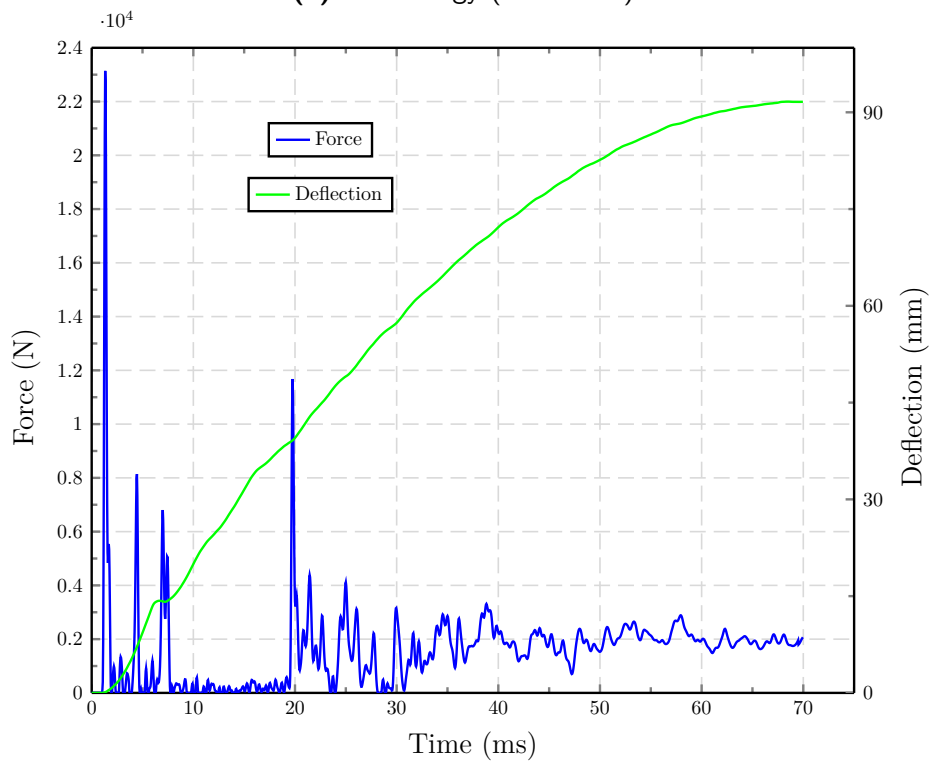
Table 3.8: Differences between teoretical and actual velocity

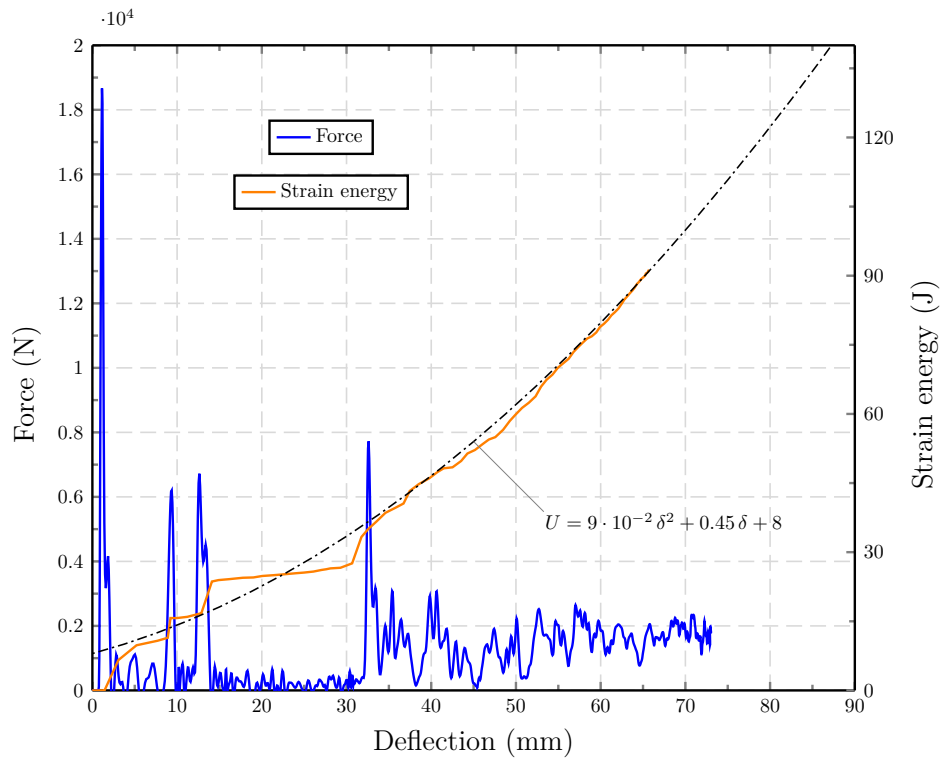
	$v_t = \sqrt{2gh}$	v_a	$1 - \Psi$ factor
$h = 0.20 \text{ m}$	1.981 m/s	1.911 m/s	3.5%
$h = 0.30 \text{ m}$	2.426 m/s	2.362 m/s	2.6%

$$\boxed{v_a = \Psi \cdot v_t} = \Psi \cdot \sqrt{2gh} \quad (3.8)$$

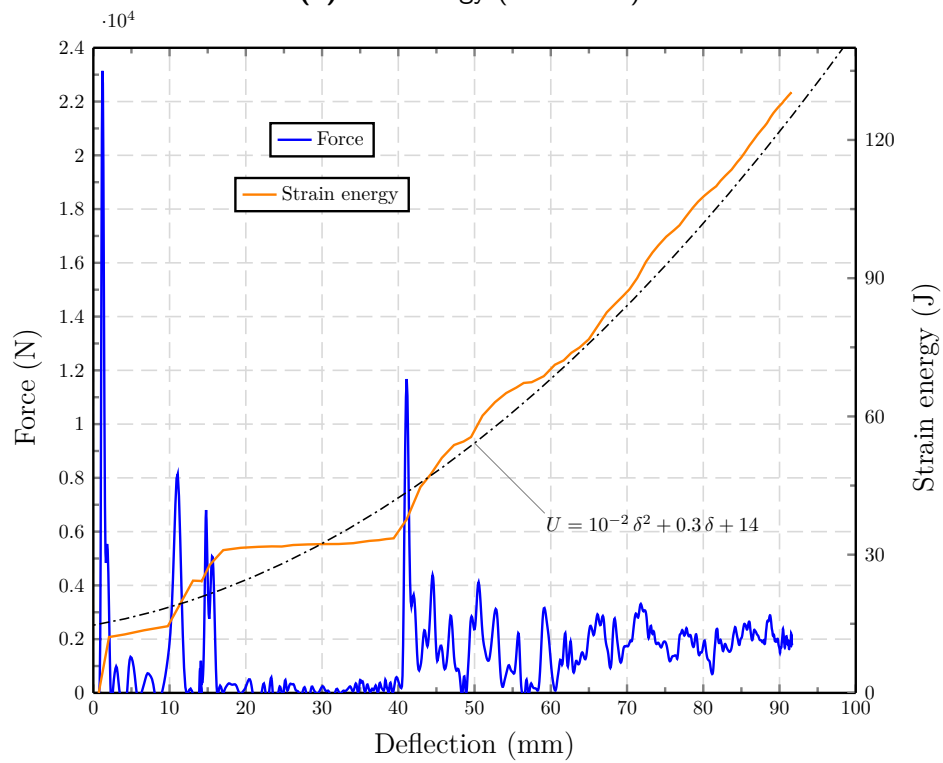
$$KE_t = \frac{1}{2} m v_t^2 \quad \text{teoretical kinetic energy} \quad (3.9)$$

$$KE_a = \frac{1}{2} m v_a^2 = \Psi^2 \cdot \frac{1}{2} m v_t^2 \quad \text{actual kinetic energy} \quad (3.10)$$

(a) Low energy ($h = 0.2$ m)(b) High energy ($h = 0.3$ m)**Figure 3.9:** Force and deflection vs. time



(a) Low energy ($h = 0.2$ m)



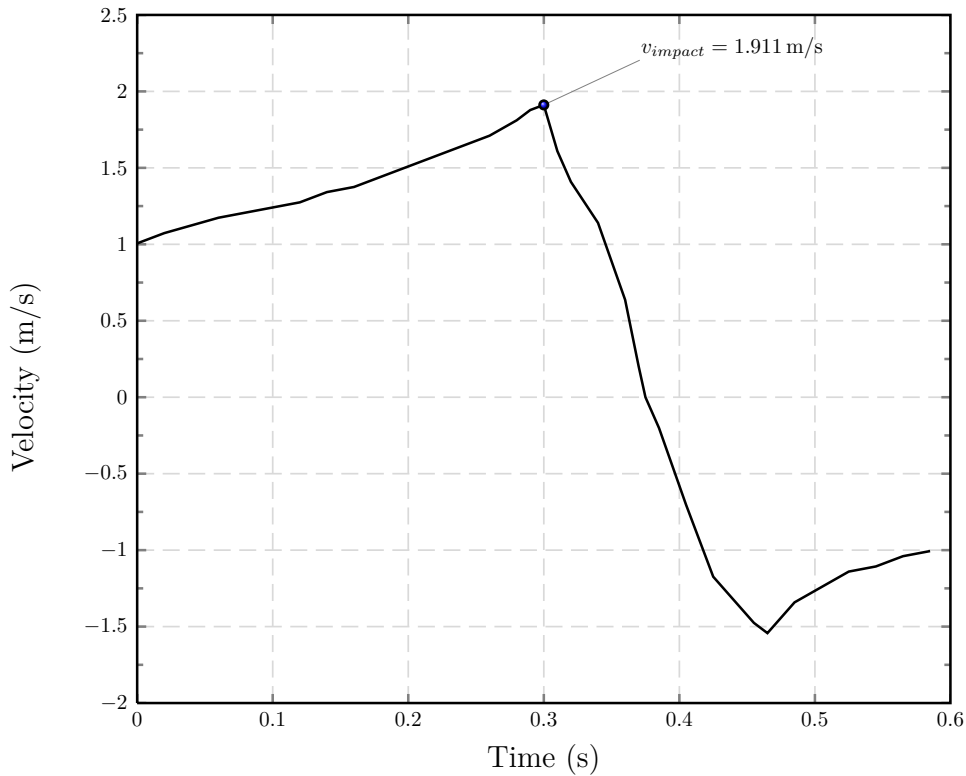
(b) High energy ($h = 0.3$ m)

Figure 3.10: Dynamic deformation

Table 3.9: Differences between teoretical and actual kinetic energy

	$KE_t = \frac{1}{2} m v_t^2$	$KE_a = \frac{1}{2} m v_a^2$	$1 - \Psi^2$
$h = 0.20$ m	88.3 J	82.2 J	6.1%
$h = 0.30$ m	132.5 J	125.7 J	6.8%

In [Figure 3.11](#) is shown the velocity evaluation of the sphere during the impact on the beam. The velocity increases up to the impact and then decreases to zero. When the sphere transferred all its kinetic energy to the beam, the beam returns the stored strain energy to the sphere. The sphere then has a velocity (the negative sign is due to the fact that the direction in which the sphere moves is opposite to the initial one) wich is lower because part of the energy is lost in friction and plastic deformation of the beam.

**Figure 3.11:** Velocity of the sphere during the impact on the beam (case $h = 0.2$ m)

The highest values of strain energy shown in [Table 3.7](#) resulting from the recorded data are due to the fact that during the deflection of the beam there is essentially an addition of potential energy not evaluable in advance because difficult to assess. An

interesting result, however, derives from the evaluation of the energy levels associated to the two heights tested; in fact, in the case $h = 0.3$ m where the impact velocity is increased there is an increase of strain energy lower than in the case $h = 0.2$ m. This is due to the fact that the impact velocity affects the event (Moberg, 1973): the higher velocity affects the impact dynamic producing a considerable energy loss due to friction and heat between the bodies in contact (Table 3.10).

Table 3.10: Differences between kinetic energy and strain energy

	v_a	$KE_a = \frac{1}{2} m v_a^2$	U	ΔE	$+\Delta E\%$
$h = 0.20$ m	1.911 m/s	82.2 J	91.1 J	8.9 J	10.8%
$h = 0.30$ m	2.362 m/s	125.7 J	130.1 J	4.4 J	3.5%

A method to measure the deformation due to a impact mass can be defined for cases of linear elastic deflection (Shigley et al., 2009).

The comparison between the measured deflection and the theoretical one was calculated on the basis of the actual impact velocity and shown in Table 3.11. The main difference is in the case $h = 0.30$ m. This test had a greater plastic deflection.

Table 3.11: Differences between actual and teoretical deflection

	v_a	δ_{max_a}	$\delta_{max_e} = v_a \cdot \sqrt{\frac{m l^3}{3 E I}}$	$\Delta\delta\%$
$h = 0.20$ m	1.911 m/s	0.073 m	0.071 m	2.7%
$h = 0.30$ m	2.362 m/s	0.092 m	0.087 m	5.5%

3.4 Comparison between Dynamic and Static tests

The impact velocity affects the energy absorbed by the structure, the results obtained in the previous section are shown and compared in the figure Figure 3.12. The strain energy in the static test necessary to produce a deflection is lower than the strain energy in the dynamic tests. The dynamic tests are different at different velocity of impact. Increasing the velocity, the strain energy to produce the same deflection must be increased (3.11). On the contrary, the deflection to produce the

same strain energy must be decreased (3.12). The effect of the loading impact is shown in Table 3.12.

Table 3.12: Effect of the loading on the strain energy and deflection

	Deflection δ	Strain energy U	Strain energy U	Deflection δ
Static test	70 mm	72 J	90 J	78 mm
Dynamic test ($h = 0.20$ m)		85 J		73 mm
Dynamic test ($h = 0.30$ m)		87 J		71 mm

$$\delta = \text{const.} : \quad v \uparrow \Rightarrow U \uparrow \quad (3.11)$$

$$U = \text{const.} : \quad v \uparrow \Rightarrow \delta \downarrow \quad (3.12)$$

It should be noted that the impact velocity affects greatly the progress of the strain energy, significantly in the first part, corresponding to an impulsive phenomenon. In the dynamic case, the sphere in the time tends to slow down and move to a phenomenon of a quasi-static so that it shows an additional an energy. In the test carried out the static deflection occurred at a constant velocity of about 0.004 m/s, the dynamic deflection, instead, started with a velocity related to the initial potential energy ($v \cong \sqrt{2gh}$) and stopped at the maximum deflection.

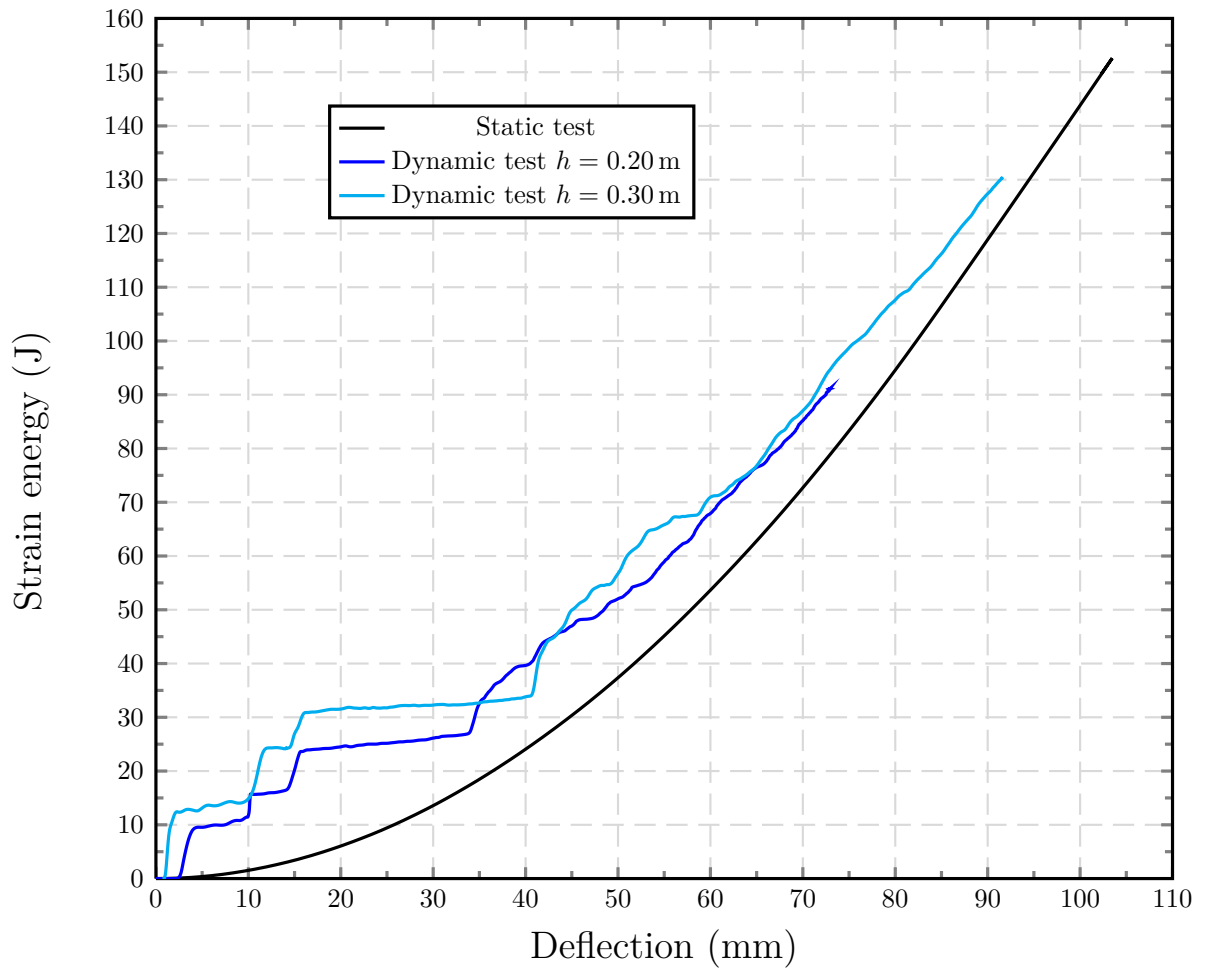


Figure 3.12: Comparison between Dynamic and Static deformation behaviour

Annex 2: Deflection due to bending, strain energy and shock and impact

Deflection due to bending

The problem of bending of beams probably occurs more often than any other loading problem in mechanical design. Shafts, axles, cranks, levers, springs, brackets, and wheels, as well as many other elements, must often be treated as beams in the design and analysis of mechanical structures and systems (Budynas and Nisbett, 2010).

The curvature of a beam subjected to a bending moment M is given by

$$\frac{1}{c} = \frac{M}{EI} \quad (3.13)$$

where c is the radius of curvature. From studies in mathematics the curvature of a plane curve is given by the equation

$$\frac{1}{c} = \frac{d^2y/dx^2}{[1 + (dy/dx)^2]^{3/2}} \quad (3.14)$$

where the interpretation here is that y is the lateral deflection of the centroidal axis of the beam at any point x along its length. The slope of the beam at any point x is

$$\theta = \frac{dy}{dx} \quad (\text{a})$$

For many problems in bending, the slope is very small, and for these the denominator of equation (3.14) can be taken as unity. Equation (3.13) can then be written

$$\frac{M}{EI} = \frac{d^2y}{dx^2} \quad (\text{b})$$

Shear force and bending moment are related by the equation $V = \frac{dM}{dx}$. Sometimes the bending is caused by a distributed load $q(x)$. $q(x)$ is called the load intensity with units of force per unit length and is positive in the positive y direction $\frac{dV}{dx} = \frac{d^2M}{dx^2} = q$. Noting equations above and successively differentiating equation (b) yields

$$\frac{V}{EI} = \frac{d^3y}{dx^3} \quad (\text{c})$$

$$\frac{q}{EI} = \frac{d^4y}{dx^4} \quad (\text{d})$$

It is convenient to display these relations in a group as follows:

$$\frac{q}{EI} = \frac{d^4y}{dx^4} \quad (3.15)$$

$$\frac{V}{EI} = \frac{d^3y}{dx^3} \quad (3.16)$$

$$\frac{M}{EI} = \frac{d^2y}{dx^2} \quad (3.17)$$

$$\theta = \frac{dy}{dx} \quad (3.18)$$

$$y = f(x) \quad (3.19)$$

Strain energy

The external work done on an elastic member in deforming it is transformed into strain, or potential, energy. If the member is deformed to distance y , and if

the force-deflection relationship is linear, this energy is equal to the product of the average force and the deflection (Figure 3.13), or

$$U = \frac{F}{2}y = \frac{F^2}{2k} \quad (3.20)$$

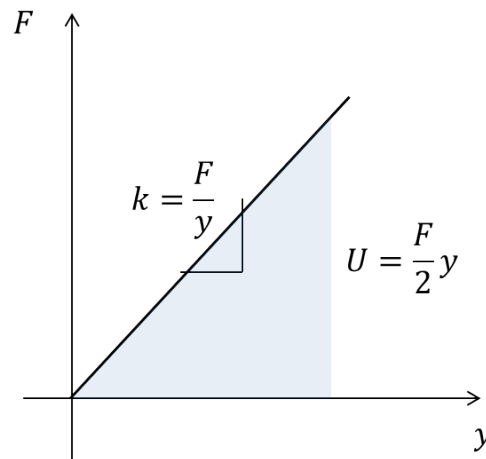


Figure 3.13: Force-deflection linear relationship

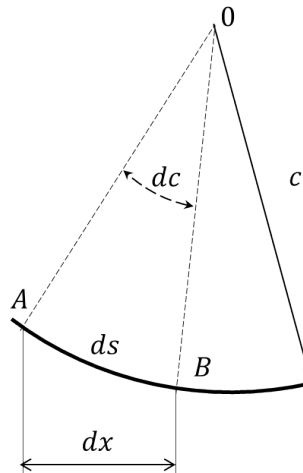


Figure 3.14: Beam bending element

This equation is general in the sense that the force F can also mean torque, or moment, provided, of course, that consistent units are used for k . By substituting appropriate expressions for k , strain-energy formulas for various simple loadings may be obtained. The strain energy stored in a beam or lever by bending may be

obtained by referring to [Figure 3.14](#). Here AB is a section of the elastic curve of length ds having a radius of curvature c . The strain energy stored in this element of the beam is $dU = (M/2)d\theta$.

Since $\rho d\theta = ds$, we have

$$dU = \frac{M ds}{2c}$$

We can eliminate c by using equation [\(3.13\)](#), $c = EI/M$. Thus

$$dU = \frac{M^2 ds}{2EI}$$

For small deflections, $ds \doteq dx$. Then, for the entire beam

$$U = \int dU = \int \frac{M^2}{2EI} dx \tag{3.21}$$

Cantilever beam with an end load

A cantilever beam with a U cross section has a concentrated load F at the end, as shown in [Figure 3.15](#). How to determine the deflection equation and the strain energy for the beam under the load F was described by [Cesari \(1994\)](#).

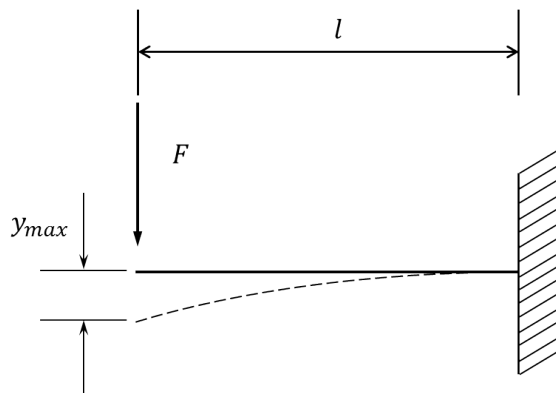


Figure 3.15: Cantilever beam with a U cross section and a concentrated load F

The differential equation of equilibrium in the transverse displacement y is given by:

$$\frac{d^4 y}{dx^4} = 0 \quad \text{no distributed load } q(x) \quad (3.22)$$

$$(3.23)$$

Integrating with the conditions:

$$\left. \begin{array}{l} \frac{d^3 y}{dx^3} = \frac{F}{EI} \\ \frac{d^2 y}{dx^2} = 0 \end{array} \right\} \text{ for } x = 0 \quad (3.24)$$

$$\left. \begin{array}{l} \theta = \frac{dy}{dx} = 0 \\ y = 0 \end{array} \right\} \text{ for } x = l \quad (3.25)$$

It is obtained the elastic deformation of beam:

$$y = \frac{F}{EI} \left(\frac{x^3}{6} - \frac{l^2}{2}x + \frac{l^3}{3} \right) = 0 \quad (3.26)$$

$$(3.27)$$

The system is equivalent to a system with one degree of freedom, as the relationship between the applied load and displacement is the following, at $x = 0$:

$$F = \frac{3EI}{l^3} y = ky \quad (3.28)$$

where k is the translational stiffness

$$k = \frac{3EI}{l^3} \quad (3.29)$$

For the bending, since M is a function of x , equation (3.21) gives:

$$U = \int \frac{M^2}{2EI} dx = \frac{1}{2EI} \int_0^l (Fx)^2 dx = \frac{F^2 l^3}{6EI} \quad (3.30)$$

therefore:

$$U = \frac{k}{2} F^2 \quad (3.31)$$

Shock and Impact: Suddenly Applied Loading

(Shigley et al., 2009)

A simple case of impact is illustrated in Figure 3.16a. Here a mass m impacts a cantilever beam of stiffness EI and length l . We want to find the maximum deflection and the maximum force exerted on the beam due to the impact. Figure 3.16b shows an abstract model of the system considering the beam as a simple spring. For the beam the spring rate was considered to be $k = F/y = 3EI/l^3$ (3.29).

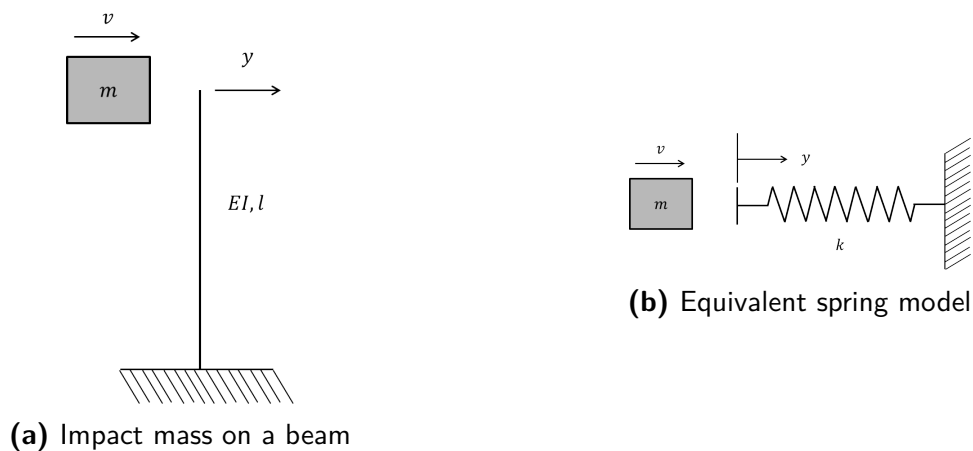


Figure 3.16: Impact model

The beam mass and damping can be accounted for, but in the example they will be considered negligible. If the beam is considered massless, there is no momentum transfer, only energy. The origin of the impact is the instant in which the mass hits the spring. Then at $t = 0$ the initial conditions are $y = 0$ and $\dot{y} = v$. The differential

equation is:

$$m \ddot{x} = -k y \quad (3.32)$$

where the spring force ky is negative, as it is opposite to the displacement y . The solution to this equation is well known and is:

$$y = A \cos \omega t + B \sin \omega t \quad (3.33)$$

where

$$\omega = \sqrt{\frac{k}{m}} \quad (3.34)$$

is the pulsation of the vibration. Considering (3.33) the velocity is

$$\dot{y} = -A\omega \sin \omega t + B\omega \cos \omega t$$

with the initial condition for $t = 0$, $y = 0$ and $\dot{y} = v$, the constant are

$$A = 0 \quad B = v/\omega$$

The solution is valid only until the mass remains in contact with the beam. The maximum deflection is

$$y_{max} = \frac{v}{\omega} = \frac{v}{\sqrt{k/m}} = v \sqrt{\frac{3EI m}{l}} \quad (3.35)$$

Chapter 4

Actual test

4.1 Tested tractor

The lateral upset of a narrow-track isodiametric-wheeled tractor was the experimental evaluation carried out after the preliminary tests. This tractor type was selected because of its specific ROPS configuration: a front ROPS rigidly fixed at the chassis and just one impact point (Figure 4.1). This allowed to simplify the tractor instrumentation and the data acquisition system.

Moreover, this kind of vehicle is often used in sloped fields, increasing the rollover risk. The geometrical and inertial parameters of the tractor were measured and are reported in Table 4.1. The height of the centre of mass (cm) and the moments of inertia (I_x, I_z) were determined using an oscillating platform (Figure 4.2), according to the methods of Casini-Ropa (1976).

4.2 Experimental set-up

In order to acquire data on the force and deflection at impact time, a dynamic triaxial force transducer was mounted on the roll-bar frame close to the vertex of the upper left hand side of the ROPS as this was the most likely point of contact with the ground (Table 4.2). Two linear displacement transducers (Table 4.2) were arranged to measure the 2D plane trajectory of the force transducer. The deflection measured allowed the strain energy absorbed by the ROPS to be calculated. The actual test



Figure 4.1: Tested tractor

Table 4.1: Tractor specifications

Tractor parameter	Value	Unit
Rear tyre size	260/70 R 20 (113 B)	
Front tyre size	260/70 R 20 (113 B)	
Rear radius wheel	0.430	m
Front radius wheel	0.430	m
Rear wheel-track	1.110	m
Front wheel-track	1.110	m
Wheelbase	1.390	m
Horizontal distance cm-rear axle	0.852	m
Horizontal distance cm-rear axle	0.538	m
Height of the centre of mass (cm)	0.600	m
Horizontal distance ROPS impact point-rear axle	1.206	m
Horizontal distance ROPS impact point-rear external wheel	0.140	m
Height of ROPS impact point	2.140	m
Moment of inertia along the Z axis	223.75	kg m ²
Moment of inertia along the X axis	1037.25	kg m ²
Tractor mass	1478	kg



(a) the moment of inertia along the Z axis

(b) the moment of inertia along the X axis

Figure 4.2: Tractor positions to determine the moment of inertia by using on oscillating platform

consisting in the tractor lateral upset was carried out on a concrete ground surface with a slope of 12° .

Table 4.2: Control, measurement and data acquisition system components of the test tractor

Quantity	Instrument	Purpose	Specifications
1	Triaxial dynamic force transducer	3 perpendicular components of force	Range $F_x \pm 40$ kN; $F_y, F_z \pm 20$ kN
2	Linear displacement transducer	Linear displacement	Range 360 mm, Max cable acc. 136 g
1	High speed camera	Event video recording	Range 1000 frames/s

The tractor was tilted laterally, elevating the right wheels with a forklift until the unstable equilibrium position was reached (Figure 4.3). To avoid overly constraining the tractor due to the friction between the tyre-fork interface, a sliding plate was added to the standard fork arrangement. The tyre effectively experienced only a vertical lifting force. The concrete surface was covered with 15 mm thick wood plates in the ROPS impact zone. The lateral rollover was video recorded with the high speed camera (AOS S series camera, 1000 frames/s). A Data Acquisition System and a Computer completed the instrumentation system, as already described in section 3.1.



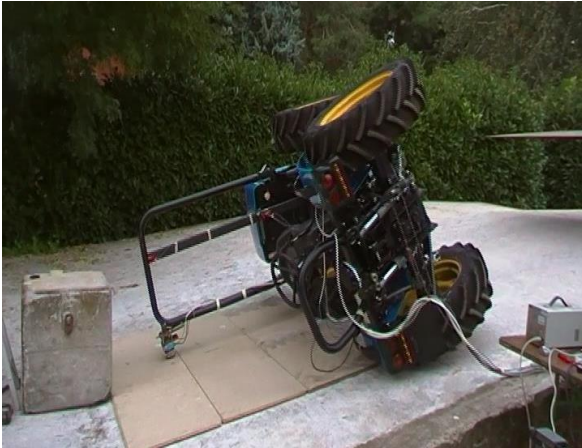
(a)



(b)



(c)



(d)

Figure 4.3: Different phases of the actual experiment

4.3 Experimental results

Analysing the tractor behaviour frame by frame, it was possible to calculate the displacement (4.1), the velocity (4.2) and the angular velocity (4.3) of the centre of mass of the tractor. As a result, the kinetic energy (4.4), assuming the hypothesis of 2D behaviour, could be computed with respect to time.

$$d_{cm}(t_i) = s(t) - s(t_{i-1}) \quad (4.1)$$

$$v_{cm}(t_i) = \frac{s(t) - s(t_{i-1})}{\Delta t} \quad (4.2)$$

$$\omega_{cm}(t) = \frac{v_{cm}(t)}{l_{cm}(t)} \quad (4.3)$$

$$KE(t) = \frac{1}{2} \cdot I_{cm} \cdot \omega_{cm}^2(t) + \frac{1}{2} \cdot m \cdot v_{cm}^2(t) \quad (4.4)$$

In [Figure 4.4](#), the kinetic energy variation of the tractor during lateral rollover is depicted together with the corresponding steps. At the beginning of the rollover, the kinetic energy increased until the tractor wheels touched the ground ($t = 1.45$ s). Subsequently, a first step of energy decrease was recorded which was due to the wheel-ground impact. Subsequently, the energy at the ROPS-ground impact suddenly decreased again (second step) as the ROPS touched the ground and the whole tractor body was subjected to a rollover rotation at the contact point with the ground. In this case, considering the kinetic energy variation depicted in [Figure 4.4](#), it can be calculated that 890 J were dissipated by the tyres while 1095 J were absorbed by the ROPS (second step). The value of the energy to be absorbed is naturally related to the tractor geometry and mass properties but also relies on the amount of energy dissipated in the tyres. The aim was to find the amount of energy absorbed in the second step. Nevertheless, this required the computation of the first step, which involved the development of a tyre impact model.

The following phases could be fixed for the tractor during the lateral upset:

- A. Unstable tractor condition
- B. Free falling rotation of the tractor
- C. Wheel-ground impact
- D. Free falling rotation of the tractor
- E. ROPS-ground impact
- F. Free falling rotation of the tractor

In [Figure 4.4](#), the free falling phases are depicted by images. The black line represents the energy absorbed by the ROPS during phase F, computed using the force and displacement data. The approach used has been already explained in the [Preliminary tests \(chapter 3\)](#).

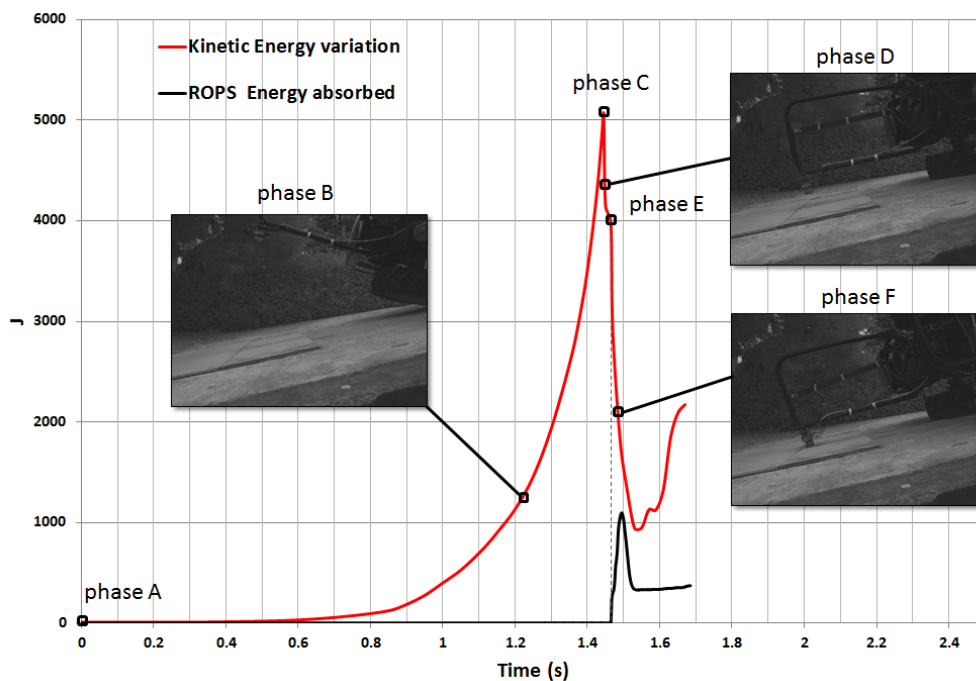


Figure 4.4: Kinetic energy during the actual lateral rollover, and the energy absorbed by the ROPS

Chapter 5

Mathematical Model

5.1 Lateral rollover model

The mathematical model used in the study was based on the general theory of dynamics. Many studies over the years have used the same approach. [Pershing and Yoerger \(1969\)](#) evaluated tractor stability and transient response in the event of interference due to bump; [Davis and Rehkugler \(1974a,b\)](#) and [Rehkugler et al. \(1976\)](#) used a mathematical model to describe the large amplitude motion of a wide-front-end wheel tractor for predicting overturning and handling behaviour in order to verify the external forces and moments applied. [Larson et al. \(1976\)](#) used a similar approach to study the motion of a tricycle-type wheel tractor in three directions to predict sideways overturning and handling behaviour. [Chisholm \(1979a,b,c,d\)](#) studied the overturning of a tractor fitted with a safety frame in a plane normal to the forward direction. [Schwanghart \(1973, 1982\)](#) developed a model analysing different stages during a tractor rollover in order to evaluate the velocity of rotation and the continuous rolling behaviour in a lateral overturning. [Song et al. \(1988\)](#) used a mathematical model for predicting tractor dynamic behaviour on soft ground. The goal was to develop a mathematical model to evaluate the energy to be absorbed by the ROPS in a tractor rollover and especially the kinetic energy variation when the ROPS touched the ground. The complexity of creating a 3D model simulating a rollover aimed at simple predictive uses was considered and therefore an alternative solution, compatible with a standardisation approach based on the consideration

of two independent planar models, one for pure longitudinal overturning and one for pure lateral rollover, was followed. Only a lateral rollover has been detailed, being the most complex to study since the intermediate impact of the tyres deeply influences the energy to be absorbed by the ROPS.

The following assumptions were made in developing the mathematical model representing the tractor lateral rollover:

- > The tractor was considered as a rigid body.
- > The plane of symmetry was the plane passing through the centre of mass and orthogonal to the rear axle.
- > The ground surface was defined as a non-deformable plane.
- > Aerodynamic forces were ignored.
- > Heat loss was ignored,
- > The event of a lateral rollover was subdivided into phases characterised by rotation about a fixed axis alternating with phases in which the axis of rotation shifted in the body-ground impact.
- > Shock absorbers and silent-blocks were ignored.

An inclined plane totally rigid with a constant slope in which the rigid body of the tractor was tilted laterally, as depicted in [Figure 5.1](#), was the computing environment. The tractor was divided into several parts. The geometry and the inertia of the tractor allowed the identification of the base points and angles in order to compute the motion equations. These points and angles are listed in [Table 5.1](#). The geometry of the tractor was characterised by the centre of mass and by the contact points. The different contact points were used to mark the boundary between the tractor and the ground. The tractor-ground contact caused various types of behaviour depending on the contact point in consideration. The various types of behaviour of the tyres and the ROPS at the time of impact with the ground required different theoretical approaches. The objective was to find the evolution of kinetic

energy during the rollover. To estimate the kinetic energy, the variation of the velocity of the tractor (angular and/or linear) based on the dynamic equations of motion (5.1), was considered. The tractor mass and inertia allowed the kinetic energy (5.2) to be calculated. The terms of the equations are defined in Table 5.2.

$$\begin{cases} \vec{F} = \frac{d\vec{p}}{dt} \\ \vec{T} = \frac{d\vec{L}}{dt} \end{cases} \implies \begin{cases} \vec{F} = m \cdot \frac{d(\vec{v}_{cm})}{dt} = m \cdot \vec{g} \\ \vec{T} = \frac{d(I \cdot \vec{\omega})}{dt} = I \cdot \frac{d(\vec{\omega})}{dt} \end{cases} \quad (5.1)$$

$$KE = \frac{1}{2} \cdot I_{cm} \cdot \omega^2 + \frac{1}{2} \cdot m \cdot v_{cm}^2 \quad (5.2)$$

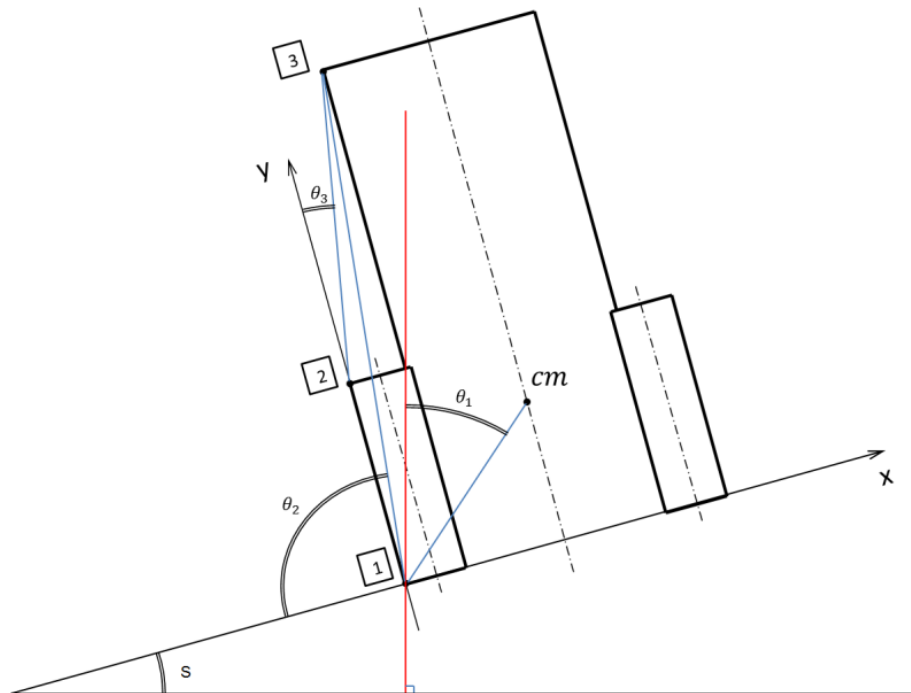


Figure 5.1: The computing environment: tractor and ground with associated points and angles

5.2 Different motion phases

The proposed model was based on the same phases observed during the actual experiment. Analysis of the lateral rollover behaviour was initiated at the static sta-

Table 5.1: Points and angles defined for tractor modelling

CP	Generic contact point
$CP1$	The lower part of the wheels (first centre of rotation)
$CP2$	The upper part of the wheels (second centre of rotation)
$CP3$	ROPS impact (third centre of rotation)
cm	Centre of mass
$Angle_s$	Ground slope
$Angle\Theta_1$	Angle between the cm and the point of unstable equilibrium
$Angle\Theta_2$	Angle between the ROPS point of impact and the ground
$Angle\Theta_3$	Angle between the ROPS point of impact and the y axis

bility limit corresponding to the centre of mass (cm) above the vertical with contact point 1 (Figure 5.1). The model was developed in two dimensions (2D) referring to the plane perpendicular to the forward direction of the tractor. The complete description of the 2D lateral overturning behaviour requires at least three degrees of freedom: two translations and one rotation, namely the different phases considered when the rollover is depicted in Figure 5.2. Reaching an unstable condition, the tractor starts rolling [phase A] and the dynamics of the tractor change. Kinematic and dynamic equations describe the behaviour of the tractor rollover. According to this approach, it was easy to define the different steps constituting the lateral rollover simulation corresponding to the one actually observed in Figure 4.3. The following step considers tractor overturn around contact point 1 [phase B]. When the wheels touch the ground, there is a change in the axis of rotation from contact point 1 to contact point 2 [phase C]. The tractor then rotates around contact point 2 [phase D] until the ROPS impacts the ground at contact point 3 [phase E]. Finally, the tractor rotates around the ROPS [phase F]. The tractor velocity variation and the corresponding kinetic energy were defined for each step.

Table 5.2: Parameters and geometrical factors included in the tractor model

Notation	
\vec{F}	Vectors of body external force
\vec{T}	Vectors of body external moments
\vec{p}	Vectors of linear momentum
\vec{L}	Vectors of angular momentum
I_{CP}	Moment of inertia for any impact point (CP=index)
m	Body mass
\vec{g}	Gravitational acceleration
\vec{v}_{cm}	Velocity of the centre of mass
$\vec{\omega}_z$	The body angular velocity
E	Total energy
KE	Kinetic energy
PE	Potential energy
LE	Deformation energy and/or energy loss due to heat or friction
cm	Centre of mass
b	Horizontal distance between the axis of rotation and the cm
Δt	Step size integration
k_e	The springback factor (elastic return)
k_g	The energy factor absorbed by the ground
k_w	The elasticity factor of the wheels
\vec{l}_{cm}	Distance between the impact point and the centre of mass
φ	Angle between the gravitational acceleration vector (\vec{g}) and \vec{l}_{cm}

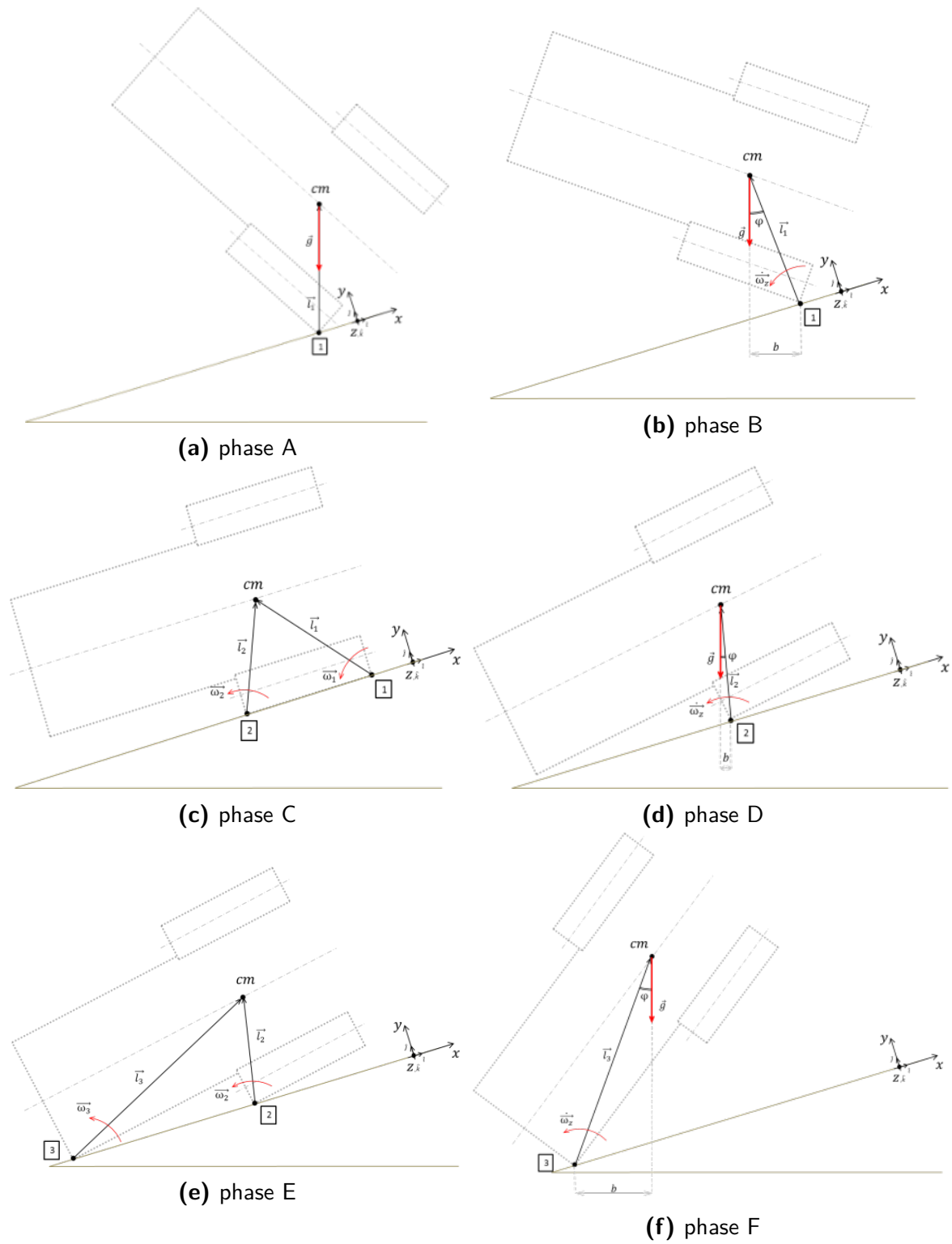


Figure 5.2: Sequence of phases in tractor lateral rollover modelling

5.3 Computation of the velocity variations during the different phases

The general form equation regarding body dynamics (5.1) was derived from body linear and angular momentum laws. It considers only the gravitational force and the invariance of the moment of inertia since the rotation occurs with respect to a fixed axis parallel to the longitudinal moment of inertia passing through the centre of mass (I_{cm}). The equations of motion of a rigid body can then be calculated:

$$\begin{cases} \vec{F} = m \cdot \frac{d(\vec{v}_{cm})}{dt} \\ \vec{T} = I_{CP} \cdot \frac{d(\vec{\omega}_z)}{dt} \end{cases} \quad (5.3)$$

The gravity was accounted for together with a pure rolling tractor and the angular acceleration was defined according to the following equation:

$$I_{CP} \cdot \frac{d(\vec{\omega}_z)}{dt} = m \cdot \vec{g} \cdot b \Rightarrow \dot{\omega}_z = \frac{m \cdot g \cdot b(t)}{I_{CP}} \quad (5.4)$$

where $b(t) = l_{CP} \cdot \sin(\varphi(t))$

5.3.1 Free falling phases (B, D, F)

The general equation (5.4) allows the computation of motion during the rotation of the rigid body with respect to a contact point as shown in [Figure 5.3](#), referred to as phase B as in the example. The integration of dynamic equations of motion permits the computation of the angular velocity (ω_z) of the ROPS and the linear velocity of centre of mass (v_{cm}), necessary to compute the kinetic energy and its variation:

$$KE = \frac{1}{2} \cdot I_{cm} \cdot |\vec{\omega}_z|^2 + \frac{1}{2} \cdot m \cdot |\vec{v}_{cm}|^2 \quad (5.5)$$

Since \vec{v}_{cm} relies on $\vec{\omega}_z$ and the distance between **cm** and **CP**, the kinetic energy

during the free falling phases is:

$$KE = \frac{1}{2} \cdot I_{CP} \cdot |\vec{\omega}_z|^2 \quad (5.6)$$

and the derivative of ω_z is defined by (5.4).

In equations (5.4) and (5.6), only the value of the length l_{CP} changes if different phases are considered. It can be subdivided into each free falling phase as follows:

Phase B:

$$\frac{d(\vec{\omega}_1)}{dt} = \frac{m \cdot g \cdot l_1 \cdot \sin(\varphi(t))}{I_1} \Rightarrow KE = \frac{1}{2} \cdot I_1 \cdot |\vec{\omega}_1(t)|^2 \quad (5.7)$$

Phase D:

$$\frac{d(\vec{\omega}_2)}{dt} = \frac{m \cdot g \cdot l_2 \cdot \sin(\varphi(t))}{I_2} \Rightarrow KE = \frac{1}{2} \cdot I_2 \cdot |\vec{\omega}_2(t)|^2 \quad (5.8)$$

Phase F:

$$\frac{d(\vec{\omega}_3)}{dt} = \frac{m \cdot g \cdot l_3 \cdot \sin(\varphi(t))}{I_3} \Rightarrow KE = \frac{1}{2} \cdot I_3 \cdot |\vec{\omega}_3(t)|^2 \quad (5.9)$$

Each free falling phase has a different index, based on the contact points (Table 5.1)

5.3.2 Impact phases (C, E)

a. Hard impact of a Rigid body

Since the objective was to compute the kinetic energy variation during the impact of the ROPS on the ground (**phase E**), an impact model had to be developed. It is useful not only in the ROPS-ground impact analysis, but also in the wheels-ground

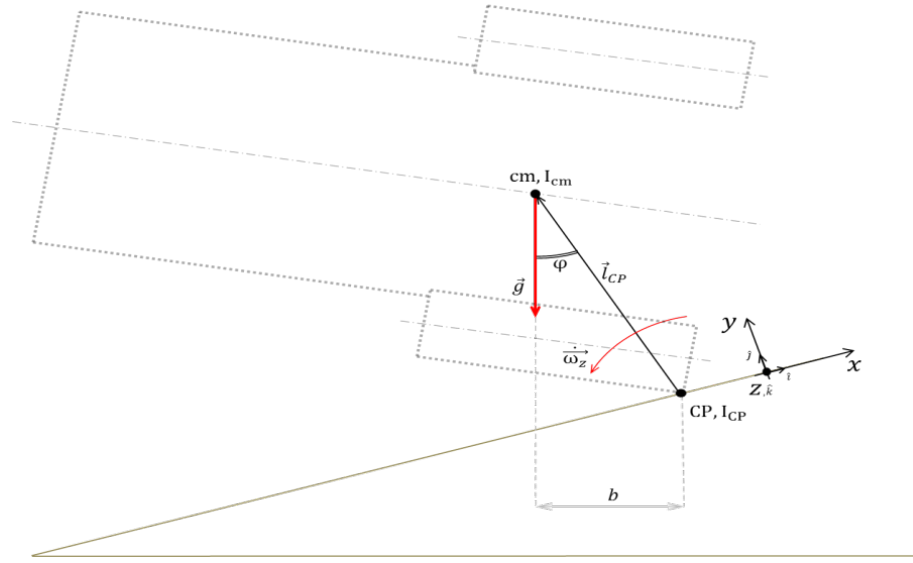


Figure 5.3: Plane motion of a rigid body around a fixed axis

interaction, as this influences the velocity of the ROPS before it touches the ground. At each impact, the change of the axis of rotation implies a variation of kinetic energy, as the condition of the isolated body and the conservation of the angular momentum are assumed. A schematic of the tractor in a hard impact phase is proposed in Figure 5.4. According to Figure 5.5 and Figure 5.6, the kinetic energy and the angular momentum before the impact can be formulated as follows:

$$KE = \frac{1}{2} \cdot I_{CP} \cdot |\vec{\omega}_{CP}|^2 \quad (5.10)$$

$$L = I_{CP} \cdot \omega_{CP} \quad (5.11)$$

Denoting the corresponding variable just after the impact by index +1, the kinetic energy before the impact could be related to the kinetic energy after the impact and the energy lost to friction (Figure 5.4):

$$KE_{CP} = KE_{CP+1} + LE_{CP+1} \quad (5.12)$$

where LE_{CP+1} denotes the loss of energy to be dissipated (in body deformation, heat transfer or friction). Considering the conservation of the angular momentum

applicable from hard shock theory, the following equation can be formulated:

$$I_{CP} \cdot \omega_{CP} = I_{CP+1} \cdot \omega_{CP+1} \quad (5.13)$$

where I_{CP+1} denotes the tractor motion along the x axis at point $CP+1$ instead of at CP . By introducing (5.10) into the expression of kinetic energy, LE_{CP+1} was computed to be:

$$LE_{CP+1} = \frac{k}{2} \cdot I_{CP} \cdot |\vec{\omega}_{CP}|^2 \quad (5.14)$$

$$\text{where: } k = \left(1 - \frac{I_{CP}}{I_{CP+1}}\right) \quad (5.15)$$

Therefore, the amount of energy lost to friction, heat or deformation following the theory of an isolated body with an inelastic impact depends only on inertia, the geometry of the body and the rotation velocity before the impact. k is the coefficient of proportionality between the kinetic energy before the impact and the energy lost during the impact.

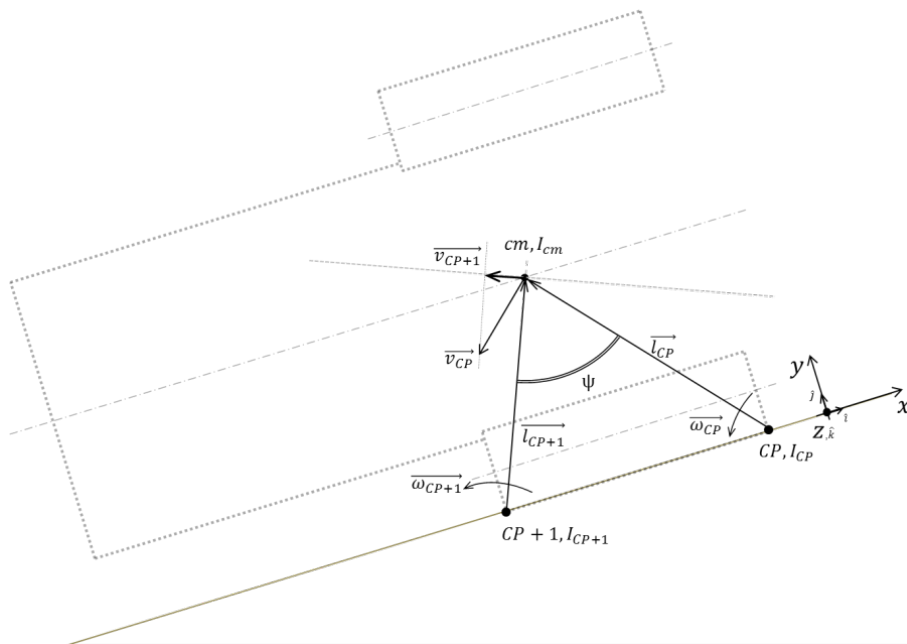


Figure 5.4: Hard impact phase

Such an approach could be representative of ROPS-ground impact behaviour, especially when considering concrete ground. Nevertheless, as can be seen regarding the experimental results, hard shock cannot be applied to the wheels-ground impact. When tyres touch the ground (**phase C**), a soft shock indeed occurs, but it is not totally inelastic. An alternative approach is then proposed, considering mixed inelastic-elastic behaviour on the basis of the actual lateral rollover test. The controlled experimental results showed that a mixed model had to be computed taking into account the predictable motion after impact (as detailed in [chapter 6](#)).

b. Wheel impact (Phase C)

A hard impact without the sliding motion of the impact point did not match the real behaviour (as it is observed when considering actual experiments describe in [chapter 4](#)). As a result, it became necessary to mitigate the condition of an inelastic impact. In phase C, the axis of rotation changes and it was assumed that the bodies are rigid. If the ground is considered infinitely rigid, the tyres absorb a quantity of energy proportional to the elastic energy generated by the impact of the wheels with the ground (potential energy). On the basis of the conservation of energy, it can be considered that part of the kinetic energy was absorbed as elastic potential energy released from the tyres and then as kinetic energy transferred to the body. The difference between the kinetic energy before the impact and the kinetic energy after the impact was lost as friction, taking into consideration that a part of this is useful for maintaining the axis of instantaneous rotation fixed.

In order to account for the actual tyres behaviour, an alternative impact was proposed. The velocity attributed to the centre of mass was subdivided parallelly and orthogonally to the ground. Depending on the kind of impact, represented by the coefficient ke (5.16), it was possible to analyse the velocity orthogonal to the ground after impact (5.17), assuming the velocity parallel to the ground is unchanged. The variation of energy was obtained (according to [Figure 5.5](#)) considering the conservation of angular momentum (5.18) and analysing the velocity v_1 (5.19) after the elastic energy initially absorbed by the wheels was released.

$$-1 < k_e < 1 \quad (5.16)$$

$k_e = +1$; inelastic impact

$k_e = -1$; elastic impact

$$v_N = -k_e \cdot v_\perp \quad (5.17)$$

$$\vec{L} = I_1 \cdot \vec{\omega}_1 = I_2 \cdot \vec{\omega}_2 \quad (5.18)$$

$$\begin{cases} I_{cm} \cdot \vec{\omega}_1 + \vec{l}_1 \wedge m \cdot \vec{v}_1 = I_{cm} \cdot \vec{\omega}_2 + \vec{l}_2 \wedge m \cdot \vec{v}_2 \\ \vec{v}_1 = (v_1 \cdot \cos(\gamma)) \hat{i} + k_e \cdot (v_1 \cdot \sin(\gamma)) \hat{j} \end{cases} \quad (5.19)$$

As is shown in [Figure 5.5](#), the indices represent different tractor motions:

1. before impact;
2. after impact.

In addition, the directions of the velocity vectors before and after the impact are defined by two angles:

γ : angle between the velocity vector before impact and the x axis;

α : angle between the velocity vector after impact and the x axis.

The point around the rotation changes; then $I_2 \neq I_1$ and the distance with respect to the **cm** also change. Given that:

$$\begin{cases} \vec{\omega}_1 = \omega_1 \cdot \hat{k} \\ \vec{\omega}_2 = \omega_2 \cdot \hat{k} \end{cases}; \quad \begin{cases} l_{2x} = l_2 \cdot \sin(\alpha) \\ l_{2y} = l_2 \cdot \cos(\alpha) \end{cases} \quad (5.20)$$

$$\vec{\omega}_2 = \frac{I_{cm} \cdot \vec{\omega}_1 + m \cdot (l_{2x} \cdot v_1 \cdot \sin(\gamma) \cdot k_e + l_{2y} \cdot v_1 \cdot \cos(\gamma)) \cdot \hat{k}}{I_{cm} + m \cdot l_2^2} \quad (5.21)$$

$$\omega_2 = \frac{I_{cm} \cdot \omega_1 + m \cdot (l_{2x} \cdot v_1 \cdot \sin(\gamma) \cdot k_e + l_{2y} \cdot v_1 \cdot \cos(\gamma))}{I_{cm} + m \cdot l_2^2} \quad (5.22)$$

c. ROPS impact (Phase E)

The ROPS-ground impact had a different behaviour because the impact occurred in a restricted area, i.e. the surface of contact of the most external part of the ROPS first coming into contact with the ground. A translational component of the motion may occur. It was considered that the pure rotational motion of the system (ROPS + wheels) was converted into two kinds of motion after ROPS impact: a rotation around contact point 3 and a translation of this point due to the sliding of the ROPS on the ground (Figure 5.6). Thus, in the ROPS-ground impact, the energy not affecting the subsequent rotation was partially maintained as translational kinetic energy and was partially lost to heat and friction. Based on the assumption of non-deformable ground and the ROPS rigidly connected to the chassis, the energy lost to friction was considered to be converted into deformation energy on the ROPS. The model assumptions allowed the energy absorbed by the ROPS at the first impact with the ground to be assessed.

Still assuming conservation of the angular momentum (5.18), the kinetic energy after the inelastic impact was:

$$KE_3 = \frac{1}{2} \cdot I_3 \cdot \omega_3^2 \quad (5.25)$$

While the energy lost in friction is:

$$\begin{cases} KE_2 = \frac{1}{2} \cdot I_2 \cdot \omega_2^2 \\ KE_3 = \frac{1}{2} \cdot I_3 \cdot \omega_3^2 \end{cases} \Rightarrow LE_C = KE_2 - KE_3 \quad (5.26)$$

Considering a friction factor (5.27) between the tractor and the ground, assuming that the part of the tractor velocity parallel to the ground (5.28) was not lost to friction but was instead converted into kinetic energy of translation, the contribution of *rotational kinetic energy* (5.29) added to the contribution of the *translational kinetic energy* (5.30) allowed the calculation of the kinetic energy after impact (5.31).

$$f = \frac{v_x}{1 + v_x} \quad (5.27)$$

$$\left. \begin{array}{l} v_2 = \omega_2 \cdot l_2 \\ v_3 = \omega_3 \cdot l_3 \end{array} \right\} \Rightarrow v_{\perp 3} = \sqrt{v_2^2 - v_3^2} \Rightarrow v_x = v_{\perp 3} \cdot \sin(\alpha) \quad (5.28)$$

$$KE_{rot} = \frac{1}{2} \cdot I_3 \cdot \omega_3^2 \quad (5.29)$$

$$KE_{trans} = \frac{1}{2} \cdot m \cdot v_x^2 \cdot f \cdot (1 - k_g) \quad (5.30)$$

$$KE_C = KE_{rot} + KE_{trans} \quad (5.31)$$

Finally, using (5.31) and (5.23), one can calculate the variation of kinetic energy E_{ROPS} during the ROPS-ground impact, detailed subsequently in section 5.5. The level of energy is considered to be absorbed by the protective structure and dissipated as deformation, theoretically preserving driver safety. The variation of kinetic energy could represent the minimum energy value to be absorbed during the ROPS official tests. This theoretical value now has to be compared with the results obtained during experiments in order to show its relevance.

5.4 Integration method and kinetic energy computation

Starting from the equation of the body in unstable equilibrium (**phase A**), the approach was an analysis through repetition over time:

$$\begin{cases} \Delta t = time_i - time_{i-1} \\ \omega_i = \omega_{i-1} + \Delta\omega \end{cases} \quad (5.32)$$

if Δt is relatively small, one can approximate $\dot{\omega}$ as a constant. Angular velocity and angular variation were computed according to the Euler Method and the Trapezoidal Rule (Monegato, 1998) (5.33).

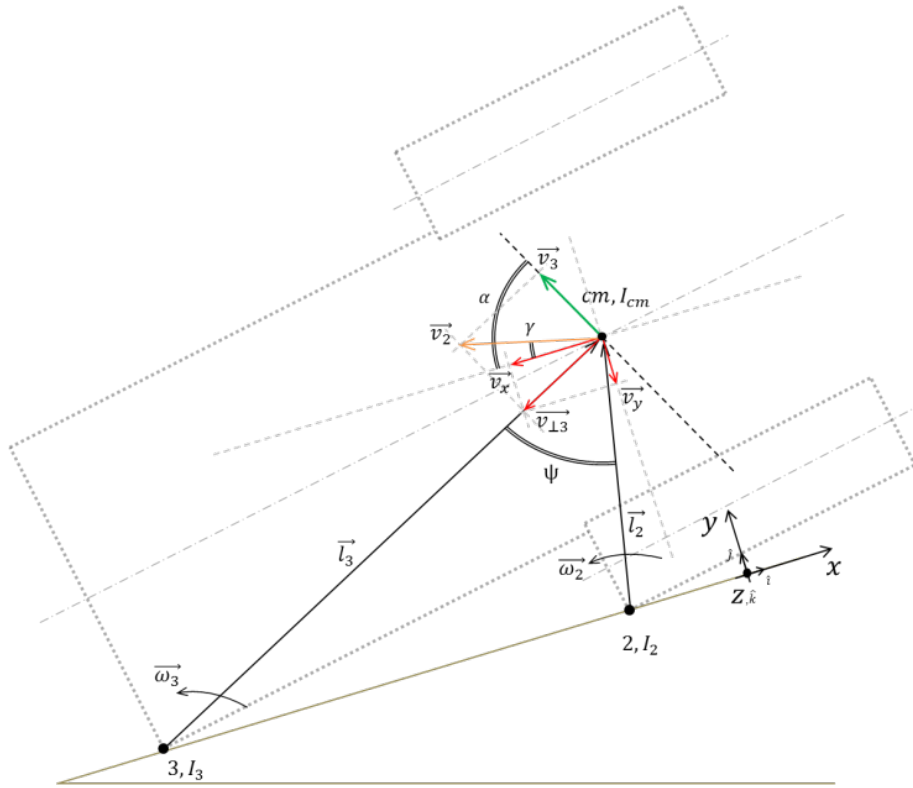


Figure 5.6: Impact of the wheels with the ground slope

$$\begin{cases} \dot{\omega}_i = \frac{m \cdot g \cdot b}{I} \\ \omega_i = \omega_{i-1} + \dot{\omega}_i \cdot \Delta t \\ \theta_i = \theta_{i-1} + \left(\frac{\omega_{i-1} + \omega_i}{2} \right) \cdot \Delta t \end{cases} \quad \begin{array}{l} \text{Euler Forward Method} \\ \text{Trapezoidal Rule} \end{array} \quad (5.33)$$

On the basis of the geometric and inertial characteristics of the tractor (Table 4.1) the kinetic energy of rotation (5.34) can be computed.

$$KE_{rot} = \frac{1}{2} \cdot I \cdot \omega^2(t) = \frac{1}{2} \cdot (I_{cm} + m \cdot l_{cm}^2) \cdot \omega^2(t) \quad (5.34)$$

When the tractor was subjected to an initial velocity of translation v_0 , a roto-translational motion affected only by gravitational force was assumed. Using the example of Figure 5.7, the translational velocity (5.35) allowed the kinetic energy of translation over time to be assessed (5.36).

$$v_{trans}(t) = \sqrt{v_{0x'}^2 + (v_{0y'} + g \cdot t)^2} \quad (5.35)$$

$$KE_{trans}(t) = \frac{1}{2} \cdot m \cdot v_{trans}^2(t) \quad (5.36)$$

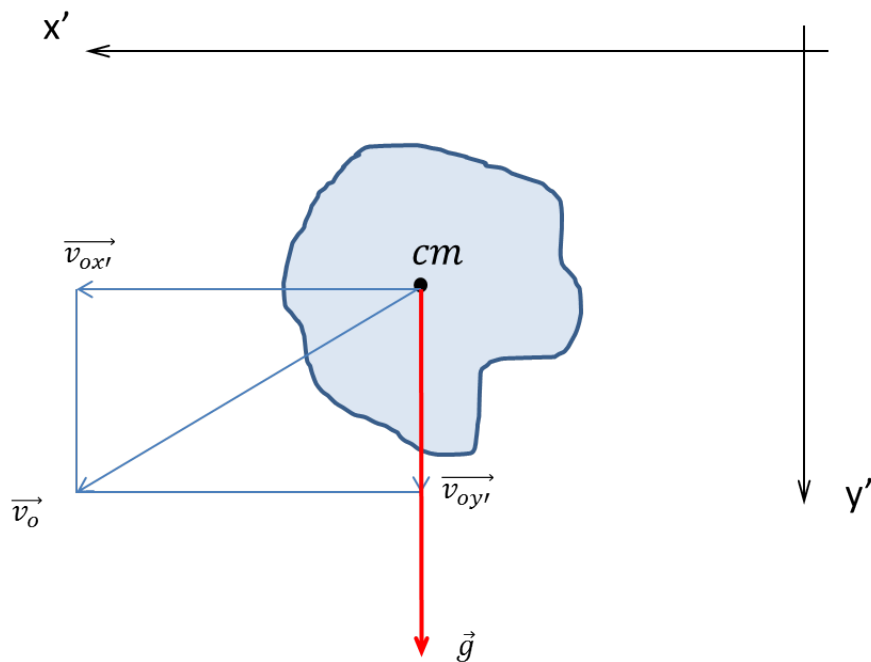


Figure 5.7: Rigid body subject only to gravitational force with initial speed

The kinetic energy (5.37) was the sum of the kinetic energy of rotation (5.34) and the kinetic energy of translation (5.36).

$$\begin{aligned} KE_{tot}(t) &= KE_{rot}(t) + KE_{trans}(t) = \frac{1}{2} \cdot (I_{cm} + m \cdot l_{cm}^2) \cdot \omega^2(t) + \frac{1}{2} \cdot m \cdot v_{trans}^2(t) \\ &= \frac{1}{2} \cdot I_{cm} \cdot \omega^2(t) + \frac{1}{2} \cdot m \cdot \left((l_{cm} \cdot \omega(t))^2 + v_{trans}^2(t) \right) \\ KE_{tot}(t) &= \frac{1}{2} \cdot I_{cm} \cdot \omega^2(t) + \frac{1}{2} \cdot m \cdot v^2(t) \end{aligned} \quad (5.37)$$

5.5 Evaluation of energy to be absorbed by the ROPS

The energy absorbed by the ROPS at the first impact with the ground was based on the variation of kinetic energy. According to a conservative analysis considering a totally non-elastic impact, the energy absorbed by the ROPS can be traced as in (5.26). It was considered that the energy of the body not involved in the action of rotation caused the deformation of the body in the impact zone. The basic idea of this study was to point out the alternative behaviour of the tractor during the ROPS-ground impact time even starting from a totally non-elastic impact. The portion of the energy of the tractor which did not produce rotation became energy lost by absorption of the ROPS, eventual absorption by the ground and residual energy of translation. The energy absorbed by the ROPS (5.38) was considered to be the sum of two separate energy components (Figure 5.6), a component perpendicular to the ground and a component parallel to the ground with the introduction of a friction factor proportional to the velocity of impact on the ground (f) and an absorption coefficient of the ground (k_g) equal to 0 in the case of zero absorption and 1 in the case of total absorption of the ground. Imposing zero absorption of the ground and a maximum value of the friction factor, the case of non-elastic impact is represented. The variation of these factors allows different scenarios.

$$E_{ROPS} = \frac{1}{2} \cdot m \cdot v_x^2 \cdot (1 - f) \cdot (1 - k_g) + \frac{1}{2} \cdot m \cdot v_y^2 \cdot (1 - k_g) \quad (5.38)$$

Chapter 6

Real data vs. mathematical model

6.1 Comparison of the real data and mathematical model

The mathematical model proposed in the previous section was simulated using to the software MatLab ([MATLAB, 2010](#)). The tractor behaviour in the lateral rollover phases was analysed, and the variation of the kinetic energy of the tractor pointed out. The approach in the development of the model was to consider the variation in the kinetic energy before and after the impact of the tractor on the ground. The difference in kinetic energy was absorbed by the body, the ground or transformed into loss due to friction. When the ground was infinitely rigid and there was negligible friction (according to the assumptions made earlier, the energy lost to friction was converted into deformation energy absorbed by the ROPS), it was assumed that the variation of kinetic energy corresponded to the amount of energy absorbed by the tractor. In [Figure 6.1](#), the maximum kinetic energy during the tractor rollover and the energy absorbed by the ROPS versus the ground slope are depicted. The results shown are based on the geometrical dimensions of the tractor prototype undergoing the experimental rollover test. Full details are summarised in [Table 6.1](#) according to the reference system used ([Figure 6.2](#)).

In order to show the relevance of the proposed mixed impact model, a computation of kinetic variations was carried out for three cases:

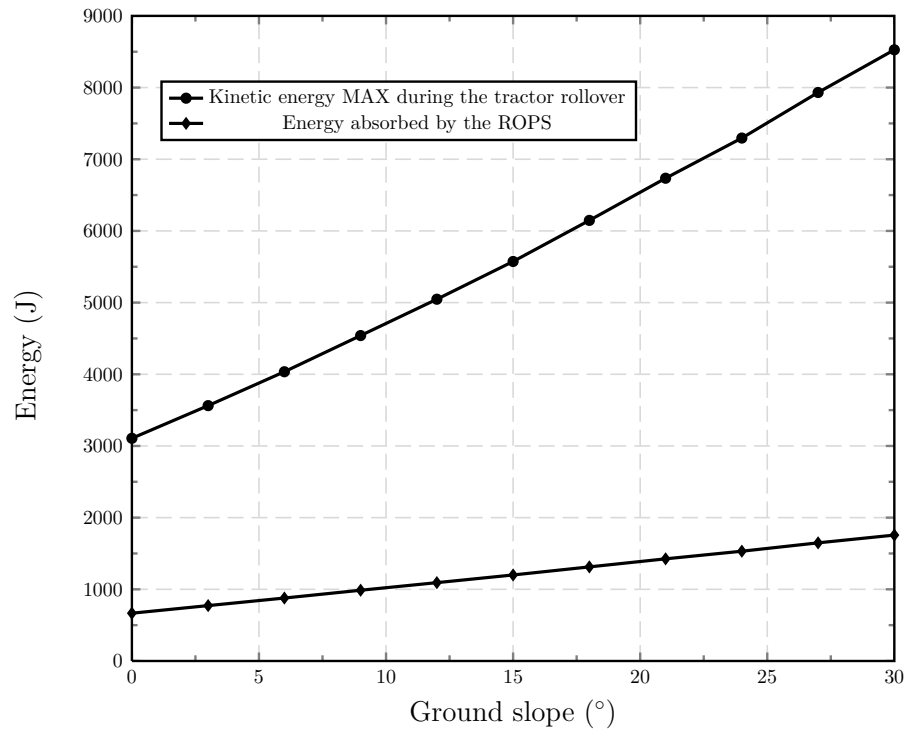


Figure 6.1: Kinetic energy and the energy absorbed by the ROPS during impact with respect to the ground slope

Table 6.1: Tractor geometrical dimension

	x	y	$Unit$	$Description$
Point 1	0.000	0.000	m	The lower part of the wheels
Point 2	0.000	0.860	m	The upper part of the left wheels
Point 3	0.140	2.140	m	ROPS impact
cm	0.688	0.600	m	Centre of mass

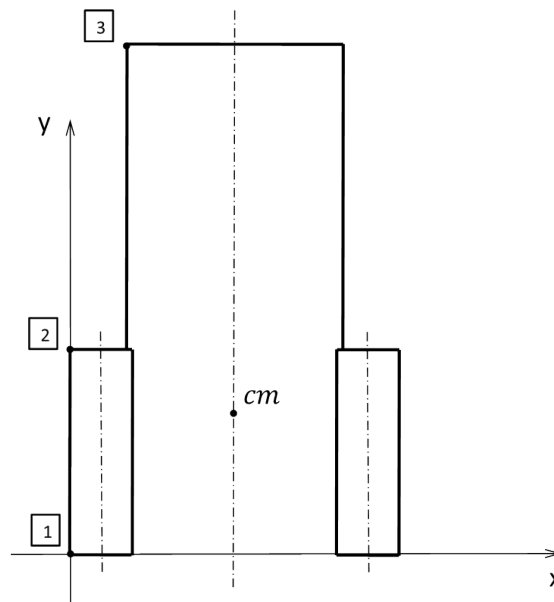


Figure 6.2: Reference system

Case a. Using totally inelastic tyres ($ke = 0$ in equation (21));

Case b. Using totally elastic tyres ($ke = 1$ in equation (21));

Case c. Using the proposed impact model with a coefficient $ke = 0.9$ and a friction factor.

The different variations are reported in [Figure 6.3](#) and compared to the actual kinetic energy variation during the lateral rollover.

The first case corresponds to the mathematical model inspired by Schwanghart's model ([Schwanghart, 1982](#)). It considers a totally inelastic impact model, and consequently overestimates the energy lost in the wheels-ground impact. This leads to an underestimation of the energy to be absorbed by the ROPS during its impact with the ground (**Case a**, [Figure 6.3](#)). This model is then not representative of the energy variation recorded during the experimental tests, and cannot then be representative of actual rollover situations. The introduction of an elastic factor on the wheels allows a higher value of available kinetic energy to be obtained after wheels-ground impact. As pointed out in **Case b**, [Figure 6.3](#), an elastic impact indeed reduces the first step of kinetic energy. Nevertheless, the second step, representative of the ROPS impact with the ground, is overestimated since the translational motion

of the tractor is ignored. Finally, the introduction of the translational effect into the proposed model produced a correct variation of kinetic energy in both impacts (Case c) with respect to the actual data recorded as is shown in Figure 6.4.

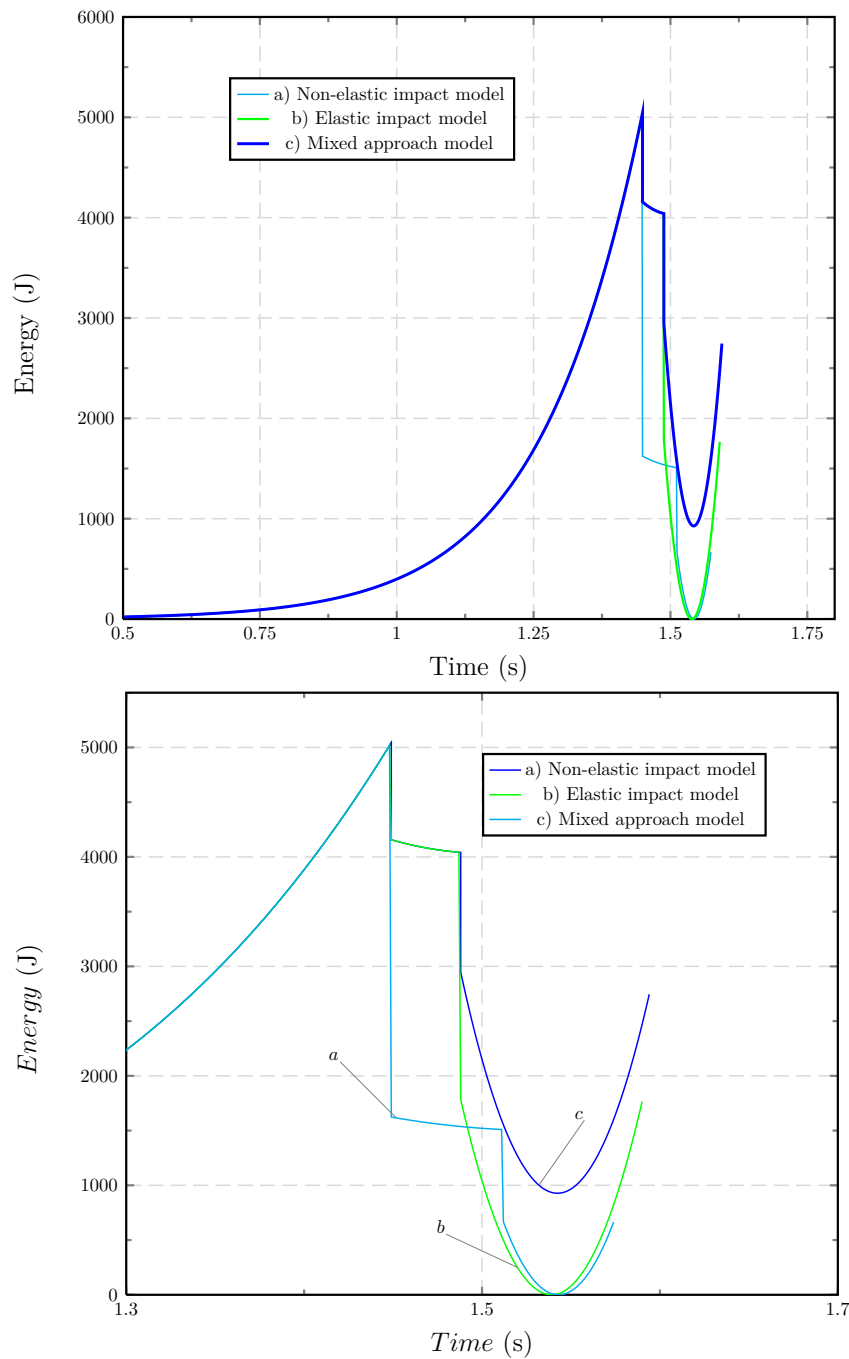


Figure 6.3: Model evolution:
a) Non-elastic Model, *b)* Elastic Model, *c)* Mixed Model

In Table 6.2, the energy values absorbed by the ROPS in the three cases consid-

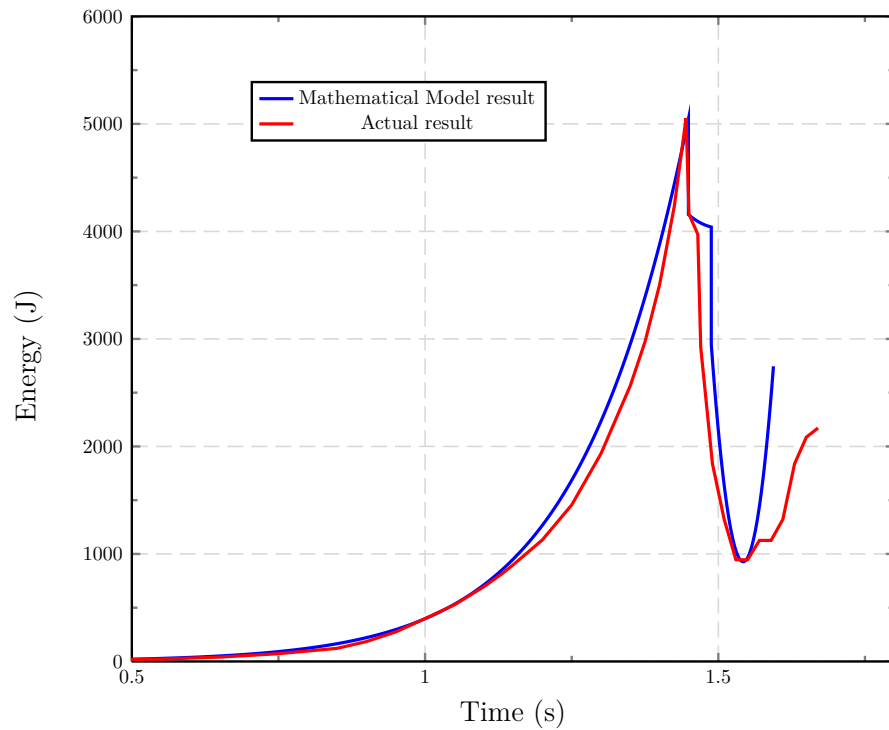


Figure 6.4: Actual Data vs. Mathematical Model

ered are compared. The energy step recorded during the experimental tests when the ROPS impacted the ground was equal to 1095 J.

Table 6.2: Energy absorbed by the ROPS in different approaches with respect to the actual value of 1095 J

Type of Model	E_{ROPS}	Unit
Inelastic Model	843	J
Introduction of the elastic factor on the wheels	2257	J
Introduction of the translational effect	1093	J

The proposed model allowed accurately evaluating the kinetic energy variation on the basis of the tyre properties. Moreover, tyre elasticity and ground absorption may be taken into consideration in order to account for several cases and/or calibrate the model to particular situations. The proposed mixed model succeeds in finding the right energy level with an error of less than 1%. It can then be used to analyse the tractor behaviour in lateral rollover in different scenarios, such as ground inclination, geometry and inertia of the tractor, boundary conditions, elasticity of the tyres, elasticity of the ROPS and ground absorption. [Figure 6.5](#) shows

the results of the energy absorbed by the ROPS when considering different slope conditions and the elasticity of the tyres for the same configuration of the tractor. When increasing both the elasticity of the tyres and the slope the energy absorbed by the ROPS increased. This can be obtained by means of tyres with a more elastic compound or tires used at a greater inflation pressure. The energy value obtained can be compared to the testing energy value foreseen in the OECD testing procedure (OECD Code 6, 2013). For this tractor, the value was 2004 J and it is depicted by the horizontal grey plane in Figure 6.5. The results showed that some conditions exist in which the energy to be absorbed by the ROPS is greater than the amount of energy computed by the testing procedure. Even if the slope does not exceed a 1/1.5 gradient (vertical grey plane in Figure 6.5, representing testing procedure recommendations), the elasticity of the tyres may lead to an important amount of energy to be absorbed by the ROPS. As a result, the value used to test ROPSs may become critical for such conditions. The proposed model enables the elaboration of software capable of measuring the relationship between the energy and the tractor parameters, or environmental conditions. This could represent a tool for validating the testing procedure relevance with respect to agro-equipment and supply a relevant value for testing the ROPS.

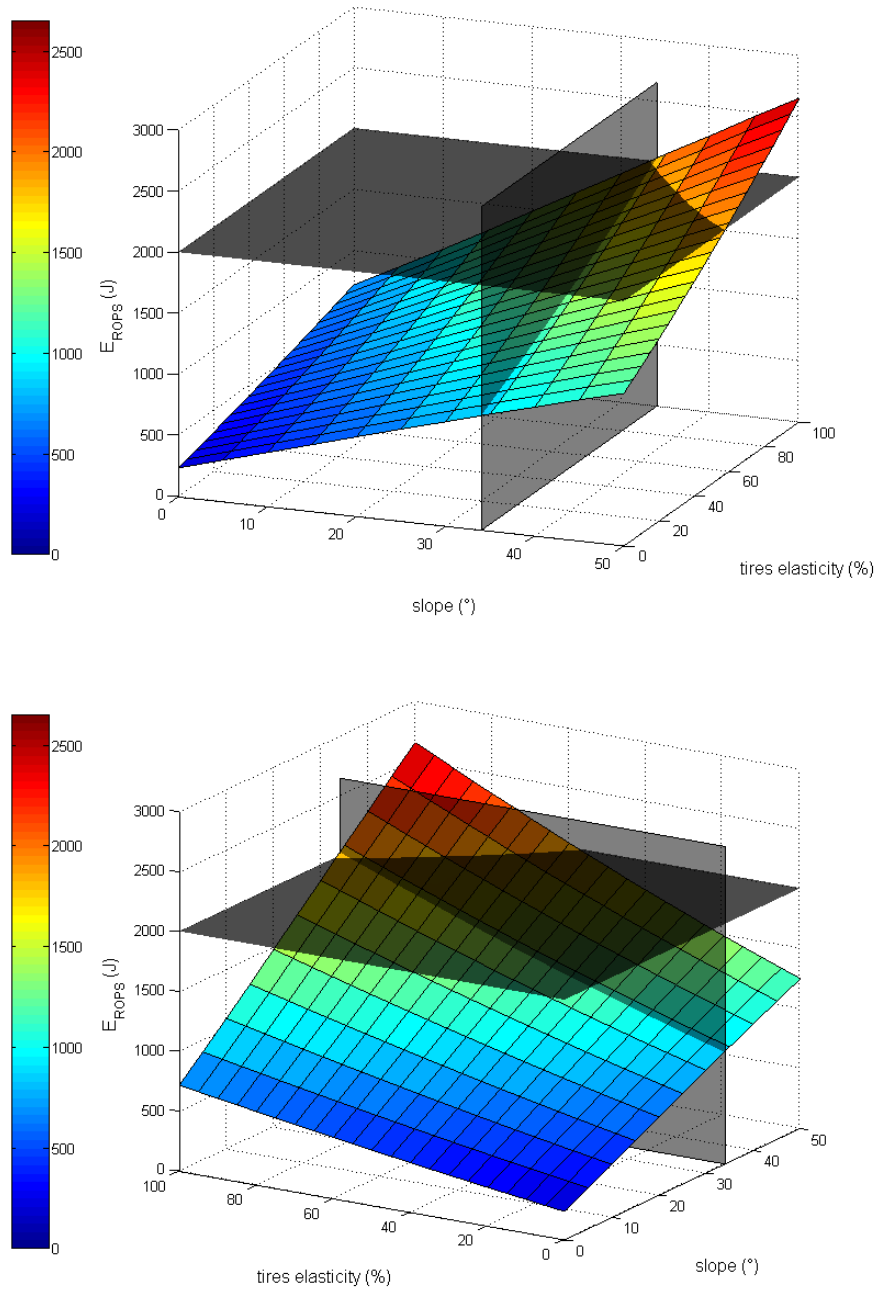


Figure 6.5: Energy absorbed by the ROPS vs. slope and tyre elasticity

Chapter 7

Conclusions

An analytical model accurately analysing tractor rollover situations was developed. In order to relevantly describe the different impacts occurring during rollover, a simple impact model (totally hard or soft) cannot be used. Actual experiments showed that the variations of energy occurring when the side of the tyre touches the ground or when the ROPS is crashing do not match the classical models. As a result, this thesis proposed an alternative model of impact, relevantly describing the rollover situation. On the one hand, it mixes soft and hard shock models of impact. This is particularly suitable in accounting for the influence of the tyres. On the other hand, an analysis of velocity directions before and after the shock is achieved. The translational motion (friction) at the contact point during impact may then be considered. As a consequence, the results obtained with the proposed model precisely match the experiments. In particular, the variation of energy during rollover was accurately computed. Other than the interest in understanding rollover dynamics, such an approach is then suitable for evaluating the energy to be absorbed by a ROPS. In particular, the influence of tractor design parameters (such as geometry, mass or moment of inertia), and environmental properties (slope, grip condition) on the level of energy to be absorbed in case of a rollover can be calculated. This can first be used to help in designing the complex tractor-ROPS. Secondly, such a model constitutes an interesting tool for checking the validity of the standards with respect to strength tests. The evolution of machine design in recent decades has indeed been important while testing procedures have not changed accordingly.

Software based on the proposed equations may then constitute a possible way of verifying the relevance of a testing procedure with respect to machine properties. Moreover, it can alternatively supply a relevant value of energy to be applied as a testing procedure, if needed. The final aim of the research was to ensure the robustness of the ROPS with respect to the evolution of agricultural machines and finally to improve the driver safety in cases of rollover. The proposed approach has herein been limited to lateral rollover accidents, but can easily be extended to longitudinal overturning. Furthermore, this study is herein focused on ROPS dimensioning and ensuring driver protection when an accident occurs. However the model may also be exploited in order to design active safety devices for avoiding an accident. The dynamic model may indeed be used to understand the conditions leading to risk of rollover situations. As a result, hazardous situations can be anticipated and then avoided by warning the driver or proposing corrective action.

Bibliography

- 2003/37/EC. European Directive of the European Parliament and of the Council relating to the type-approval of agricultural or forestry tractors, their trailers and interchangeable towed machinery, together with their systems, components and separate technical units, 2003. URL <http://eur-lex.europa.eu/>.
- 2005/67/EC. European Directive relating to the type-approval of agricultural or forestry tractors, 2005. URL <http://eur-lex.europa.eu/>.
- 2010/52/EU. European Directive relating to the type-approval of agricultural or forestry tractors, 2010. URL <http://eur-lex.europa.eu/>.
- 87/402/EEC. European Directive on roll-over protection structures mounted in front of the driver's seat on narrow-track wheeled agricultural and forestry tractors, 1987. URL <http://eur-lex.europa.eu/>.
- I. Ahmadi. Dynamics of tractor lateral overturn on slopes under the influence of position disturbances (model development). *Journal of Terramechanics*, 48(5):339 – 346, 2011. ISSN 0022-4898. doi: <http://dx.doi.org/10.1016/j.jterra.2011.07.001>. URL <http://www.sciencedirect.com/science/article/pii/S0022489811000437>.
- J.R. Alfaro, I. Arana, S. Arazuri, and C. Jarén. Assessing the safety provided by sae j2194 standard and code 4 standard code for testing rops, using finite element analysis. *Biosystems Engineering*, 105(2):189 – 197, 2010. ISSN 1537-5110. doi: <http://dx.doi.org/10.1016/j.biosystemseng.2009.10.007>. URL <http://www.sciencedirect.com/science/article/pii/S1537511009003146>.

- J. I. Arana, J.R. Alfaro, S. Arazuri, J.L. Ponce de León, and C. Jarén. A proposal to improve the sae standard and oecd code 4 standard code for testing rops. *Transactions of the ASABE*, 54(4):1189–1197, 2011. URL <http://elibrary.asabe.org/abstract.asp?adid=39017&t=3>.
- F. Boyer, C.J. Chisholm, and H. Schwanghart. Rollover protective structures for wheeled agricultural or forestry tractors. Expertise for EEC commission XI/1036/76-D, Brussels., 1976.
- R. Budynas and K. Nisbett. *Shigley's Mechanical Engineering Design*. McGraw-Hill series in mechanical engineering. McGraw-Hill Education, 2010. ISBN 9780073529288. URL <http://books.google.it/books?id=eT1DPgAACAAJ>.
- G. Casini-Ropa. Attrezzatura e metodo per il rilievo dell'altezza da terra del bari-centro delle macchine agricole [equipment and methods for the measurement of the height from the ground of the centre of gravity on agricultural machinery]. *Rivista di Ingegneria Agraria*, 2:81–85, 1976.
- F. Cesari. *Calcolo matriciale delle strutture*. Pitagora, 1994. ISBN 9788837107024. URL <http://books.google.it/books?id=yqqTAAAACAAJ>.
- C.J. Chisholm. A survey of 114 tractor sideways overturning accidents in the uk - 1969 to 1971. Department note DN/TE/238/1425. National Institute of Agricultural Engineering, Silsoe., 1972.
- C.J. Chisholm. Tractor overturning tests: 1973-75. Department note DN/E/693/1425. National Institute of Agricultural Engineering, Silsoe., 1977.
- C.J. Chisholm. A mathematical model of tractor overturning and impact behaviour. *Journal of Agricultural Engineering Research*, 24(4):375 – 394, 1979a. ISSN 0021-8634. doi: 10.1016/0021-8634(79)90079-9. URL <http://www.sciencedirect.com/science/article/pii/0021863479900799>.
- C.J. Chisholm. Experimental validation of a tractor overturning simulation. *Journal of Agricultural Engineering Research*, 24(4):395 – 415, 1979b. ISSN 0021-

8634. doi: 10.1016/0021-8634(79)90080-5. URL <http://www.sciencedirect.com/science/article/pii/0021863479900805>.
- C.J. Chisholm. The effect of parameter variation on tractor overturning and impact behaviour. *Journal of Agricultural Engineering Research*, 24(4):417 – 440, 1979c. ISSN 0021-8634. doi: 10.1016/0021-8634(79)90081-7. URL <http://www.sciencedirect.com/science/article/pii/0021863479900817>.
- C.J. Chisholm. Analysis of rigid-body motion from cine film measurements. *Journal of Agricultural Engineering Research*, 24(4):441 – 446, 1979d. ISSN 0021-8634. doi: 10.1016/0021-8634(79)90082-9. URL <http://www.sciencedirect.com/science/article/pii/0021863479900829>.
- C.J. Chisholm and P.C. Seward. The correlation between damage to rollover protective structure in tractor overturning accident and in standard tests. Department note DN/E/674/4600. National Institute of Agricultural Engineering, Silsoe., 1976.
- D.C. Davis and G.E. Rehkugler. Agricultural wheel-tractor overturns. part i: Mathematical model. *Transactions of the ASABE*, 17(3):477–483, 1974a. URL <http://elibrary.asabe.org/abstract.asp?adid=36887&t=3>.
- D.C. Davis and G.E. Rehkugler. Agricultural wheel-tractor overturns. part ii: Mathematical model verification by scale-model study. *Transactions of the ASABE*, 17(3):484–488, 492, 1974b. URL <http://elibrary.asabe.org/abstract.asp?adid=36888&t=3>.
- J.R. Etherton, R.G. Cutlip, J.R. Harris, M. Ronaghi, K.H. Means, and S. Howard. Dynamic performance of the mechanism of an automatically deployable rops. *Journal of Agricultural Safety and Health*, 8(1):113–118, 2002. URL <http://elibrary.asabe.org/abstract.asp?adid=7222&t=3>.
- A. Fabbri and S. Ward. Validation of a finite element program for the design of rollover protective framed structures (rops) for agricultural tractors. *Biosystems Engineering*, 81(3):287 – 296, 2002. ISSN 1537-5110. doi: <http://dx.doi.org/10.1006/>

- bioe.2001.0012. URL <http://www.sciencedirect.com/science/article/pii/S1537511001900121>.
- C.E. Goering and W.F. Buchele. Computer simulation of an unsprung vehicle part i. *Transactions of the ASABE*, 10(2):–, 1967a. URL <http://elibrary.asabe.org/abstract.asp?adid=39652&t=3>.
- C.E. Goering and W.F. Buchele. Computer simulation of an unsprung vehicle part ii. *Transactions of the ASABE*, 10(2):–, 1967b. URL <http://elibrary.asabe.org/abstract.asp?adid=39653&t=3>.
- A.L. Guzzomi and V. Rondelli. Narrow-track wheeled agricultural tractor parameter variation. *Journal of Agricultural Safety and Health*, 19(4):237–260, 2013. URL <http://elibrary.asabe.org/abstract.asp?adid=44181&t=3>.
- A.L. Guzzomi, V. Rondelli, A. Guarnieri, G. Molari, and P.G. Molari. Available energy during the rollover of narrow-track wheeled agricultural tractors. *Biosystems Engineering*, 104(3):318 – 323, 2009. ISSN 1537-5110. doi: <http://dx.doi.org/10.1016/j.biosystemseng.2009.07.005>. URL <http://www.sciencedirect.com/science/article/pii/S1537511009002220>.
- J.R. Harris, V.H. Mucino, J.R. Etherton, K.A. Snyder, and K.H. Means. Finite element modeling of rops in static testing and rear overturns. *Journal of Agricultural Safety and Health*, 6(3):215–225, 2000.
- J.R. Harris, E.A. McKenzie, Jr., J.R. Etherton, D.M. Cantis, and M. Ronaghi. Rops performance during field upset and static testing. *Journal of agricultural safety and health*, 16(1):5–18, 2010.
- ISO 12003-1:2013. Agricultural and forestry tractors – Roll-over protective structures on narrow-track wheeled tractors – Part 1: Front-mounted ROPS. Geneva, Switzerland: ISO, 2008.
- ISO 3463:2006. Tractors for agriculture and forestry – Roll-over protective structures (ROPS) – Dynamic test method and acceptance conditions. Geneva, Switzerland: ISO, 2006.

- ISO 5700:2013. Tractors for agriculture and forestry – Roll-over protective structures (ROPS) – Static test method and acceptance conditions. Geneva, Switzerland: ISO, 2013.
- R.W. Job. Roll-over protective structure development; an industry perspective. In *ASABE Meeting Presentation*, Providence, Rhode Island, June 29-July 2 2008. St. Joseph, Michigan: American Society of Agricultural and Biological Engineers (USA). Paper Number: 083751.
- K.U. Kim and G.E. Rehkugler. A review of tractor dynamics and stability. *Transactions of the ASABE*, 30(3):–, 1987. URL <http://elibrary.asabe.org/abstract.asp?adid=30449&t=3>.
- J.A. Koch, W.F. Buchele, and S.J. Marley. Verification of a mathematical model to predict tractor tipping behavior. *Transactions of the ASABE*, 13(1):67–72, 76, 1970. URL <http://elibrary.asabe.org/abstract.asp?adid=38538&t=3>.
- D.L. Larson, D.W. Smith, and J.B. Liljedahl. The dynamics of three-dimensional tractor motion. *Transactions of the ASABE*, 19(1):195–200, 1976. URL <http://elibrary.asabe.org/abstract.asp?adid=35993&t=3>.
- R. Lenain, E. Hugo, and T. Langle. Sensitivity of the absorbed energy into a rops during a rollover situation: comparison to the security level proposed into oecd code 4. In *International Conference on Agricultural Engineering (AgEng 2010)*, pages 137–147, Aubiere, 6-8 September 2010. Cemagref.
- J. Liu and P.D. Ayers. Application of a tractor stability index for protective structure deployment. *Journal of Agricultural Safety and Health*, Special Issue(1):171–181, 1998. URL <http://elibrary.asabe.org/abstract.asp?adid=15367&t=3>.
- MATLAB. *version 7.10.0 (R2010a)*. The MathWorks Inc., Natick, Massachusetts, 2010.
- E.G. McKibben. *The Kinematics and Dynamics of the Wheel-type Farm Tractor*. Agricultural Engineering, 1927. URL <http://books.google.it/books?id=uycbnQEACAAJ>.

- H.A. Moberg. *Tractor safety cabs: test methods and experiences gained during ordinary farm work in Sweden*. National Swedish Testing Institute for Agricultural Machinery, 1964. URL <http://books.google.fr/books?id=JAgXmAEACAAJ>.
- H.A. Moberg. *Dynamic Testing of Tractor Protection Cabs - Development of Method, Practical Experiences*. Society of Automotive Engineers, 1973. URL <http://books.google.it/books?id=0wVpHwAACAAJ>.
- G. Monegato. *Fondamenti di Calcolo Numerico [Fundamentals of Numerical Computing]*. Clut, 1998.
- OECD Code 3. *Standard code for the official testing of protective structures on agriculture and forestry tractors (DYNAMIC TEST)*. Organisation for Economic Co-operation and Development, Available at. Paris, France: OECD Headquarters, 2013. URL <http://www.oecd.org>.
- OECD Code 4. *Standard code for the official testing of protective structures on agriculture and forestry tractors (STATIC TEST)*. Organisation for Economic Co-operation and Development, Available at. Paris, France: OECD Headquarters, 2013. URL <http://www.oecd.org>.
- OECD Code 6. *Standard Code for the official testing of front mounted roll-over protective structures on narrow-track wheeled agricultural and forestry tractors*. Organisation for Economic Co-operation and Development, Available at. Paris, France: OECD Headquarters, 2013. URL <http://www.oecd.org>.
- OECD Code 7. *Standard Code for the official testing of rear mounted roll-over protective structures on narrow-track wheeled agricultural and forestry tractors*. Organisation for Economic Co-operation and Development, Available at. Paris, France: OECD Headquarters, 2013. URL <http://www.oecd.org>.
- OECD Codes. *Standard codes for the official testing of agricultural and forestry tractors*. Organisation for Economic Co-operation and Development, Available at. Paris, France: OECD Headquarters, 2013. URL <http://www.oecd.org>.

- R.L. Pershing and R.R. Yoerger. Simulation of tractors for transient response. *Transactions of the ASABE*, 12(5):715–719, 1969. URL <http://elibrary.asabe.org/abstract.asp?adid=38935&t=3>.
- G.E. Rehkugler, V. Kumar, and D.C. Davis. Simulation of tractor accidents and overturns. *Transactions of the ASABE*, 19(4):602–609, 613, 1976. URL <http://elibrary.asabe.org/abstract.asp?adid=36078&t=3>.
- V. Rondelli and A.L. Guzzomi. Selecting rops safety margins for wheeled agricultural tractors based on tractor mass. *Biosystems Engineering*, 105(3):402 – 410, 2010. ISSN 1537-5110. doi: <http://dx.doi.org/10.1016/j.biosystemseng.2009.12.013>. URL <http://www.sciencedirect.com/science/article/pii/S1537511010000036>.
- V. Rondelli, E. Capacci, B. Franceschetti, and A. Guarnieri. Rops design evolution with respect to the requirements of the strength test procedures. In *International Conference on Agricultural Engineering (AgEng 2012)*, page 6, 8-12 July 2012.
- SAE J 2194. Roll-Over Protective Structures (ROPS) for Wheeled Agricultural Tractors. Warrendale, PA (USA): SAE, 2009.
- A.J. Scarlett, J.N. Reed, D.A. Semple, P.C. Seward, A.D. Stockton, and J.S. Price. Operator rollover protection on small vehicles. Research report 432. UK: HSE Books, 2006.
- H. Schwanghart. Schlepperumsturz und prüfung von umsturz-schutzeinrichtungen. *Landtechnische Forschung*, 19(1):1–5, 1971.
- H. Schwanghart. Berechnungsmethode für das umsturzverhalten eines achrschleppers am hang [method for calculating the overturning behaviour of tractors on slopes]. *Grundl. Landtechnik*, 23(6):170–176., 1973.
- H. Schwanghart. Der statische test als prüfung der festigkeit von schlepper- umsturzschutzvorrichtungen in der europäischen gemeinschaft. *Grundl. Landtechnik*, 28(5):184–189, 1978.

- H. Schwanghart. *Umsturzverhalten von Traktoren und Auswirkungen auf die Schutzvorrichtungen und die Sicherheit /vorgel. von H[elmut] Schwanghart*. Institut für Kraftfahrtechnik, Förderwesen und Agrartechnik Lehrstuhl für Landmaschine, 1982. URL <http://books.google.fr/books?id=MST5MgAACAAJ>.
- J.E. Shigley, C.R. Mischke, and R.G. Budynas. *Progetto e costruzione di macchine*. Ingegneria meccanica. McGraw-Hill Companies, 2009. ISBN 9788838665035. URL <http://books.google.com/books?id=4QFCPwAACAAJ>.
- W. Söhne and H. Schwanghart. Stand und entwicklung von prüfmethoden bei schleperumsturzschutzvorrichtungen. *Grundl. Landtechnik*, 28(5):178–184, 1978.
- H. Silleli, M.A. Dayioglu, A. Gültekin, K. Ekmekçi, M.A. Yildiz, E. Akay, and G. Saranlı. Anchor mechanism to increase the operator clearance zone on narrow-track wheeled agricultural tractors: Prototype and first tests. *Biosystems Engineering*, 97(2):153 – 161, 2007. ISSN 1537-5110. doi: <http://dx.doi.org/10.1016/j.biosystemseng.2007.02.016>. URL <http://www.sciencedirect.com/science/article/pii/S1537511007000451>.
- H. Silleli, M.A. Dayioglu, A. Gültekin, G. Saranlı, M.A. Yildiz, E. Akay, and K. Ekmekçi. Anchor mechanism to increase the operator clearance zone on narrow-track wheeled agricultural tractors: Static and field upset test results. *Biosystems Engineering*, 99(2):196 – 204, 2008. ISSN 1537-5110. doi: <http://dx.doi.org/10.1016/j.biosystemseng.2007.10.014>. URL <http://www.sciencedirect.com/science/article/pii/S1537511007002954>.
- D.W. Smith and J.B. Liljedahl. Simulation of rearward overturning of farm tractors. *Transactions of the ASABE*, 15(5):818–821, 1972. URL <http://elibrary.asabe.org/abstract.asp?adid=38017&t=3>.
- A. Song, B.K. Huang, and H.D. Bowen. Simulating a powered model wheel-tractor on soft ground. *Transactions of the ASABE*, 32(1):2–11, 1988. URL <http://elibrary.asabe.org/abstract.asp?adid=30954&t=3>.

- H.B. Spencer and G. Gilfillan. An approach to the assessment of tractor stability on rough sloping ground. *Journal of Agricultural Engineering Research*, 21(2):169 – 176, 1976. ISSN 0021-8634. doi: [http://dx.doi.org/10.1016/0021-8634\(76\)90071-8](http://dx.doi.org/10.1016/0021-8634(76)90071-8). URL <http://www.sciencedirect.com/science/article/pii/0021863476900718>.
- B. Springfeldt. Rollover of tractors - international experiences. *Safety Science*, 24(2):95 – 110, 1996. ISSN 0925-7535. doi: [http://dx.doi.org/10.1016/S0925-7535\(96\)00069-0](http://dx.doi.org/10.1016/S0925-7535(96)00069-0). URL <http://www.sciencedirect.com/science/article/pii/S0925753596000690>.
- X. Wang. *Modification and Evaluation of Continuous Roll Prediction Model for Front Drive Mowers*. University of Tennessee, Knoxville, 2005. URL <http://books.google.it/books?id=dS3ENwAACAAJ>.
- X. Wang, P. Ayers, and A.R. Womac. Static simulation and analyses of mower's rops behavior in a finite element model. *Journal of Agricultural Safety and Health*, 15(4):335–351, 2009.